New constraints on the early formation of the Western Dharwar Craton (India) from igneous zircon U-Pb and Lu-Hf isotopes

Martin Guitreau, Samuel B. Mukasa, Lorne Loudin, Sajeev Krishnan

New constraints on the early formation of the Western Dharwar Craton (India) from igneous zircon U-Pb and Lu-Hf isotopes

Highlights:

- We present new U-Pb and Lu-Hf isotope data for igneous zircons from the WDC (75 characters)
- We found the oldest granitoid of the WDC which is a 3411 Ma peraluminous orthogneiss (85 characters)
- This orthogneiss is suggested to mark the beginning of the WDC formation (72 characters)
- Our results reveal that ancient crust up to 3607 Ma is present as inherited zircons (83 characters)
- No crust older than 3410 Ma was involved in the WDC formation prior to ~3200 Ma (79 characters)

New constraints on the early formation of the Western Dharwar Craton (India) from igneous zircon U-Pb and Lu-Hf isotopes

Martin Guitreau[1,2,3*], Samuel B. Mukasa[1,4], Lorne Loudin[1,5], Sajeev Krishnan[6]

[1] *CEPS-Department of Earth Sciences, University of New Hampshire, James Hall, 56 College Road, Durham, NH 03824, USA*

[2] *School of Earth and Environmental Sciences, The University of Manchester, Williamson building, Oxford road, Manchester, M13 9PL, UK*

[3] *Université Clermont Auvergne, Laboratoire Magmas et Volcans, IRD, CNRS, UMR 6524, 6 avenue Blaise Pascal, 63178 Aubière, France*

[4] *Department of Earth Sciences, University of Minnesota, Pillsbury Hall, 310 Pillsbury Drive SE, Minneapolis, MN 55455, USA*

[5] *Gemological Institute of America, Inc., 50 W 47th Street, New York, NY 10036, USA*

[6] *Centre for Earth Sciences, Indian Institute of Science, Bangalore 560 012, India*

** Corresponding author: martin.guitreau@uca.fr*

Keywords: Western Dharwar Craton, zircon U-Pb geochronology, Lu-Hf isotope system, continents, Archean

Word count: abstract = 344; Main text = 10492; Figures = 9 (+ 6 in supplementary) and Tables = 4 (+6 in supplementary); refs = 124

Abstract:

The Western Dharwar Craton (WDC) is an Archean crustal segment for which the earliest stages of development have remained poorly constrained because the oldest identified lithologies are chronologically indistinguishable despite vastly different compositions and origins (i.e., 3352 ± 110 Ma Sargur-group komatiites and 3342 ± 6 Ma Hassan-Gorur TTG gneiss). Indication for older crust come from ancient detrital zircons (3450-3610 Ma), although their genetic link to the WDC is purely conjectural. In order to bring new understanding to early development of the WDC, we studied orthogneisses around the Holenarsipur Schist Belt (HSB) for their petrography, major-oxide concentrations, zircon U-Pb geochronology, and Lu-Hf isotope systematics. Our results reveal that the WDC igneous record contains crust older than 3350 Ma in the form of a 3410.8 ± 3.6 Ma granitic gneiss and inherited zircons with ages ranging from 3295 ± 18 to 3607 ± 16 Ma that were found within a 3178 ± 10 Ma trondhjemitic gneiss and a biotite-rich enclave found within it. The presence of muscovite and the peraluminous signature of the granitic gneiss, in spite of mildly-depleted Hf isotopic signature (ε_{Hf} = +2.2 ± 0.6 at 3410.8 Ma), suggest that this sample formed by reworking of a felsic precursor with short crustal residence time, possibly marking the beginning of WDC formation. The oldest inherited zircons display variable ε_{Hf} ranging from +10.4 at 3414 Ma to -2.3 at 3607 Ma that did not seem to have influenced the Hf isotopic composition of granitoids of the WDC that formed between 3200 and 3410 Ma, except perhaps in the Sargur area. We suggest that the WDC formed remote from continental crust until a crustal block containing >3410 Ma zircons was accreted to it ~3200 My ago. This event resulted in the stabilization of the WDC which is marked by diapiric granitoids to which the 3178 Ma trondhjemitic gneiss belongs.

After 3200 Ma, the crustal block together with granitoids formed between 3410 and 3200 Ma buffered the Hf isotopic signature of newly formed granitoids, hence, indicating that, by then, the WDC already was a stable continental segment.

1. Introduction:

The Western Dharwar Craton (WDC; Southern India) is amongst the best-preserved pieces of Archean crust and therefore has been well studied (e.g., Naqvi and Rogers, 1987; Bouhallier et al., 1995; Chardon et al., 2008; Ramakrishnan, 2009; Dey, 2013; Jayananda et al., 2015). It has recorded multiple episodes of magmatic and volcanic activity as well as several sedimentary cycles and tectonic events that started in the Paleoarchean (~3400 Ma) and ended around the Archean-Proterozoic transition (~2500 my ago), although later metamorphic events have also occured (e.g., Naqvi and Rogers, 1987; Bhaskar Rao et al., 1992; Meen et al., 1992; Miller et al., 1996; Table 1). Despite a large number of studies, including recent ones, having addressed the question of the evolution of the Dharwar craton (e.g., Naqvi and Rogers, 1987; Chadwick et al., 2000; Jayananda et al., 2008; Lancaster et al., 2015), there still is uncertainty in the timing and the nature of WDC's first crust formation. This is because the two oldest known lithologies appear coeval within analytical uncertainty, and yet have vastly different compositions. These units are the 3352 ± 110 Ma Sargur-group komatiites (Jayananda et al., 2008) and the Hassan-Gorur gneisses, ranging from dioritic amphibolites to typical TTGs (e.g., Beckinsale et al., 1980; Bhaskar Rao et al., 1991; Naqvi et al., 2009; Jayananda et al., 2015). These orthogneisses have been dated at 3358 ± 66 Ma by Beckinsale et al., (1980), and more recently refined to 3342 ± 6 Ma by Jayananda et al. (2015). Yet, zircons from detrital metasediments (i.e., quartzites and conglomerates; Nutman et al., 1992; Lancaster et al., 2015; Bhaskar Rao et al., 2008; Sarma et al., 2012)

reveal the presence of sialic crust as old as 3542 ± 9 to 3634 ± 10 Ma in the vicinity of WDC between ~3300 My and ~2500 My ago, as deduced from the estimated age of deposition for the studied detrital sediments of the WDC (Table 1). Some of the Nd isotopic signatures displayed by Hassan-Gorur gneisses are consistent with the involvement of pre-existing crust in their genesis (Jayananda et al., 2015), but closed-system evolution of the Sm-Nd isotope system in these gneisses cannot be verified. Therefore, the actual age of the oldest generations of WDC's peninsular gneisses remains uncertain (e.g., Jayananda et al., 2008, 2015; Naqvi et al., 2009; Dey, 2013; Lancaster et al., 2015), while it bears a great deal on our understanding of the early history of the Dharwar Craton.

Zircons derived from terranes adjacent, or accreted, to a craton, after its major stages of formation, can contribute to the local detrital zircon record. Interestingly, neighboring Bastar and Bundelkhand cratons, as well as the Coorg Block, contain old gneisses dated at 3509 ± 14 Ma (Sarkar et al., 1993), 3561 ± 11 Ma (Ghosh, 2004), 3582.6 ± 4 Ma (Rajesh et al., 2009), 3550.9 ± 5.9 Ma (Kaur et al., 2014), and 3502 ± 11 Ma (Santosh et al., 2016). Rare ancient zircon cores have also been found in TTG gneisses from the Karwar Block (3473-3601 Ma; Ishwar-Kumar et al., 2013). However, while WDC's oldest detrital zircons show coherent Hf isotopic signatures (see Sarma et al., 2012; Lancaster et al., 2015), they generally differ from those of their coeval igneous counterparts from Coorg Block and Bundelkhand Craton's oldest gneiss (Santosh et al., 2016; Kaur et al., 2014), possibly indicating a different origin. Quartzites and greywackes in which Paleoarchean detrital zircons have been found, are assumed to have been deposited at respective ages of ~3300-3200, ~2900 Ma, and ~2500 Ma (e.g., Nutman et al., 1992; Bhaskar Rao et al., 1992, 2008; Peucat et al., 1995; Sarma et al., 2012; Hokada et al., 2013; Table 1). Therefore, it remains uncertain

100 if the ages indicated by detrital zircons accurately depict the age of the oldest crusts
101 involved in development of the WDC.
102 To shed new light on the context of early formation of the Western Dharwar
103 Craton, we have conducted a field survey of some of the oldest generations of
104 peninsular gneisses in the Hassan-Gorur area. Here, we report on two felsic gneisses
105 and an enclave found within one of them, as well as on their zircon U-Pb ages and Hf
106 isotopic signatures. Our new results considered with available data on the WDC bring
107 important constraints on the early development of the WDC.
108

109 **2. Geological background**

110 The Dharwar craton (Southern India) is subdivided into a western (WDC) and an
111 eastern (EDC) part that are separated by a major shear zone along the Chitradurga
112 greenstone belt ("Ch" in Fig. 1), and a N-S trending intrusion composed of late Archean
113 K-rich granites (i.e., Closepet batholith; e.g., Moyen et al., 2003; Fig. 1). Most of the
114 rocks of the EDC exhibit Neoarchean ages, whereas those found in the WDC have
115 protoliths dated at ~2500 and up to ~3360 Ma (e.g., Beckinsale et al., 1980; Naqvi and
116 Rogers, 1987; Meen et al., 1992; Bhaskar Rao et al., 1992; Jayananda et al., 2008, 2015;
117 Sarma et al., 2012; Dey, 2013). The Dharwar craton had been northwardly tilted,
118 probably sometime between 2400 and 1600 Ma (Ramakrishnan, 2009), and therefore
119 displays an almost entire conformable crustal sequence characterized by a continuous
120 increase in metamorphic grade from greenschist to granulite toward South (e.g.,
121 Pichamuthu, 1965; Rollinson et al., 1981; Hansen et al., 1985; Raase et al., 1986).
122 Tonalite-trondhjemite-granodiorite (TTG) gneisses, locally named peninsular gneisses,
123 make up the basement of the WDC and dominantly crop out in the southern regions
124 (Fig. 1). These orthogneisses are intercalated with highly deformed supracrustal

sequences of the ~3.4-3.0 Ga Sargur group (e.g., Naqvi and Rogers, 1987; Yoshida et al., 1994; Jayananda et al., 2008, 2015) that were equilibrated in high-metamorphic grade in the late-Archean (i.e., ~8kbar and ~700-750°C around 2430 Ma; Janardhan et al., 1982; Raith et al., 1983; Jayananda et al., 2013). Both the Peninsular gneisses and the Sargur group are unconformably overlain by the 2.9-2.5 Ga Dharwar supergroup (Table 1), which is less deformed and less metamorphosed than the Sargur group. Therefore, the oldest remnants are located in the South, in high-grade metamorphic conditions, and the youngest, less metamorphosed greenstones, are located in northern regions of the WDC (Fig. 1). Some younger granites (2700-2500 Ma) are also found throughout the WDC (e.g., Taylor et al., 1984; Meen et al., 1992). The general dome-and-basin structure exhibited by the WDC have been documented in several studies that concluded that denser greenstone belts sunk into the basement gneisses by sagduction (e.g., Bouhallier et al., 1993, 1995; Chardon et al., 1996, 1998).

Supracrustal (greenstone) belts are very abundant in the WDC and they contain either one or both volcano-sedimentary groups (e.g. Hokada et al., 2013); the Sargur group (~3350-3000 Ga) and the Dharwar supergroup (2900-2500 Ga), the latter of which is further sub-divided into Chitradurga (upper section) and Bababudan groups (lower section) based on lithologies and ages (e.g., Naqvi and Rogers, 1987; Ramakrishnan, 2009; Table 1). Sargur Group volcanic sequences are dominated by komatiites and tholeiitic basalts, with subordinate felsic lava flows, whereas the Dharwar Supergroup volcanics contain abundant tholeiitic to felsic volcanics with subordinate komatiitic basalts. Sediments composing Sargur and Dharwar groups are conglomerate, quartzite, pelite, carbonate, and banded iron formation. According to Ramakrishnan (2009), the Sargur Group occurs in two types of lithological association, namely: (i) linear ultramafic-mafic belts containing subordinate clastic sediments and

150 BIF (e.g. Nuggihalli, Nagamangala and Krishnarajpet), and (ii) scattered ultramafic-
151 mafic enclaves associated with quartzite-carbonate-pelite-BIF assemblage (e.g. Sargur
152 and Mercara). The same author, together with Chadwick et al. (1989), indicates that the
153 Dharwar sequence consists of three lithological packages that are, in the ascending
154 order, (1) a basal quartz-pebble conglomerate with amygdular metabasalt alternations,
155 local felsic volcanics, and banded-iron formation (BIF), which correspond to the
156 Bababudan Group, (2a) a polymict conglomerate, quartzite, pelite, carbonate, and
157 Mn/Fe formations that define the Vanivilas Subgroup of the Chitradurga Group, (2b)
158 pillowed metabasalts, felsic volcanics, and BIF which form the Ingaldhal Subgroup of
159 the Chitradurga Group, and (3) a greywacke turbidite, a polymict conglomerate, and a
160 BIF horizon that correspond to the Ranibennur Subgroup of the Chitradurga Group.
161 The peninsular gneisses exhibit ages from 3360 to 3000 Ma and are somewhat
162 heterogeneous in age and composition (e.g., Beckinsale et al., 1980; Rogers et al., 1986;
163 Bhaskar Rao et al., 1991; Jayananda et al., 2015). Multiple generations of peninsular
164 gneisses have been identified and classified using different criteria (e.g., Janardhan et
165 al., 1978; Bhaskar Rao et al., 1983; Naqvi et al., 1983; Monrad, 1983) but the most
166 commonly used classification has been that of Monrad (1983), which is mainly based
167 on geochemistry. The latter author, through the example of the Hassan District
168 (Karnataka), proposed a low-Rb group (~3360-3200 Ma), a low-Al group (~3200-3100
169 Ma), a high-Al group (~3000 Ma) and a post-tectonic group (~3000-2900 Ma)
170 corresponding to massive diapiric bodies (e.g., Halekote trondhjemite, Chikmagalur
171 granite; Stroh et al., 1983; Taylor et al., 1984; Meen et al., 1992). A recent study (i.e.,
172 Jayananda et al., 2015) refined the classification of peninsular gneisses around the
173 Hassan district as follows: older TTG gneisses, which contain a low-Al and high-Al
174 group (3340-3280 Ma), younger trondhjemites, including Halekote-type, (3230-3200

175 Ma), eastern gneisses (3100 Ma) and the Chikmagalur granite (3150 Ma). The older
176 TTG gneisses have chemical characteristics suggesting that they formed by partial
177 melting of essentially undepleted heterogeneous mafic crusts at shallow depth and high
178 pressure, for the low-Al and high-Al group, respectively. In addition, older TTG
179 gneisses indicate possible interaction with pre-existing crust during emplacement.
180 Similar mafic sources can account for the formation of the trondhjemites (e.g.,
181 Halekote-type) with significant interaction with pre-existing crust as testified to by the
182 presence of inherited zircon cores (e.g., Jayananda et al., 2015). The eastern gneisses
183 more likely represent shallow level melting of depleted mafic sources subsequently
184 contaminated by older TTG gneisses (low-Al type), whereas the Chikmagalur granite
185 most likely originate from partial melting of newly formed TTG crust at lower crustal
186 level.

187 In a craton-wide compilation of available Nd isotope data, Dey, (2013) proposed
188 that the WDC formed through essentially juvenile addition (mafic and felsic) between
189 3360 and 3000 Ma (ε_{Nd} = +1.5 to +6.4), followed by dominantly mafic crust addition
190 between 2900 and 2600 Ga (ε_{Nd} = -0.3 to +0.4), and major crust reworking at 2600-
191 2500 Ma, accompanied by minor juvenile input. A recent study dealing with detrital
192 zircon U-Pb and Lu-Hf isotope systematics (Lancaster et al., 2015) concluded that there
193 had been significant juvenile crust extraction from ~3.3. to 2.7 Ga and cratonization at
194 ~3.0 Ga in the WDC. These authors also suggested continuous extraction of mantle
195 melts from as far back as 3.7 Ga to 3.3 Ga, which matches ages of some detrital zircons
196 (Table 1 and references therein) but are mostly absent from the igneous record.
197

198 **3. Sampling strategy and sample description**

Samples analyzed in this study were collected in two separate locations around the Holenarsipur Schist Belt (HSB; Fig. 2; Table 2) because this area hosts WDC's oldest peninsular gneisses reported so far (e.g., Beckinsale et al., 1980; Bhaskar Rao et al., 1991; Meen et al., 1992; Jayananda et al., 2015). The HSB area consists of volcano-sedimentary successions that mostly belong to the Sargur group (e.g., Peucat et al., 1995; Jayananda et al., 2008) and that sunk by sagduction into 3350-3300 Ma peninsular gneisses (e.g., Beckinsale et al., 1980; Bouhallier et al., 1993; Jayananda et al., 2015). Both peninsular gneisses and the HSB were intruded by Halekote trondhjemites ~3200 My ago (e.g., Taylor et al., 1984; Jayananda et al., 2015). Most of the gneisses analyzed in previous studies were collected in quarries (e.g., Beckinsale et al., 1980; Bhaskar Rao et al., 1991; Jayananda et al., 2015), hence possibly missing the oldest generations of peninsular gneisses. Consequently, we have purposely sampled gneisses both inside, and outside quarries where, however, outcrops are limited. Nevertheless, we made every effort to collect fresh samples, free of any altered surfaces.

3.1. Field occurrence of orthogneiss 13DC12

Sample 13DC12 is a fine-grained and massive to very weakly foliated brownish orthogneiss collected from meter- to decameter-scale outcrops protruding from weathered soils (Fig. 3A). Medium-grained pegmatite veins, which belong to only one identifiable generation, crosscut the orthogneiss (Fig. 3A), but these were avoided in collecting sample 13DC12. As summarized in Table 2, this sample is composed dominantly of quartz, plagioclase, K-Feldspar (microcline), but also contains biotite, muscovite, and very few opaque phases (e.g., oxide, sulfide). At the hand-sample scale some rare 1-5 mm octahedral metallic phases are also visible. In thin section (see Figs.

3B and 3C), quartz consists of medium-sized to large xenomorphs that sometimes contain smaller euhedral to subhedral quartz grains, likely recrystallized statically. Plagioclase often appears as medium to large sub-euhedral to xenomorphic crystals showing variable degrees of sericitization. K-Feldspar is commonly found as small xenomorphs intercalated between larger quartz or plagioclase grains, although big crystals can sometimes be found. Biotite is always present as small subhedral crystals, often altered into chlorite. In places, zircon is visible within biotite because of the halo generated through radioactive decay of zircon-hosted U and Th. Muscovite forms bigger crystals than biotite and they are often subhedral. Although the rock appears massive to weakly foliated, and displays a granoblastic texture (Figs. 3B and 3C), bands of grain-size reduction down to a factor of ~5, are visible at the thin section scale. However, no noticeable change in mineralogy is observed in these bands.

3.2. Field occurrence of orthogneiss 13DC13

Sample 13DC13 is a fresh, grey, and fine-grained orthogneiss (Fig. 3D), that is massive to weakly foliated. In contrast to the field occurrence of orthogneiss 13DC12, this sample was collected in a large (~500 x 500 m) active quarry (Fig. 3D; Table 2) throughout which the outcrops are homogeneous. It is, nevertheless, crosscut by multiple generations of pegmatite veins of various sizes and spatial distribution (Fig. 3D), and some biotite-rich enclaves ranging in size from ~5 x 2 to ~30 x 10 cm can also be found sparsely distributed within it. Sample 13DC13 is composed essentially of plagioclase, quartz, K-Feldspar (microcline), biotite, and muscovite (Table 2). In thin section (see Figs. 3E and 3F), quartz appears as medium-sized and relatively fresh xenomorphs. Plagioclase show little sericitization and also occurs as subhedral crystals to xenomorphs of substantial size, in contrast to K-Feldspar which is commonly small

with the exception of some rare large and fresh xenomorphs that are likely secondary. Biotite is more abundant than in the orthogneiss 13DC12 and crystals are usually subhedral and fresh (no or very little alteration into chlorite). Zircon halos are visible in some biotite crystals. Muscovite is slightly less abundant than biotite but has a similar habitus and size. Both biotite and muscovite seem to have been co-genetically crystallized as they form coherent masses of interspersed crystals. Almost no opaque phase can be seen in thin section. Sample 13DC13 is characterized by a granoblastic texture visible in thin section (Figs. 3E and 3F).

3.3. Biotite-rich enclave (13DC15)

Sample 13DC15 is a fresh ~20 x 10 cm biotite-rich enclave found in the orthogneiss that 13DC13 represents. Due to its high-biotite content, this type of enclave is very often deeply weathered and friable but the ongoing work in the quarry exhumed some fresh samples such as 13DC15. This rock contains approximately 70% biotite (sometimes turned into chlorite), 10% quartz, 10% plagioclase, and 10% of various minerals (e.g., K-Feldspar, muscovite, opaque phases; Table 2).

4. Analytical details

4.1. Major and minor element analysis

Major- and minor-oxide results are given in Table S1. Measurements were done by ICP-AES (Jobin-Yvon ULTIMA C) at the Laboratoire Magmas et Volcans (Clermont-Ferrand, France). The rock standard BHVO-1 was also analyzed so as to determine the precision and accuracy of the measurements. Major- and minor-oxide concentrations were within <1% up to 5% of consensus values (Flanagan, 1976; Abbey, 1983;

273 Govindaraju, 1994) whereas analytical precisions were better than 1% for both major
274 and minor oxides, except for P_2O_5 concentration which had 3% uncertainty.
275
276 **4.2. Zircon U-Pb geochronology by LA-ICP-MS**
277 Zircon crystals were separated at the University of Colorado (Boulder, CO, USA) using
278 standard mineral separation techniques (see Mojzsis et al., 2003). The most optically
279 clear zircon grains devoid of cracks and inclusions were selected and mounted in epoxy
280 together with fragments of the zircon standards AS3 (1099.1 ± 0.5 Ma; Paces and
281 Miller, 1993) and 91500 (1065.4 ± 0.3 Ma; Wiedenbeck et al., 1995). The selected
282 crystals were euhedral to subhedral, pale pink to orange, and transparent to slightly
283 cloudy. The spots analyzed on each grain were selected based on internal textures as
284 revealed by cathodoluminescence (CL) images acquired at the University of New
285 Hampshire using a Tescan Lyra 3 scanning electron microscope.
286 Zircon U-Pb analyses were carried out by LA-ICP-MS at the University of New
287 Hampshire (UNH). Details regarding operating conditions are given in Table S2 and
288 results can be found in Table 3, and the supplementary Tables S3 and S4. A gold trap
289 was used to lower ^{204}Hg interferences on ^{204}Pb and, hence, more accurately detect the
290 presence of common Pb. Measurements were started ~5s after the beginning of the
291 ablation to allow a steady flow of the aerosol from the laser to the mass spectrometer.
292 Time-resolved signals were carefully monitored throughout each and every analysis to
293 ensure optimization and data reproducibility. Further, because of down-hole
294 fractionation, we used the t_0 intercept method based on data regression through linearly
295 shifting isotopic ratios as a function of time (see Košler and Sylvester, 2003; Fisher et
296 al., 2010). Both $^{207}Pb/^{235}U$ and $^{206}Pb/^{238}U$ ratios were measured, but the former was
297 only used as a quality check by comparing it to $^{207}Pb/^{235}U$ calculated from measured

298 $^{206}Pb/^{238}U$ and $^{207}Pb/^{206}Pb$, as well as a $^{238}U/^{235}U$ of 137.88. Decay constant used are
299 the followings: $^{238}\lambda = 1.55125.10^{-10}$, $^{235}\lambda = 9.8485.10^{-10}$ (Jaffey et al., 1971), and $^{232}\lambda =$
300 $4.9475.10^{-11}$(Le Roux and Glendenin, 1963). $^{207}Pb/^{206}Pb$ ages were calculated using
301 iterative convergence. The ISOPLOT program (Ludwig, 2008) was used to display the
302 processed data on Concordia diagrams and to determine the sample ages. We further
303 measured semi-quantitative (no internal standardization) concentrations of Pb, U, and
304 Th, by using AS3 as an external standard (Paces and Miller, 1993). Finally, $^{232}Th/^{238}U$
305 ratios were calculated from $^{208}Pb/^{206}Pb$ values and determined $^{207}Pb/^{206}Pb$ ages.
306 91500 zircon standard was analyzed as an unknown throughout the session for
307 quality check. The weighted average $^{207}Pb/^{206}Pb$ and upper-intercept U-Pb age obtained
308 for 91500, over the course of this study, were both 1061.6 ± 7.1 Ma (2σ; n = 10; Fig.
309 S1). These ages agree well within uncertainty with the commonly accepted ID-TIMS
310 age of 1065.4 ± 0.3 Ma (Wiedenbeck et al., 1995). 91500 zircon standard Pb, U, and
311 Th mean concentrations determined over the course of this study gave 14.4 ± 2.1 (2σ;
312 n = 10), 66.3 ± 7.9, and 23.0 ± 4.5 ppm (Table S3), respectively. These values are in
313 reasonably good agreement with the respective recommended values of 15 ± 4 (2σ), 80
314 ± 16, and 29.9 ± 4.2 ppm (Wiedenbeck et al., 2004), which are means of analyses
315 performed in 5 different laboratories. The mean calculated $^{232}Th/^{238}U$ obtained for
316 91500 was 0.37 ± 0.01 (2σ; n = 10; Table S3), which is in agreement with values of
317 0.3444 ± 0.0018 (2σ), determined by Wiedenbeck et al. (1995) on 2 zircon fragments,
318 and 0.38 ± 0.09 determined by numerous LA-ICP-MS analyses (Wiedenbeck et al.,
319 2004).
320
321 **4.3. Zircon Lu-Hf isotope analysis by LA-MC-ICP-MS**

Lu-Hf isotope analyses were done by LA-MC-ICP-MS at Laboratoire Magmas et Volcans (LMV), Clermont-Ferrand (France). Details regarding the operating conditions are given in Table S2 and results can be found in Tables 3, S5, and S6. Lu-Hf isotope measurements were done using the cup configuration recommended by Fisher et al. (2014a). The Yb and Hf instrumental mass biases used to correct data were determined using $^{173}Yb/^{171}Yb$ normalized to the value of 1.132685 (Chu et al., 2002) and $^{179}Hf/^{177}Hf$ normalized to the value of 0.7325 (Stevenson and Patchett 1990). It was further assumed that Lu fractionation followed that of Yb (Fisher et al., 2014a). A value of 0.79618 for $^{176}Yb/^{173}Yb$ (Chu et al., 2002) and 0.02655 for $^{176}Lu/^{175}Lu$ (Fisher et al., 2014a) were used to correct data for the isobaric interferences of ^{176}Yb and ^{176}Lu on ^{176}Hf. In order to monitor instrumental fractionation and data quality, zircon standards 91500, MudTank, Plešovice, and R33 were measured multiple times over the course of the LA-MC-ICP-MS analyses. Lu-Hf isotope analyses were done on top of the pits developed by ablation during the U-Pb isotope analyses in order to acquire linked information. Much like for U-Pb isotope analyses, time-resolved signals were carefully monitored throughout each and every analysis. The ^{176}Lu decay constant of Scherer et al. (2011) and S□derlund et al. (2004), which is $1.867.10^{-11}$, was used to calculate initial Hf isotopic compositions. Uncertainties associated with the radiogenic-ingrowth correction were propagated using the algorithms of Ickert (2013). Epsilon notations were derived from normalization to the Bulk Silicate Earth (BSE) Lu-Hf isotopic parameters published by Iizuka et al. (2015).

Obtained mean $^{176}Hf/^{177}Hf$ for 91500, MudTank, Plešovice, and R33 were 0.282299 ± 0.000018 (2σ; n=16), 0.282501 ± 0.000017 (2σ; n=17), 0.282472 ± 0.000013 (2σ; n=7), and 0.282757 ± 0.000039 (2σ; n=9), respectively (Table S5; Fig. S2). These values are well within uncertainty of the accepted values of 0.282308 ±

0.000006 (Blichert-Toft, 2008) for 91500, 0.282507 ± 0.000006 (Woodhead and Hergt, 2005) for MudTank, 0.282482 ± 0.000012 (Sláma et al., 2008) for Plešovice, and 0.282764 ± 0.000014 (Fisher et al., 2014b) for R33. Determined $^{176}Yb/^{177}Hf$ and $^{176}Lu/^{177}Hf$ for these zircon standards also comply well with those recommended by other authors (Table S5; e.g., Fisher et al., 2014a, 2014b).

5. Results

5.1. Orthogneiss 13DC12 composition and ages

This sample is characterized by high silica content (74 wt%), moderately high Al_2O_3 (13.9 wt%), similar Na_2O and K_2O contents (3.9 and 4.3 wt%, respectively), and low Fe_2O_3 (1.47 wt%), CaO (0.95 wt%), MgO (0.19 wt%), TiO_2 (0.11 wt%), P_2O_5 (0.11 wt%), and MnO (0.02 wt%) (Table S1). On an Ab-An-Or normative plot (O'Connor, 1965; Barker, 1979), sample 13DC12 falls in the granite field (Fig. 4A). Major elements further indicate that sample 13DC12 has a peraluminous character (A/CNK and A/NK > 1; Table S1; Fig. 4B). In addition, it can be seen in Figure 4C that 13DC12 plots at the high-silica end of the domain that characterizes calc-alkalic rock suites, more specifically in the field of Bt- and two-mica granites and on the edge of the field for TTG. Similarly, in the ternary diagram proposed by Laurent et al. (2014) for classification of Archean granitoids, 13DC12 falls in a zone where the fields for Bt- and two-mica granites and hybrid granites overlap (Fig. 4D). Finally, Figure 4E shows that 13DC13 major element concentrations comply with those of melts produced by partial melting of tonalites.

Zircons recovered from this sample have similar habits but exhibit variable internal structures, as revealed by CL images, ranging from simple oscillatory zoning to patchy and/or chaotic domains resembling alteration/recrystallization textures (Fig.

S3). This is in line with the U-Pb data being concordant to highly discordant. Similarly, U and Th concentrations vary from relatively low (<300 ppm for U and <100 ppm for Th; Tables 3 and S4) to high (>1000 ppm; Tables 3 and S4) and positively correlate with degrees of discordance with a change of slope beyond ~1000 ppm U. Measured $^{207}Pb/^{206}Pb$ ages do not show any correlation with discordance in the range 0-40% where they vary between 3310 ± 15 and 3425 ± 18 Ma (Table 3 and S4), but steadily decrease from 3235 ± 14 to 2696 ± 11 Ma between 40 and 71% discordance. The only truly concordant data correspond to two analyses done on the crystal labelled "13DC12_5" which gave ages of 3413 ± 7 and 3410 ± 4 Ma. The oldest $^{207}Pb/^{206}Pb$ ages determined on 13DC12's zircon population are in excellent agreement with the age of this concordant zircon. When used together these ages define an upper intercept age and weighted average $^{207}Pb/^{206}Pb$ age of 3410.8 ± 3.6 and 3408.6 ± 3.6 Ma, respectively (Fig. 6). All other zircons taken together, define a single broad Discordia with upper- and lower-intercepts at 3440 ± 39 and 576 ± 90, respectively (Fig. 6C). Note that the upper-intercept age is consistent, within uncertainty, with that determined from oldest and least discordant zircons. No global correlation is observed between Th/U ratios, which for the vast majority fall within the common range of magmatic zircons (e.g., Wang et al., 2011; Kirkland et al., 2015), and other chemical nor isotopic parameters. None of the observed internal structures indicate the presence of xenocrystic cores, nor of overgrowths (Fig. S3).

Zircons from the granitic gneiss exhibit high $^{176}Yb/^{177}Hf$ and $^{176}Lu/^{177}Hf$ values that are strongly correlated with each other (Table S6). Also, both ratios correlate positively with the measured $^{176}Hf/^{177}Hf$ values, which vary between 0.280685 ± 0.000032 and 0.281124 ± 0.000029. This correlation almost vanishes when $^{176}Yb/^{177}Hf$ and $^{176}Lu/^{177}Hf$ are plotted against initial $^{176}Hf/^{177}Hf$ (calculated using determined

397 $^{207}Pb/^{206}Pb$ ages) because these latter all agree within error-bars except for two data
398 points which exhibit the most radiogenic $^{176}Hf/^{177}Hf$ (Tables 3 and S4; Fig. 5). These
399 two errant data points resulted from analyses done on two separate crystals (zircons #1
400 and #2) that exhibit advanced discordance (Tables 3 and S4) and that have been
401 analyzed twice. The other analyses done on these crystals show initial Hf isotopic
402 compositions that comply well with the general Hf isotope initials, especially with those
403 determined on the concordant zircon 13DC12_5 (i.e., $^{176}Hf/^{177}Hf$ = 0.280635 ±
404 0.000018 and 0.280625 ± 0.000015). If all initial $^{176}Hf/^{177}Hf$ are calculated at the age
405 given by the concordant crystal, the positive correlation between $^{176}Yb/^{177}Hf$ and
406 $^{176}Hf/^{177}Hf$, as well as between $^{176}Lu/^{177}Hf$ and $^{176}Hf/^{177}Hf$ completely vanishes. Broad
407 positive correlations are observed between U concentration and $^{176}Lu/^{177}Hf$, and
408 therefore $^{176}Yb/^{177}Hf$.
409
410 **5.2. Orthogneiss 13DC13 composition and ages**
411 This sample has high SiO_2 content (72.6 wt%), high Al_2O_3 (15 wt%), relatively high
412 Na_2O (4.9 wt%) and CaO (1.82 wt%), moderately low K_2O (2.5 wt%) and Fe_2O_3 (1.69
413 wt%), and low MgO (0.50 wt%), TiO_2 (0.27 wt%), P_2O_5 (0.08 wt%), and MnO (0.02
414 wt%) (Table S1). On an Ab-An-Or normative plot (O'Connor, 1965; Barker, 1979),
415 sample 13DC13 falls in the trondhjemite field (Fig. 4). Major elements further indicate
416 that sample 13DC13 has a peraluminous character, much like 13DC12 (A/CNK and
417 A/NK > 1; Table S1). Figure 4C shows that 13DC13 plots at the high-silica end of the
418 domain that characterizes calc-alkalic rock suites, where the field for TTG and Bt- and
419 two-mica granites overlap. Similarly, in the ternary diagram proposed by Laurent et al.
420 (2014) for the classification of late-Archean granitoids (Fig. 4D), 13DC13 plots where
421 the fields for Bt- and two-mica granites, hybrid granites, and TTG overlap. Finally, in

Figure 4E 13DC13 fall in the compositional range of melts produced by partial melting of tonalities but near the boundary with low-K and high-K mafic rocks.

Zircons from this sample show variable crystal habits from stubby to elongated, and exhibit very different types of internal structures as revealed by CL images (Fig. S4). For example, zircon #5 exhibits a concentrically zoned dark and bright core with sinuous outlines surrounded by an oscillatory-zoned outer part. Zircon #11 has a homogeneous and barely zoned core surrounded by a darker and more chaotic outer rim. In this zircon, part of the core seems to have been resorbed and replaced by the same zircon material as that forming the outer rim. Similar to 13DC12 zircons, those from 13DC13 universally show a correlation between degrees of discordance and U, as well as Th, contents, which respectively vary from a few hundred to a few thousand ppm, and from a few tens to a few hundred ppm (Tables 3 and S4). Measured $^{207}Pb/^{206}Pb$ ages vary between 3441 ± 16 (5% discordant) and 2836 ± 20 Ma (80% discordant) (Fig. 7), and a broad correlation is observed between degrees of discordance and $^{207}Pb/^{206}Pb$ ages. Zircons from sample 13DC13 do not define a single Discordia but instead a funnel-shaped discordance pattern on a Concordia plot with upper-intercept ages ranging from ~3100 to ~3450 Ma (Fig. S5).

Zircons from the trondhjemitic gneiss with Th/U below 0.2 yield dates from 3355 down to 2964 Ma, whereas zircons with Th/U values that characterize the common magmatic range (>0.2-0.8; e.g., Wang et al., 2011; Kirkland et al., 2015) exhibit less variability and older dates (~3450-3320 Ma). Finally, zircons with Th/U >1 exhibit younger dates of 3278-2836 Ma (Tables 3 and S4; Fig.S5).

Determined $^{176}Lu/^{177}Hf$ and $^{176}Yb/^{177}Hf$ for zircons from the trondhjemitic gneiss are moderately low (Tables 3 and S6; Fig. 7) and strongly correlated with each

446 other. Initial Hf isotope ratios show modest variability between 0.280717 ± 0.000022
447 and 0.280860 ± 0.000016 and do not correlate with any elemental or isotopic parameter.
448
449 **5.3. Biotite-rich enclave (13DC15)**
450 Only two zircons have been recovered from the biotite-rich enclave 13DC15 and they
451 both show simple oscillatory zoning in CL images (Fig. S6). Each zircon has been dated
452 twice (see Tables 3 and S4 and Fig. S6). The first zircon (i.e., 13DC15_1) gave
453 $^{207}Pb/^{206}Pb$ ages of 3473 ± 21 Ma (2% discordant) and 2973 ± 30 Ma (23% discordant).
454 $^{176}Yb/^{177}Hf$ and $^{176}Lu/^{177}Hf$ determined on the same crystal are both low and close to
455 each other (Tables 3 and S5). In contrast to the differences exhibited by U-Pb ages, the
456 two measured $^{176}Hf/^{177}Hf$ are in excellent agreement within uncertainty, which is also
457 the case for the initial ratios (i.e., 0.280477 ± 0.000022 and 0.280487 ± 0.000013;
458 Tables 3 and S6; Fig. 8).
459 The two U-Pb analyses performed on the second zircon crystal are very
460 consistent with each other and gave respective $^{207}Pb/^{206}Pb$ ages of 3603 ± 23 Ma (9%
461 discordant) and 3610 ± 23 Ma (11% discordant). Determined $^{176}Yb/^{177}Hf$ and
462 $^{176}Lu/^{177}Hf$ are both low and close to each other (Tables 3 and S6), and the two
463 measured $^{176}Hf/^{177}Hf$ are in excellent agreement within uncertainty, which is also the
464 case for the initial ratios (i.e., 0.280374 ± 0.000019 and 0.280373 ± 0.000021; Tables
465 3 and S6; Fig. 8).
466 The oldest ages, obtained for 13DC15_1a, 2a, and 2b, are associated with Th/U
467 ratios in the common magmatic range, whereas the significantly discordant data of
468 13DC15_1b, which indicates a $^{207}Pb/^{206}Pb$ age of 2973 Ma, is coupled to a Th/U below
469 0.2 (Tables 3 and S6).
470

6. Discussion

6.1. Origin of studied orthogneisses based on petrographic observations and geochemical data

6.1.1. Granitic gneiss (13DC12)

One of the most notable petrographic observation that one can make in 13DC12 is the presence of significant amounts of muscovite which is a strong indicator for the crustal origin of granites (e.g., Barbarin, 1999). This is reinforced by the peraluminous flavor of this sample (Fig. 4B) together with the fact that it plots in the field of crustally-derived granites (i.e., Bt- and two-mica granites) in some key geochemical diagrams for late-Archean granitoids (Figs 4C and 4D). Finally, the major element composition of 13DC12 matches well with that of melts expected from partial melting of tonalitic sources with possible involvement of metasediments (Figs 4E). Taken altogether, we consider that petrographic and geochemical observations point to a dominant crustal origin for the protolith of the granitic gneiss 13DC12.

6.1.2. Trondhjemitic gneiss (13DC13)

The sample 13DC13 also contains significant amounts of muscovite that points to a crustal contribution to the formation of 13DC13 protolith. This is consistent with the peraluminous signature of this sample (Fig. 4B) together with the fact that it plots in the field of crustally-derived granites (i.e., Bt- and two-mica granites) and hybrid granites in some key geochemical diagrams for late-Archean granitoids (Figs 4C and 4D). Much as for 13DC12, the major element content in 13DC13 matches well with that of melts expected from partial melting of tonalitic sources with probable involvement of mafic sources (low-K and/or high-K; Figs 4E). Consequently, we

interpret petrographic and geochemical observations made on the trondhjemitic gneiss 13DC13 as evidence for its dominant crustal origin.

6.2. Interpretation of the zircon U-Pb ages and primary Hf isotopic signatures

6.2.1. Granitic gneiss (13DC12)

As illustrated in Figure 5, zircons from granitic gneiss sample 13DC12 display large variations in $^{207}Pb/^{206}Pb$ ages, but only a small variation in initial $^{176}Hf/^{177}Hf$. This behavior is quite common in old zircons (e.g., Patchett, 1983; Gerdes and Zeh, 2009; Guitreau et al., 2012) and can be attributed to different sensitivities to perturbation of the U-Pb and Lu-Hf isotope systems by thermal means and/or fluid activity (e.g., Lenting et al., 2010). Because all data points, except for 13DC12_1a, comply with the closed-system evolution model for the Lu-Hf isotope system in the analyzed crystals – based on the measured $^{176}Lu/^{177}Hf$ (Figure 5) – the observed variability in initial $^{176}Hf/^{177}Hf$ is not considered to be geological. Rather, this variability is the result of under-correction of radiogenic ^{176}Hf ingrowth that merely derives from the use of $^{207}Pb/^{206}Pb$ ages that are younger than the actual crystallization ages. Zircons from the granitic gneiss, therefore, form a single population. The age of 3410.8 ± 3.6 Ma (Fig. 6A) determined using the most concordant, and oldest least discordant zircons, is hence interpreted to be the actual crystallization age of this zircon population, and by extension that of 13DC12. Figure 5 shows that zircons used to establish this age also provide very consistent initial $^{176}Hf/^{177}Hf$ of 0.280631 ± 0.000018, which translates into an ε_{Hf} of +2.2 ± 0.6 at 3410.8 Ma (Table 4), and that we interpret as best reflecting the Lu-Hf isotope systematic of sample 13DC12. The upper-intercept age obtained from zircons that underwent post-crystallization U-Pb disturbance (i.e., 3440 ± 39 Ma) (Fig. 6C) is in agreement, within uncertainty, with the established crystallization age for

13DC12, reinforcing the notion that there is a single zircon population in the granitic gneiss. Finally, the lower-intercept age of 576 ± 90 Ma (Fig. 6C) that is interpreted as the timing of Pb-loss in some of 13DC12 zircons, matches well with metamorphic episodes recorded by rocks of the WDC and the southern granulite province (e.g., Bhaskar Rao et al., 1992; Miller et al., 1996; Meiβner et al., 2002; Santosh et al., 2006). This date corresponds to widespread Pan-African metamorphic events in the southern continents which previously comprised the supercontinent Gondwana (e.g., Yoshida et al., 1996; Meert, 2003; Santosh et al., 2005, 2006; Sato et al., 2011).

The age and initial Hf isotopic signature of zircons from the granitic gneiss sample 13DC12 match well with those of ancient detrital zircons from the WDC analyzed by Sarma et al. (2012), Lancaster et al. (2015) and Maibam et al. (2016), which are presented in Figure 9. These authors rationally interpreted this slightly positive initial ε_{Hf} signature as marking juvenile crust addition. However, if one assumes that ~3410 Ma detrital zircons were derived from lithologies similar to the granitic gneiss studied herein, which is the only rock >3350 Ma identified so far in the WDC, then, the positive ε_{Hf} signatures become misleading because sample 13DC12 is interpreted as a crust reworking product based on petrographic and geochemical arguments (see *section 5.1.1*). This example illustrates the fact that Hf isotopic signatures cannot unambiguously discriminate between juvenile addition and crustal reworking when used alone in the detrital zircon record. However, positive ε_{Hf} in a crustally-derived granitoid indicates that its precursor had a crustal residence time that was short enough so that its Hf isotopic composition was still close to that of its mantle source when it got reworked. In the absence of constraints on the nature of this precursor and its mantle source, we can speculate on lower- and upper-limits for crustal residence time by, respectively, assuming that the minimum time-span between emplacement and

545 reworking of a granitic unit is on the order of ~10 My, and by calculating two-stage
546 model ages (e.g., Blichert-Toft and Albarède, 2008; Hawkesworth et al., 2010). In order
547 to minimize issues inherent to model ages (e.g., Arndt and Goldstein, 1987; Laurent
548 and Zeh, 2015; Payne et al., 2016), we have used end-members from a large range of
549 crustal $^{176}Lu/^{177}Hf$ which characterize average Archean TTGs (0.004; Guitreau et al.,
550 2012) and average continental crust (0.015; Griffin et al., 2004). Assuming a mantle
551 source similar to the arc-mantle (ε_{Hf} = +13.3; Dhuime et al., 2011; Iizuka et al., 2013),
552 the calculated model ages range from 3466 to 3492 Ma. If, instead, a depleted mantle
553 source (DM) similar to that of MORB (ε_{Hf} = +17; Chauvel and Blichert-Toft, 2001) is
554 assumed, the model ages become 3503 to 3545 Ma. We cannot conclude on the actual
555 residence time of the precursor to 13DC12 but we note that it can range from ~10 to
556 ~130 My and is, hence, relatively short and included in the range displayed by the oldest
557 detrital zircons (e.g., Nutman et al., 1992; Sarma et al., 2012; Lancaster et al., 2015;
558 Maibam et al., 2016) and igneous zircons (this study) of the WDC.
559
560 **6.2.2. Trondhjemitic gneiss (13DC13)**
561 Internal textures associated with variable U-Pb ages, Th/U, and initial Hf isotopic
562 compositions in 13DC13 zircons (Figs. 7 and S5) led us to conclude that there is more
563 than one population in this sample, each variably affected by post-crystallization
564 disturbance(s). In order to characterize these populations, we have determined
565 Discordia lines at the scale of each zircon every time analyses done on a same crystal
566 showed consistent initial $^{176}Hf/^{177}Hf$ and that $^{207}Pb/^{206}Pb$ ages correlated with degrees
567 of U-Pb discordance. Otherwise, $^{207}Pb/^{206}Pb$ ages and their associated initial $^{176}Hf/^{177}Hf$
568 were considered separately. Doing so results in the emergence of five groups (Table 4).

The first one is represented by three zircon crystals in which the laser-ablation spots were located in zones that we interpreted as xenocrystic cores because they appear as rounded and/or resorbed domains surrounded by oscillatory-zoned outerparts in CL images (Fig. S4). These three zircons exhibit ages of 3468 ± 41 (upper-intercept zircon #4), 3456 ± 20 (upper-intercept zircon #7), and 3414 ± 23 Ma (concordant $^{207}Pb/^{206}Pb$ zircon #12) that are associated with respective initial Hf isotopic compositions of 0.280742 ± 0.000014, 0.280721 ± 0.000017, and 0.280860 ± 0.000016. These latter are equivalent to ε_{Hf} of +7.5 ± 0.5, +6.4 ± 0.6, and +10.4 ± 0.6 (Table 4), respectively.

The second group is represented by three crystals in which laser-ablation measurements were done in domains resembling xenocrystic cores much like for the first group and that gave ages of 3342 ± 19 (upper-intercept zircon #5), 3356 ± 25 (upper-intercept zircon #11), and 3359 ± 110 (upper-intercept zircon #3). The initial Hf isotopic signatures obtained on the same locations are 0.280720 ± 0.000018, 0.280733 ± 0.000012, and 0.280778 ± 0.000016 (Table 4), respectively, which translates into ε_{Hf} values of +3.7 ± 0.6, +4.5 ± 0.4, and +6.1 ± 0.6.

The third group is represented by only one crystal that gave an age of 3295 ± 18 Ma (grain #6; Fig. S4). This crystal has very reproducible initial Hf isotopic compositions (Table 3) that, when calculated at 3295, give a weighted average of 0.280752 ± 0.000010 which is equivalent to an ε_{Hf} of +3.7 ± 0.4.

The fourth group exhibits ages of 3170 ± 32 and 3179 ± 11 Ma that have been obtained in oscillatory-zoned outer margins of two different crystals. The corresponding initial $^{176}Hf/^{177}Hf$ are 0.280756 ± 0.000013 and 0.280822 ± 0.000011, which gives ε_{Hf} of +0.8 ± 0.5 and +3.4 ± 0.4, respectively (Table 4).

The fifth group corresponds to an age of 3101 ± 25 Ma that was obtained from two analyses done in one very elongated zircon (Fig. S5). Initial Hf isotopic signature

for this zircon is 0.280739 ± 0.000021, which is equivalent to an ε_{Hf} of -1.4 ± 0.7 (Table 4).

The calculated lower-intercept ages for the identified Discordia lines, different from ~0 Ma, form two groups with one ranging from 542 ± 160 to 749 ± 90 Ma and another poorly constrained one from 969 ± 770 to 1792 ± 640 Ma, which is due to the limitedly discordant data that define the Discordia lines. The accuracy of the latter group is debatable. However, the first group exhibit ages very compatible with that observed for the granitic gneiss (Fig. 6C) and that comply well with known Pan-African metamorphic events that occurred in southern India (e.g., Bhaskar Rao et al., 1992; Miller et al., 1996).

We interpret the trondhjemitic gneiss (13DC13) to have been emplaced at 3178 ± 10 Ma, which is the average age of the fourth group, because it corresponds to the age of oscillatory zoned outer margins. Older ages, which are for the most part located in identifiable xenocrystic cores are interpreted as inherited. The age of the fifth group is assumed to be metamorphic because of the internal texture of the crystal and its high Th/U of ~1.2, which is often seen in zircons that formed during high-temperature metamorphism (e.g., Vavra et al., 1999; Möller et al., 2003). This is consistent with the finding of Jayananda et al. (2015) that titanite recovered from neighboring 3200 Ma Halekote-type trondhjemite exhibit ages ranging from 3217 to 3091 Ma, and that these authors interpreted as marking a ca. 3100 Ma metamorphic event in the area around the HSB. We note that the estimated age of crystallization for the trondhjemitic gneiss is close to that of the Chikmagalur granite, which crops out south from the Bababudan belt (Fig. 1; Jayananda et al., 2015), and to that of diapiric trondhjemites observed in the Holenarsipur Schist Belt (Figs. 1 and 2; Jayananda et al., 2015). The inherited zircon ages of 3295, 3342-3359, and 3414 Ma match well with, respectively, a 3298 ± 7 Ma

volcanic flow identified within the HSB by Peucat et al., (1995), the 3342 ± 6 Ma Hassan-Gorur gneiss studied by Beckinsale et al., (1980), Bhaskar Rao et al., (2008), and Jayananda et al. (2015), and the 3410.8 ± 3.6 Ma granitic gneiss (13DC12) from this study. Further, the ε_{Hf} of +4 to +7 determined by Bhaskar Rao et al. (2008) for a 3346 ± 10 Ma Gorur gneiss match very well with the values of +3.7 to +6.1 obtained for inherited zircons of the second group, which gave ages of 3342 to 3359 Ma. However, the ε_{Hf} signature of the granitic gneiss (13DC12), +2.2 ± 0.6, differs significantly from that of the 3414-Ma zircon (i.e., +10.4 ± 0.6) which indicates that although coeval, they did not record the same event. Finally, the trondhjemitic gneiss zircons dated at 3456-3468 Ma do not correspond to any known lithology in the WDC, although such old zircons have been found as detrital crystals (e.g., Nutman et al., 1992; Sarma et al., 2012; Lancaster et al., 2015; Maibam et al., 2016). These oldest detrital zircons exhibit less radiogenic Hf isotope signatures than the inherited ones studied herein.

The trondhjemitic gneiss (13DC13) is petrographically similar to the Halekote trondhjemites and Chikmagalur granite, which also contain primary muscovite according to descriptions provided in Jayananda et al. (2015). Given all these similarities, as well as the fact that the trondhjemitic gneiss has been sampled in a zone of low strain resembling the central part of a diapir (Fig. 2; Bouhallier et al., 1993), we propose that it is related to the diapiric trondhjemites of the WDC, which are known to contain enclaves of older rocks (e.g., Naqvi and Rogers, 1987; Meen et al., 1992; Jayananda et al., 2015), such as the Bt-rich enclave (13DC15) which itself contains older zircons. Stroh et al. (1983) interpreted these diapiric granitoids as markers of WDC stabilization through removal of heat-producing radioactive elements from the lower crust by reworking. This interpretation is supported by data recently presented in

644 Jayananda et al. (2015), who also concluded that the dome-and-basin structure of the
645 WDC had been acquired during the emplacement of these trondhjemites ~3200 My ago.
646 This process of stabilization of Archean continental crust has also been suggested for
647 other cratons (e.g., Schoene et al., 2008). When evolutionary paths for felsic and mafic
648 lithologies are taken into account (see Fig. 9), the ε_{Hf} signatures of the trondhjemitic
649 gneiss 13DC13, represented by the fourth group (+0.8 ± 0.5 and +3.4 ± 0.4 at 3178 Ma;
650 Table 4) can be accounted for by the reworking of various crustal lithologies
651 represented by inherited zircons older than 3200 Ma within 13DC13. Therefore, this Hf
652 isotope variability could be indicative of isotopic heterogeneity within the magma
653 parental to 13DC13 which originated from distinct crustal sources involved during
654 anatexis and/or acquired through interactions with various crustal lithologies. However,
655 we cannot rule out some mixing between unrelated domains because the two analyzed
656 crystals both contained two zones with slightly different Hf isotope signatures (Fig. 6
657 and S5). According to the $^{176}Hf/^{177}Hf$ of the corresponding domains (Tables 4 and S6),
658 the ε_{Hf} values mentioned above (i.e., +0.8 and +3.4) could be interpreted as,
659 respectively, minimum and maximum values for the fourth group. Nevertheless,
660 whether or not this heterogeneity is real or analytical is not important for the rest of the
661 discussion. Yet, we note that the Hf isotopic signatures of 13DC13 cognate zircons
662 match very well with those of coeval zircons from all detrital zircon datasets for the
663 WDC (Fig. 9).

664 The first group (3414-3468 Ma) has ε_{Hf} signatures more radiogenic than coeval
665 zircons from the detrital record (Fig. 9) implying that either the original host-rocks of
666 zircons from the first group were rare or they were not available for sampling at the
667 surface at the time of sedimentation. These high values (+6 to +10) imply that a strongly
668 depleted mantle source was tapped during the formation of the magma parental to

669 zircons from the first group. Such highly depleted source is rare in the Archean and
670 mostly limited to boninites and komatiites (e.g., Hoffmann et al., 2010; Nebel et al.,
671 2014; Hoffmann and Wilson, 2017).
672
673 **6.2.3. Biotite-rich enclave (13DC15)**
674 The two zircon crystals recovered from this sample show remarkably simple Lu-Hf
675 isotope systematics between the two analyses performed in each zircon (Fig. 8).
676 However, the first zircon (13DC15_1) exhibit a significant variation in age in spite of
677 consistent initial Hf isotopic compositions (Fig 8). This consistency likely indicates that
678 U-Pb systematics have been disturbed at some point in this zircon's evolution. This is
679 also consistent with the fact that oldest zircon $^{207}Pb/^{206}Pb$ age is associated with a Th/U
680 value that falls within the common magmatic range whereas the youngest age (i.e., 2973
681 Ma; Table 3) is associated with a Th/U <0.2 that can be interpreted as resulting from
682 metamorphism. The oldest age determined for 13DC15_1 is not strictly concordant and,
683 therefore, we have fitted a Discordia line through the two U-Pb analyses, which gave
684 upper- and lower-intercept ages of 3499 ± 29 and 1719 ± 190 Ma, respectively (Fig.
685 S6). Note that the upper-intercept age overlaps within uncertainty with the oldest
686 $^{207}Pb/^{206}Pb$ age determined for this zircon (13DC15_1). U-Pb ages are very consistent
687 in the second crystal which gives a combined crystallization age of 3607 ± 16 Ma (Fig.
688 S6)
689 Average initial $^{176}Hf/^{177}Hf$ for the two zircons analyzed (i.e., 13DC15_1 and
690 13DC15_2) are 0.280476 ± 0.000011 and 0.280374 ± 0.000014, respectively, which
691 correspond to ε_{Hf} values of -1.3 ± 0.4 and -2.3 ± 0.5 at 3499 and 3607 Ma, respectively
692 (Table 4).

The zircons from the biotite-rich enclave exhibit not only ages >3400 Ma but, contrary to zircons from other samples studied herein, negative initial ε_{Hf} that, hence, suggest that the magmas parental to these zircons originated from, or were buffered by, crustal lithologies with long crustal residence times. Using an arc-mantle source (see *section 5.1.1*) and assuming that the precursor can be either felsic ($^{176}Lu/^{177}Hf = 0.004$) or mafic ($^{176}Lu/^{177}Hf = 0.022$), calculated two-stage model ages (e.g., Blichert-Toft and Albarède, 2008; Hawkesworth et al., 2010) are 3684 and 3891 Ma for zircon #1, and 3821 and 4060 Ma for zircon #2. If instead we use a depleted mantle source (see *section 5.1.1*), the model ages become 3713 and 3937 Ma for zircon #1, and 3846 and 4094 Ma for zircon #2. Finally, using BSE composition from Iizuka et al. (2015) for the mantle source of the precursors we obtain ages of 3558 and 3649 Ma for zircon #1, and 3715 and 3880 Ma for zircon #2. These model ages are too variable and rely on too unconstrained assumptions to be interpreted as are but nevertheless illustrate the fact that very old crust, up to 4000 Ma, could have been involved in the formation of the magma parental to 13DC15 zircons.

6.3. Early formation of the Western Dharwar Craton

Our new results, though limited, bring important constraints that can be used in combination with previous studies to discuss the early formation of the WDC in terms of sources involved. We can further compare these latter to the latest models for WDC formation (e.g., Jayananda et al., 2008, 2015; Lancaster et al., 2015) to speculate on the geological setting of WDC early formation. Figure 9 presents our results in the context of detrital zircon datasets available for the WDC and that have been used to depict the big-picture evolution of the WDC (i.e., Sarma et al., 2012; Lancaster et al., 2015; Maibam et al., 2016). Figure 9 also includes the age range for Sargur-group komatiites

718 (Jayananda et al., 2008) and U-Pb ages alongside ε_{Hf} for Gorur gneiss from Bhaskar
719 Rao et al., (2008). It can be seen that all zircons analyzed in this study have detrital
720 equivalents, except for the most radiogenic zircons from 13DC13's first group (3414-
721 3468 Ma; Fig. 9). Although essentially consistent, slight differences can be observed
722 between the ages and ε_{Hf} displayed in the detrital records of Figure 9, which likely arise
723 from distinct catchment basins and possibly the number of analyses. The early
724 formation of the WDC can be divided into three time-periods: (1) pre-3400 Ma, (2)
725 3400-3200 Ma, (3) post-3200 Ma.

726 Zircons older than 3400 Ma exhibit large variations in ε_{Hf} signatures (Fig. 9)
727 testifying to various sources which likely points to different contexts of formation for
728 their parental granitoids. These sources are mantle domains with ancient depletion
729 history, mantle domains with moderately depleted signatures that are equivalent to
730 those observed in WDC granitoids formed during the second period, and enriched crusts
731 of possibly old ages (up to 4000 Ma). Most zircons that testify to this period are
732 inherited crystals in the 3178 Ma trondhjemitic gneiss (13DC13) and detrital zircons
733 from the Sargur-group, which have deposition ages estimated between 3100 and 3300
734 Ma. The role of the source to these zircons parental granitoids is discussed later on.

735 In the time-span 3400-3200 Ma, all detrital zircon records show positive ε_{Hf}
736 varying within the same restricted range, except for zircons from the Sargur Schist Belt
737 (Lancaster et al., 2015) which, nevertheless, also show a restricted range but around
738 chondritic values. This indicates that during this time-period, granitoids were sourced
739 in a common mantle domain that had mildly-depleted to near-chondritic Hf isotopic
740 compositions, with limited or no continental influence, similar to global data for TTGs
741 presented by Guitreau et al. (2012). In Figures 9B and 9D, an enhanced variability of
742 ε_{Hf} is visible around 3250-3200 Ma and is associated with a shift towards negative

743 values that can be seen in Figures 9C and 9D. Moreover, the ~3220 Ma granitic clast
744 analyzed in Maibam et al. (2016) contains pre-3400 Ma zircons that have ε_{Hf} similar to
745 that of the granitic sample (13DC12) from this study (Fig. 9D). These features can be
746 accounted for by reworking of WDC's oldest lithologies, buffering of newly formed
747 magmas by older lithologies, and/or a continental influence similar to what can be seen
748 in Svecofennian provinces of northern Sweden (e.g., Öhlander et al., 1993), the
749 Kohistan-Ladakh arc (e.g., Bouilhol et al., 2013), and the Sunda-Banda arc (e.g., Elburg
750 et al., 2005; Herrington et al., 2011), for example.

751 After ~3200 Ma, all datasets, but that for Bababudan-group sediments for which
752 there is no data younger than 3200 Ma (Lancaster et al., 2015), exhibit a drift of ε_{Hf}
753 towards increasingly negative values as age decreases. The deposition age of the
754 sediments from which detrital zircons were recovered are not well constrained, except
755 for the Gadag Greenstone Belt (Sarma et al., 2012). Sargur-group sediments are
756 assumed to have been deposited between ~3300 and ~3100 Ma depending on their
757 location within the WDC and the way the sedimentation age was estimated (e.g.,
758 Nutman et al. ,1992; Ramakrishnan et al., 1994; Peucat et al., 1995; Sarma et al., 2012;
759 Hokada et al., 2013). When minimum deposition ages are taken into account (Fig. 9),
760 the major part of the drifts in ε_{Hf} through time appear artificial for datasets related to
761 Sargur-group sediments because most ages are younger than that of deposition and are
762 most likely related to ancient U-Pb disturbance and/or recrystallization as noted by
763 Lancaster et al. (2015). It is interesting to note that datasets from Lancaster et al. (2015)
764 and Maibam et al. (2016) contain zircons with ages and ε_{Hf} that comply well with the
765 fifth group of the trondhjemitic gneiss (13DC13) and that we interpreted as
766 metamorphic (Figs. 9C and 9D). This example illustrates the fact that detrital zircons
767 are very powerful at unveiling big-picture information about the continental crust

768 formation and evolution but they can also provide ambiguous information because
769 evolution patterns of crustal segments (e.g., Zeh et al., 2011; Laurent and Zeh, 2015)
770 and artificial trends resulting from ancient Pb-loss look the same in ε_{Hf} versus age
771 diagrams, as already pointed out elsewhere (e.g., Amelin et al., 2000; Guitreau and
772 Blichert-Toft, 2014; Payne et al., 2016). As a consequence, we have not considered
773 detrital zircon data for ages younger than 3100 Ma. Yet, the drift observed in Sarma et
774 al. (2012) dataset is real and is also visible with data from the Eastern Dharwar craton
775 (e.g., Maibam et al., 2016). This indicates that after ~3200 Ma, the WDC magmatic
776 events dominantly involved crust reworking processes and/or buffering of magmas by
777 dominant lithologies, not unlike what was proposed by Laurent and Zeh (2015) for the
778 Pietersburg block. This is consistent with conclusions of Bhushan and Sahoo (2010)
779 and Maibam et al. (2011) that stable continental crust was formed in the WDC prior to
780 3 Ga. Further, Taylor et al. (1984) and Jayananda et al. (2015) concluded from major
781 and trace elements, as well as Sr, Pb, and Nd isotopes that granitoids younger than 3200
782 Ma contained a pre-existing crust component.

783 Sargur-group komatiites have long been considered as the oldest units of the
784 WDC (e.g., Naqvi, 1983) until the discovery of detrital zircons as old as 3600 Ma by
785 Nutman et al. (1992). The best age estimate for these komatiites is 3352 ± 110 Ma
786 (Jayananda et al., 2008), which is, hence, not precise enough to conclude on the actual
787 role of these ultramafic rocks in the early development of the WDC. Nevertheless,
788 Naqvi et al. (1983) and Jayananda et al. (2008) noted that some of the oldest identifiable
789 generations of peninsular gneisses intruded into the surrounding greenstones of the
790 HSB, hence, indicating that most of the peninsular gneisses are younger than Sargur-
791 group komatiites. Jayananda et al. (2008, 2016) concluded from elemental and isotopic
792 geochemistry that Sargur-group komatiites formed remote from continental crust.

793 Therefore, these authors proposed that komatiites of the Sargur group formed in an
794 oceanic-plateau-like environment and were accreted to a continental nucleus that
795 contained lithologies represented by the >3400 Ma detrital zircons (e.g., Kunugiza et
796 al., 1996; Jayananda et al., 2008). This scenario is not unlike what was proposed for
797 other Precambrian terranes (e.g., Boher et al., 1992; Puchtel et al., 1999; Rey et al.,
798 2003; Guitreau et al., 2012; Martin et al., 2014), and it is consistent with our
799 observations for the WDC. Recently, Baes et al. (2016) illustrated using numerical
800 modeling that the fact that the emplacement of a mantle plume in the lithosphere could
801 initiate subduction. We propose a similar scenario whereby the emplacement of an
802 oceanic plateau, comprising the Sargur-group komatiites, initiated subduction beneath
803 it that resulted in the generation of the oldest peninsular gneisses. We further propose
804 that this subduction acted as a "conveyor belt" that induced the accretion to this oceanic
805 plateau of oceanic arcs, smaller oceanic plateaus and crustal segments much like it has
806 been proposed for North America (e.g., Hoffman, 1988; Whitmeyer and Karlstrom,
807 2007), the Svecofennian Orogen (e.g., Weihed et al., 2005; Guitreau et al., 2014) and
808 the Kohistan-Ladakh arc (e.g., Bouilhol et al., 2013). The accretion to the oceanic
809 plateau of several oceanic arcs and smaller oceanic plateaus would account for the
810 various unrelated chemical and isotopic signatures of peninsular gneisses found
811 throughout the WDC (e.g., Bhaskar Rao et al., 1983; Monrad, 1983; Naqvi et al., 2009;
812 Jayananda et al., 2015). Further, this scenario can account for the low- and high-
813 pressure sources for peninsular gneisses identified by Jayananda et al. (2015) because
814 the size and buoyancy of these mafic-ultramafic segments can control the modality of
815 subduction (i.e., fast or low; shallow or steep). Accretion of oceanic arcs and oceanic
816 plateaus could also account for the short-crustal residence time of sources to peninsular
817 gneisses, as interpreted by Bhaskar Rao et al. (1991), Jayananda et al. (2015), and as

818 concluded for sample 13DC12 (this study). We surmise that accretion of oceanic arcs
819 could induce crustal reworking which would be consistent with the fact that some of
820 the oldest granitoids of the WDC have peraluminous characteristics despite Nd and Hf
821 isotope signatures similar to mildly depleted mantle sources (Jayananda et al., 2015;
822 this study). If we interpret the granitic gneiss 13DC12 as the reworking product of
823 oceanic arc granitoids during accretion to an oceanic plateau represented by Sargur-
824 group komatiites, then, the sample 13DC12 gives a minimum age of 3410 Ma for this
825 oceanic plateau and the initiation of the WDC growth. The role of ancient crust
826 represented by 3500-3600 Ma zircons is hard to understand and needs further
827 investigation. However, it appears from Figure 9 that such ancient crust did not
828 influence the ε_{Hf} signatures of granitoids in the catchment basins of sediments from
829 Bababudan, Chitradurga, and Gadag Schist belt before ~3200 Ma. In contrast,
830 sediments in the Sargur Schist Belt had a distinct catchment basin as testified to by the
831 ε_{Hf} of detrital zircons in Figure 9C. The granitoids parental to these latter zircons appear
832 to have been possibly influenced by 3500-3600 Ma crust, as represented by zircons
833 from 13DC15, earlier than 3200 Ma. Further, the granitoids parental to these latter
834 could have been part of the catchment basin of Sargur Schist Belt sediments. However,
835 the large uncertainty on detrital zircon ages in Figure 9C, prevents accurate conclusions
836 to be drawn. Nevertheless, we see the absence of influence of the ancient crust,
837 represented by zircons from 13DC15, in the ε_{Hf} signatures of most of detrital zircons
838 from the WDC (Fig. 9) as an argument in favor of the absence of this ancient crust in
839 the vicinity of the HSB prior to ~3200 Ma. We suggest that a large crustal block
840 containing 3500-3600 Ma zircons was accreted to the WDC around 3200 Ma, which
841 initiated the stabilization of, at least, portions of the WDC (e.g., HSB) and the buffering
842 of newly formed magmas by dominant enriched lithologies represented by 3400-3200

843 Ma peninsular gneisses and 3600-3400 Ma granitoids (Fig. 9). This event marked a
844 change in the growth style of the WDC that is substantiated by the drift of detrital
845 zircons ε_{Hf} values (Fig. 9) which could correspond, at least in part, to hidden crustal
846 growth (see Laurent and Zeh, 2015; Payne et al., 2016; Couzinié et al., 2016). Remnants
847 of this crustal block, which is intrinsic to the WDC record, may be in the vicinity of the
848 HSB but more likely around the Sargur Schist Belt.

849 In order to reconstruct the detailed tectono-magmatic history of the WDC and
850 test models for its geological setting, future work will have to focus on documenting
851 ages and signatures of peninsular gneisses in greater details, as well as understanding
852 their stratigraphic relationships and spatial distribution. One important aspect to target
853 is the role of the ancient crust identified herein. Doing so will help refine the above-
854 explained scenario and its local variations that can account for differences in Hf isotopic
855 signatures exhibited by the various detrital zircon records shown in Figure 9. Finally,
856 the same work will have to be conducted in supracrustal belts in order to clarify their
857 origin and relationships with peninsular gneisses.

858

859 **7. Conclusions**

860 We have studied the petrography of a Western Dharwar Craton granitic gneiss and
861 trondhjemitic gneiss, as well as a Bt-rich enclave within the latter, and measured their
862 zircon U-Pb ages and Lu-Hf isotope systematics to shed new light on crustal formation
863 processes during the early formation of the WDC. Our study reveals that crust older
864 than the oldest known granitoid of the WDC (3342-Ma Hassan-Gorur gneiss;
865 Beckinsale et al., 1980; Jayananda et al., 2015), which was known from the detrital
866 zircon record (e.g., Nutman et al., 1992), is also present in the igneous record in the
867 form of a 3410.8 ± 3.6 Ma granitic gneiss and inherited zircons, with ages up to 3607

± 16 Ma, in a 3178 Ma trondhjemitic gneiss and a mica-rich enclave found within this trondhjemite. Hf isotopic signatures indicate short-crustal residence time for the precursor to the granitoids parental to analyzed zircons, except for the oldest ones that could have been sourced from Eoarchean-Hadean precursor(s).

Our results compared with similar data for detrital zircons from four locations throughout the WDC allow three time periods to be distinguished. The first one is pre-3400 Ma and exhibit multiple zircon ε_{Hf} signatures (very depleted to slightly enriched; ε_{Hf} of +10.4 to -2.3) testifying to the involvement of several distinct sources in the formation of pre-3400 Ma units. The second period is from 3400 to 3200 Ma and corresponding zircons display either mildly-depleted or near-chondritic Hf isotopic signatures, depending on the sampling location of sediments, that vary within a restricted range throughout this period. This indicates involvement of a common juvenile source with limited or no continental influence until ~3200 Ma, when the third period started. This latter is characterized by dominant crust reworking or buffering of newly formed granitoids by pre-existing ones, which translates into a drift of ε_{Hf} signatures towards increasingly negative values. We propose a scenario updated from that of Jayananda et al. (2008) for the early formation of the WDC in which the arrival of a mantle plume in the upper-mantle gave rise to an oceanic plateau that contained Sargur-group komatiites. The formation of this oceanic plateau triggered subduction on its egdes in a way similar to that described in models from Baes et al. (2016). The subducted oceanic-like crust acted as a conveyor belt that dragged crustal blocks in the vicinity of the oceanic plateau which included short-lived oceanic arcs and small oceanic plateaus which ultimately contributed to the growth of the WDC. We suggest that this subduction started at least 3410 My ago and lasted until at least 3200 Ma when a continental block containing the granitoids parental to the >3410 Ma zircons got

accreted to the WDC, hence, inducing its stabilization. The WDC further grew and evolved but newly formed granitoids were buffered by, or sourced in, dominant lithologies of the WDC.

Acknowledgements:

We thank Steve Mozjsis and the CRiO group for help with zircon separation, Nancy Cherim and Mark Townley for help with CL image acquisition, Julia G. Bryce and Maria F. Fahnestock for technical help at UNH. Jean-Louis Paquette and Abdel-Mouhcine Gannoun are thanked for assistance with analyses at the Laboratoire Magmas et Volcans. We are grateful to Claire Fonquernie and Mhammed Benbakkar for rock crushing and major-oxide analyses at Laboratoire Magmas et Volcans. Discussions with Hervé Martin helped improve the present manuscript. Martin Guitreau acknowledges financial support from Matthias Willbold through NERC grant R117299 and the Région Auvergne through the Auvergne Fellowship program. This is a Laboratory of Excellence ClerVolc contribution. The University of New Hampshire supported this research project through start-up funds granted to Dr. Samuel B. Mukasa. Last but not least, we would like to thank Randall Parrish for efficient editorial handling as well as Tsuyoshi Iizuka, Sukanta Dey, and an anonymous reviewer for insightful comments that helped improve this manuscript.

References

Abbey, S., 1983. Studies in "Standard Samples" of Silicate Rocks and Minerals 1969-1982. Canadian Geological Survey Paper 83-15, p. 114.

916 Amelin, Y., Lee, D.-C., Halliday, A.N., 2000. Early–middle archaean crustal evolution
917 deduced from Lu–Hf and U–Pb isotopic studies of single zircon grains.
918 Geochimica et Cosmochima Acta 64, 4205–4225.
919 Arndt, N.T., Goldstein, S.L., 1987. Use and abuse of crust-formation ages. Geology 15,
920 893-895.
921 Baes, M., Gerya, T., Sobolev, S.V., 2016. 3-D thermos-mechanical modeling of plume-
922 induced subduction initiation. Earth and Planetary Science Letters 453, 193-
923 203.
924 Barbarin, B., 1999. A review of the relationships between granitoid types, their origins
925 and their geodynamic environments. Lithos 46, 605-626.
926 Barker, F., 1979. Trondhjemites: definition, environment and hypotheses of origin. In:
927 Barker, F. Ed.**.**, Trondhjemites, Dacites and Related Rocks. Elsevier,
928 Amsterdam, pp. 1–12.
929 Beckinsale, R.D., Drury, S.A., Holt, R.W., 1980. 3300-Myr old gneisses from the South
930 Indian Craton. Nature 283, 469–470.
931 Bhaskar Rao, Y.J., Beck, W., Murthy, V.R., Charan, S,N., Naqvi, S.M., 1983. Geology,
932 geochemistry and age of metamorphism of Archaean grey gneisses around
933 Channarayapatna Hassan district, Karmataka, South India. Geological Society
934 of India Memoirs 4, 309–328.
935 Bhaskar Rao, Y.J., Naha, K., Srinivasan, R., Gopalan, K., 1991. Geology, geochemistry
936 and geochronology of the Archaean Peninsular Gneiss around Gorur, Hassan
937 District, Karnataka, India. Proceedings of the Indian Academy of Science 100,
938 399-412.
939 Bhaskar Rao, Y.J., Sivaraman, T.V., Pantulu, G.V.C., Gopalan, K., Naqvi, S.M., 1992.
940 Rb–Sr ages of late Archean metavolcanics and granites, Dharwar craton, South

941 India and evidence for Early Proterozoic thermotectonic event. Precambrian
942 Research 59, 145–170.
943 Bhaskar Rao, Y.J., Griffin, W.L., Ketchum, J., Pearson, N.J., Beyer, E., O'Reilly, S.Y.,
944 2008. An outline of juvenile crust formation and recycling history in the
945 Archaean Western Dharwar craton, from zircon in situ U-Pb dating and Hf-
946 isotopic compositions. Goldschmidt conference abstracts p.81.
947 Blichert-Toft, J., 2008. The Hf isotopic composition of zircon reference material 91500.
948 Chemical Geology 253, 252-257.
949 Blichert-Toft, J., Albarède, F., 2008. Hafnium isotopes in Jack Hills zircons and the
950 formation of the Hadean crust. Earth and Planetary Science Letters 265, 686-
951 702.
952 Bhushan, S.K., Sahoo, P., 2010. Geochemistry of clastic sediments from Sargur
953 supracrustals and Bababudan group, Karnataka: Implications on Archaean
954 Proterozoic boundary. Journal of the Geological Society of India 75, 829-840.
955 Boher, M., Abouchami, W., Michard, A., Albarede, F., Arndt, N.T., 1992. Crustal
956 growth in West-Africa at 2.1 Ga. Journal of Geophysical Research 97, 345–369.
957 Bouhallier, H., Choukroune, P., Ballèvre, M., 1993. Diapirism, bulk homogeneous
958 shortening and transcurrent shearing in the Archaean Dharwar craton: The
959 Holenarsipur area, southern India. Precambrian Research 63, 43-58.
960 Bouhallier, H., Chardon, D., Choukroune, P., 1995. Strain patterns in Archaean dome-
961 and-basin structures: The Dharwar craton (Karnataka, South India). Earth and
962 Planetary Science Letters, 135, 57-75.
963 Bouilhol, P., Jagoutz, O., Hanchar, J.M., Dudas, F.O., 2013. Dating the India-Eurasia
964 collision through arc magmatic records. Earth and Planetary Science Letters
965 366, 163-175.

966 Chadwick, B., Ramakrishnan, M., Vasudev, V.N., Viswanatha, M.N., 1989. Facies
967 distribution and structure of a Dharwar volcano-sedimentary basin: Evidence
968 for late Archaean transpression in south India. Journal of the Geological Society
969 of London 146, 825-834.
970 Chadwick, B., Vasudev, V.N., Hedge, G.V., 2000. The Dharwar craton, southern India,
971 interpreted as the result of Late Archaean oblique convergence. Precambrian
972 Research 99, 91-111.
973 Chardon, D., Choukroune, P., Jayananda, M., 1996. Strain patterns, décollement and
974 incipient sagducted greenstone terrains in the Archaean Dharwar craton (south
975 India). Journal of structural geology 18, 991-1004.
976 Chardon, D., Choukroune, P., Jayananda, M., 1998. Sinking of the Dharwar Basin
977 (South India): implications for Archaean tectonics. Precambrian Research 91,
978 15-39.
979 Chardon, D., Jayananda, M., Chetty, T.R.L., Peucat, J.-J., 2008. Precambrian
980 continental strain and shear zone patterns; South Indian case. Journal of
981 Geophysical Research 113, 1-16.
982 Chauvel, C., Blichert-Toft, J., 2001. A hafnium isotope and trace element perspective
983 on melting of the depleted mantle. Earth and Planetary Science Letters 190,
984 137–151.
985 Chu, N., Taylor, R.N., Chavagnac, V., Nesbitt, R.W., Boella, R.M., Milton, J.A.,
986 German, C.R., Bayon, G., Burton, K., 2002. Hf isotope ratio analysis using
987 multi-collector inductively coupled plasma mass spectrometry: an evaluation of
988 isobaric interference corrections. Journal of Analytical Atomic Spectrometry
989 17, 1567–1574.

990 Couzinié, S., Laurent, O., Moyen, J.-F., Zeh, A., Bouilhol, Villaros, A., 2016. Post-
991 collisional magmatism: crustal growth not identified by zircon Hf-O isotopes.
992 Earth and Planetary Science Letters 456, 182-195.
993 Dey, S., 2013. Evolution of the Archaean crust in the Dharwar craton: The Nd isotope
994 record. Precambrian Research 227, 227-246.
995 Dhuime, B., Hawkesworth, C., Cawood, P.A., 2011. When continents formed, Science
996 331, 154-155.
997 Elburg, M.A., Foden, J.D., van Bergen, M.J., Zulkarnain, I., 2005. Australia and
998 Indonesia in collision: geochemical sources of magmatism. Journal of
999 Volcanology and Geothermal Research 140, 25–47.
1000 Fisher, C.M., Longerich, H.P., Jackson, S.E., Hanchar, J.M., 2010. Data acquisition and
1001 calculation of U-Pb isotopic analyses using laser ablation (single collector)
1002 inductively coupled plasma mass spectrometry. Journal of Analytical Atomic
1003 Spectrometry 25, 1905-1920.
1004 Fisher, C.M., Vervoort, J.D., Hanchar, J.M., 2014a. Guidelines for reporting zircon Hf
1005 isotopic data by LA-MC-ICP-MS and potential pitfalls in the interpretation of
1006 these data. Chemical Geology 363, 125–133.
1007 Fisher, C.M., Vervoort, J.D., DuFrane, S.A., 2014b. Accurate Hf isotope
1008 determinations of complex zircons using the “laser ablation split stream”
1009 method. Geochemistry Geophysics Geosystem 15, 121-139.
1010 Flanagan, F.J., 1976, Descriptions and Analysis of Eight New USGS Rock Standards,
1011 U.S. Geological Survey Professional Paper 840, p. 192.
1012 Gerdes, A., Zeh, A., 2009. Zircon formation versus zircon alteration – New insights
1013 from combined U-Pb and Lu-Hf in-situ LA-ICP-MS analyses, and

consequences for the interpretation of Archean zircon from the Central Zone of the Limpopo Belt. Chemical Geology 261, 230-243.

Ghosh, J.G., de Wit, M., Zartman, R.E., 2004. Age and tectonic evolution of Neoproterozoic ductile shear zone in the Southern Granulite Terrain of India, with implications for Gondwana studies. Tectonics 23, 1-38.

Govindaraju, K., 1994, 1994 Compilation of Working Values and Descriptions for 383 Geostandards, Geostandards Newsletter, 18:1-158.

Griffin, W.L., Belousova, E.A., Shee, S.R., Pearson, N.J., O'Reilly, S.Y., 2004. Archean crustal evolution in the northern Yilgarn Craton: U-Pb and Hf-isotope evidence from detrital zircons. Precambrian Research 131, 231-282.

Guitreau, M., Blichert-Toft, J., 2014. Implications of discordant U-Pb ages on Hf isotope studies of detrital zircons. Chemical Geology 385, 17-25.

Guitreau, M., Blichert-Toft, J.,Martin, H.,Mojzsis, S.J., Albarède, F., 2012. Hafnium isotope evidence from Archean granitic rocks for deep mantle origin of continental crust. Earth and Planetary Science Letters 337–338, 211–223.

Guitreau, M., Blichert-Toft, J., Billström, K., 2014. Hafnium isotope evidence for early-Proterozoic volcanic arc reworking in the Skellefte district (northern Sweden) and implications for the Svecofennian orogeny. Precambrian Research 252, 39-52.

Hawkesworth, C., Dhuime, B., Pietranik, A., Cawood, P., Kemp, T., and Storey, C., 2010, The generation and evolution of the continental crust: Journal of the Geological Society 167, 229–248.

Herrington, R.J., Scotney, P.M., Roberts, S., Boyce, A.J., Harrison, D., 2011. Temporal association of arc–continent collision, progressive magma contamination in arc

volcanism and formation of gold-rich massive sulphide deposits on Wetar Island (Banda arc). Gondwana Research 19, 583–593.

Hokada, T., Horie, K., Satish-Kumar, M., Ueno, Y., Nasheeth, A., Mishima, K., Shiraishi, K., 2013. An appraisal of Archaean supracrustal sequences in Chitradurga Schist Belt, western Dharwar craton, southern India. Precambrian Research 227, 99–119.

Hoffman, P., 1988. United Plates of America, the birth of a craton: early Proterozoicassembly and growth of Laurentia. Annual Reviews in Earth and Planetary Science. 16, 543–603.

Hoffmann, J.E., Münker, C., Polat, A., König, S., Mezger, K., Rosing, M.T., 2010. Highly depleted Hadean mantle reservoirs in the sources of early Archean arc-like rocks, Isua supracrustal belt, southern West Greenland. Geochimica et Cosmochimica Acta 74, 7236-7260.

Hoffmann, J.E., Wilson, A.H., 2017. The origin of highly radiogenic Hf isotope compositions in 3.33 Ga Commondale komatiite lavas (South Africa). Chemical Geology 455, 6-21.

Ickert, R., 2013. Algorithms for estimating uncertainties in initial radiogenic isotope ratios and model ages. Chemical Geology 340, 131–188.

Iizuka, T., Campbell, I.H., Allen, C.M.,Gill, J.B.,Maruyama, S.,Makoka, F., 2013. Evolution of the African continental crust as recorded by U–Pb, Lu–Hf and O isotopes in detrital zircons from modern rivers. Geochimica et Cosmochimica Acta 107, 96–120.

Iizuka, T., Yamaguchi, T., Hibiya, Y., Amelin, Y., 2015. Meteorite zircon constraints on the bulk Lu-Hf isotope composition and early differentiation of the Earth. Proceedings of the National Academy of Science 112, 5331-5336.

1063 Ishwar-Kumar, C., Windley, B.F., Horie, K., Kato, T., Hokada, T., Itaya, T., Yagi, K.,
1064 Gouzu, C., Sajeev, K., 2013. A Rodinian suture in western India: New insights
1065 on India-Madagascar correlations. Precambrian Research 236, 227-251.
1066 Jaffey, A.H., Flynn, K.F., Glendenin, L.E., Bentley, W.C., Essling, A.M., 1971.
1067 Precision measurement of half-lives and specific activities of 235U and 238U.
1068 Physical Reviews C 4, 1889.
1069 Janardhan, A.S., Srikantappa, C., Ramachandra, H.M., 1978. The Sargur schist
1070 complex – An Archaean high-grade terrane in southern India. In: B.F.
1071 Windleyand S.M. Naqvi (Eds.) Archaean Geochemistry, Elsevier, Amsterdam,
1072 pp. 127-149.
1073 Janardhan, A.S., Newton, R.C., Hansen, E.C., 1982. The transformation of amphibolite
1074 facies gneiss to charnockite in southern Karnataka and northern Tamil Nadu,
1075 India. Contributions to Mineralogy and Petrology 79, 130-149.
1076 Jayananda, M., Kano, T., Peucat, J.-J., Channabasappa, S., 2008. 3.35 Ga komatiite vol-
1077 canism in the western Dharwar craton: constraints from Nd isotopes and
1078 wholerock geochemistry. Precambrian Research 162, 160–179.
1079 Jayananda, M., Tsutsumi Y., Miyazaki, T., Gireesh, R.V., Kapfo, K.-u., Tushipokla,
1080 Hidaka, H., Kano, T., 2013. Geochronological constraints on Meso- and
1081 Neoarchean regional metamorphism and magmatism in the Dharwar craton,
1082 southern India. Journal of Asian Earth Sciences 78, 18-38.
1083 Jayananda, M., Chardon, D., Peucat, J.-J., Tushipokla, Fanning, C.M., 2015. Paleo- to
1084 Mesoarchean TTG accretion and continental growth in the western Dharwar
1085 craton, Southern India: Constraints from SHRIMP U-Pb zircon geochronology,
1086 whole-rock geochemistry and Nd-Sr isotopes. Precambrian Research 268, 295-
1087 322.

1088 Jayananda, M., Duraiswami, R.A., Aadhiseshan, K.R., Gireesh, R.V., Prabhakar, B.C.,
1089 Kafo, K.-u, Tushipokla, Namratha, R., 2016. Physical volcanology and
1090 geochemistry of Palaeoarchaean komatiite lava flows from the western Dharwar
1091 craton, southern India: implications for Archaean mantle evolution and crustal
1092 growth. International geology review 58, 1569-1595.
1093 Kaur, P., Zeh, A., Chaudhri, N., 2014. Characterisation and U-Pb-Hf isotope record of
1094 the 3.55 Ga felsic crust from the Bundelkhand Craton, northern India.
1095 Precambrian Research 255, 236-244.
1096 Kirkland, C.L., Smithies, R.H., Taylor, R.J.M., Evans, N., McDonald, B., 2015. Zircon
1097 Th/U ratios in magmatic environs. Lithos 212-215, 397-414.
1098 Košler, J., Sylvester, P.J., 2003. Present trends and the Future of Zircon in
1099 Geochronology: Laser Ablation ICPMS. Zircon. Reviews in Mineralogy and
1100 Geochemistry, 53, 243–275.
1101 Kunugiza, K., Kato, Y., Kano, T., Takaba, Y., Kuruma, I., Sohma, T., 1996. An
1102 Archaean tectonic model of the Dharwar craton, Southern India: the origin of
1103 the Holenarsipur greenstone belt (Hassan district, Karnataka) and
1104 reinterpretation of the Sargur-Dharwar relationship. Journal of Southeast Asian
1105 Earth Sciences 14, 149-160.
1106 Lancaster, P.J., Dey, S., Storey, C.D., Mitra, A., and Bhunia, R.K., 2015. Contrasting
1107 crustal evolution processes in the Dharwar craton: insights from detrital zircon
1108 U-Pb and Hf isotopes. Gondwana Research 28, 1361-1372.
1109 Laurent, O., Martin, H., Moyen, J.F., Doucelance, R., 2014. The diversity and evolution
1110 of late-Archean granitoids: Evidence for the onset of “modern-style” plate
1111 tectonics between 3.0 and 2.5 Ga. Lithos 205, 208-235.

1112 Laurent, O., Zeh, A., 2015. A linear Hf isotope-age array despite different granitoid
1113 sources and complex Archean geodynamics: Example from the Pietersburg
1114 block (South Africa). Earth and Planetary Science Letters 430, 326-338.
1115 Lenting, C.,Geisler, T.,Gerdes, A.,Kooijman, E.,Scherer, E.E.,Zeh, A., 2010. The
1116 behavior of the Hf isotope system in radiation-damaged zircon during
1117 experimental hydrothermal alteration. American Mineralogist 95, 1343–1348.
1118 Le Roux, L.J., Glendenin, L.E., 1963. Half-life of 232Th. In: National Conference on
1119 Nuclear Energy, Application of Isotopes and Radiation. Proceedings of the
1120 National Conference on Nuclear Energy held in Pretoria, April 5–8 1963. South
1121 African Atomic Energy Board, Pelindaba, pp. 83–94.
1122 Ludwig, K.R., 2008. User's Manual for Isoplot 3.6, a Geochronological Toolkit for
1123 Microsoft Excel. Berkeley Geochronology Center Special Publication **4**.
1124 Maibam, B., Goswami, J.N., Srinivasan, R., 2011. Pb–Pb zircon ages of Archaean
1125 metasediments and gneisses from the Dharwar craton, southern India:
1126 implications for the antiquity of the eastern Dharwar craton. J. Earth Syst. Sci.
1127 120 (4),643–661.
1128 Maibam, B., Gerdes, A., Goswami, J.N., 2016. U-Pb and Hf isotope records in detrital
1129 and magmatic zircon from eastern and western Dharwar craton, southern India:
1130 Evidence for coeval Archaean crustal evolution. Precambrian Research 275,
1131 496-512.
1132 Moyen, J.-F., Martin, H., 2012. Forty years of TTG research. Lithos 148, 312–336.
1133 Martin, H., Moyen, J.-F., Guitreau, M., Blichert-Toft, J., Le Pennec, J.-L., 2014. Why
1134 Archaean TTG cannot be generated by MORB melting in subduction zones.
1135 Lithos 198-199, 1-13.

1136 Meißner, B., Deters, P., Srikantappa, C., Köhler, H., 2002. Geochronological evolution
1137 of the Moyar, Bhavani and Palghat shear zones of Southern India: Implications
1138 for east Gondwana correlations. Precamb. Res., 114, 149-175.
1139 Meen, J.K., Rogers, J.J.W., Fullagar, P.D., 1992. Lead isotopic compositions in
1140 thewestern Dharwar craton, southern India: evidence for distinct middle
1141 Archaeanterrains in a late Archaean craton. Geochim. Cosmochim. Acta 56,
1142 2455–2470.
1143 Meert, J.G., 2003. A synopsis of events related to the assembly of eastern Gondwana.
1144 Tectonophysics 362, 1-40.
1145 Miller, J.S., Santosh, M., Pressley, R.A., Clements, A.S., Rogers, J.J.W., 1996. A Pan-
1146 African thermal event in southern India. Journal of Southeast Asian Earth
1147 Sciences 14, 127-136.
1148 Mojzsis, S.J., Devaraju, T.C., Newton, R.C., 2003. Ion microprobe U-Pb age
1149 determinations on zircon from the late Archean granulite facies transition zone
1150 of Southern India. Journal of Geology 111, 407-425.
1151 Möller, A., O'Brien, P.J., Kennedy, A., Kröner, A., 2003. Linking growth episodes of
1152 zircon and metamorphic textures to zircon chemistry: an example from the
1153 ultra-high temperature granulites of Rogaland (SW Norway). Geological
1154 Society, London, Special Publications 220, 65-81.
1155 Monrad, 1983. Evolution of sialic terranes in the vicinity of the Holenarasipur belt,
1156 Hassan district, Karnataka, India. Geological Society of India Memoirs 4, 343–
1157 364.
1158 Moyen et al., 2003. Syntectonic granite emplacement at different structural levels: the
1159 Closepet granite, South India. Journal of Structural Geology 25, 611-631.

1160 Naqvi, S.M., 1983. Early Precambrian clastic metasediments of Dharwar greenstone
1161 belts; Implications to sial-sima transformation processes. Geological Society of
1162 India Memoirs 4, 220-236.
1163 Naqvi, S.M., Divakara Rao, V., Hussain, S.M., Narayana, B.L., Nirmal Charan, S.,
1164 Govil, P.K., Bhaskar Rao, Y.J., Jafri, S.H., Rama Rao, P., Balram, V., Masood
1165 Ahmad, Pantulu, K.P., Gnaneswar Rao, Subba Rao, D.V., 1983. Geochemistry
1166 of gneisses from Hassan district and adjoining areas, Karnataka, India.
1167 Geological Society of India Memoirs 4, 401-413.
1168 Naqvi, S.M., Ram Mohan, M., Rana Prathap, J.G., Srinivasa Sarma, D., 2009.Adakite–
1169 TTG connection and fate of Mesoarchaean basaltic crust of Holenarsipur
1170 nucleus, Dharwar Craton, India. Journal of Asian Earth Sciences 35, 416–434.
1171 Naqvi and Rogers, 1987. Precambrian Geology of India. Oxford monographs on
1172 Geology and Geophysics 6.
1173 Nutman, A.P., Chadwick, B., Ramakrishnan, M., Viswanatha, M.N., 1992. SHRIMP
1174 U-Pb ages of detrital zircon in Sargur supracrustal rocks in western Karnataka,
1175 southern India. Journal of the Geological Society of India 39, 367–374.
1176 Nebel, O., Campbell, I.H., Sossi, P.A., van Kranendonk, M.J., 2014. Hafnium and iron
1177 isotopes in early Archean komatiites record a plume-driven convection cycle in
1178 the Hadean Earth. Earth and Planetary Science Letters 397, 111–120.
1179 O'Connor, J.T., 1965. A classification for quartz-rich igneous rocks based on feldspar
1180 ratios. U.S. Geological Survey Professionnal Paper, 525(B): 79-84.
1181 Öhlander, B., Skiöld, T., Elming, S.-Å., BABEL working group, Claesson, S.,
1182 Nisca,D.H., 1993. Delineation and character of the Archaean-Proterozoic
1183 boundary innorthern Sweden. Precambrian Res. 64, 67–84.

1184 Paces, J.B. and Miller, J.D.Jr, 1993, Precise U-Pb ages of Duluth Complex and related
1185 mafic intrusions, Northeastern Minnesota: geochronological insights to
1186 physical, petrogenetic, paleomagnetic, and tectonomagmatic processes
1187 associated with the 1.1 Ga Midcontinent Rift System. Journal of Geophysical
1188 Research 98, 13997-14013.
1189 Patchett, P.J., 1983. Importance of the Lu–Hf isotopic system in studies of planetary
1190 chronology and chemical evolution. Geochimica et Cosmochimica Acta 47, 81–
1191 91.
1192 Payne, J.L., McInerney, D.J., Barovich, K.M., Kirkland, C.L., Pearson, N.J., Hand, M.,
1193 2016. Strengths and limitations of zircon Lu–Hf and O isotopes in modelling
1194 crustal growth. Lithos 248–251, 175–192.
1195 Peucat et al., 1995. Age of the Holenarsipur greenstone belt, relations with the
1196 surrounding gneisses (Karnataka, South India). Journal of Geology 103, 701-
1197 710.
1198 Puchtel, I.S., Hofmann, A.W., Amelin, Y.V., Garbe-Schönberg, C.-D., Samsonov,
1199 A.V., Shchipansky, A.A., 1999. Combined mantle plume-island arc model for
1200 the formation of the 2.9 Ga Sumozero-Kenozero greenstone belt, SE Baltic
1201 Shield: Isotope and trace element constraints. Geochimica et Cosmochimica
1202 Acta 63, 3579-3595.
1203 Raase, P., Raith, M., Ackermand, D., Lal, R.K., 1986. Progressive metamorphism of
1204 mafic rocks from greenschist to granulite facies in the Dharwar craton of South
1205 India. The Journal of Geology 94, 261-282.
1206 Raith, M., Raase, P, Ackermand, D., Lal, R.K., 1983.Regional geothermobarometry in
1207 the granulite facies terrane of South India. Transactions of the Royal Society of
1208 Edinburgh: Earth Sciences 73, 221-244.

1209 Rajesh et al., 2009. Evidence for an early Archaean granite from Bastar craton, India.
1210 Geological Society, London, Special Publications 166, 193-196.
1211 Ramakrishnan, M., Venkata Dasu, S.P., Kröner, A., 1994. Middle Archean ages of
1212 Sargur group by single grain zircon dating and geochemical evidences for the
1213 clastic origin of metaquartzite from J. C. Pura greenstone belt, Karnataka.
1214 Journal of the Geological Society of India, 44, 605–616.
1215 Ramakrishnan, M., 2009. Precambrian mafic magmatism in the Western Dharwar
1216 craton, Southern India. Journal of the Geological Society of India 73, 101-116.
1217 Rey, P.F., Phiippot, P., Thébaud, N., 2003. Contribution of mantle plumes, crustal
1218 thickening and greenstone blanketing to the 2.75-2.65 Ga global crisis.
1219 Precambrian Research 127, 43-60.
1220 Rogers, J.J.W., Callahan, E.J., Dennen, K.O., Fullagar, P.D., Stroh, P.T., Wood, L.F.,
1221 1986. Chemical evolution of peninsular gneiss in the Western Dharwar craton,
1222 Southern India. The Journal of Geology 94, 233-246.
1223 Rollinson, H.R., Windley, B.F., Ramakrishnan, M., 1981. Contrasting high and
1224 intermediate pressures of metamorphism in the Archaean Sargur Schists of
1225 Southern India. Contributions in Mineralogy and Petrology 76, 420-429.
1226 Santosh, M., Tanaka, K., Yokoyama, K., Collins, A.S., 2005. Late Neoproterozoic-
1227 Cambrian Felsic Magmatism Along Transcrustal Shear Zones in Southern
1228 India: U-Pb Electron Microprobe Ages and Implications for the Amalgamation
1229 of the Gondwana Supercontinent. Gondwana Research 8, 31-42.
1230 Santosh, M., Morimoto, T., Tsutsumi, Y., 2006. Geochronology of the khondalite belt
1231 of Trivandrum, Southern India: Electron probe ages and implications for
1232 Gondwana tectonics. Gondwana Research 9, 261-278.

1233 Santosh, M., Yang, Q.-Y., Shaji, E., Ram Mohan, M., Tsunogae, T., Satyanarayanan,
1234 M., 2016. Oldest rocks from Peninsular India: Evidence for Hadean to
1235 Neoarchean crustal evolution. Gondwana Research 29, 105-135.
1236 Sarkar, G., Corfu, F., Paul, D.K., McNaughton, N.J., Gupta, S.N., Bishui, P.K., 1993.
1237 Early Archaean crust in Bastar craton, central India—a geochemical and
1238 isotopic study. Precambrian Research 62, 127–137.
1239 Sarma, S.D., McNaughton, N.J., Belousova, E., Mohan, M.R., Fletcher, I.R., 2012.
1240 Detrital zircon U-Pb ages and Hf-isotope systematics from the Gadag Greenston
1241 Belt: Archean crustal growth in the western Dharwar Craton, India. Gondwana
1242 Research 22, 843-854.
1243 Sato, K., Santosh, M., Tsunogae, T., Chetty, T.R.K., Hirata, T., 2011. Subduction-
1244 accretion-collision history along the Gondwana suture in southern India: A laser
1245 ablation ICP-MS study of zircon chronology. Journal of Asian Earth Sciences,
1246 40, 162-171.
1247 Shand, S.J., 1943. Eruptive rocks. Their genesis, composition, classification, and their
1248 relations to ore-deposits. Wiley, New York, 444pp.
1249 Scherer, E., Münker, C.,Mezger, K., 2001. Calibration of the lutetium–hafnium clock.
1250 Science 293, 683–687.
1251 Schoene, B., de Wit, M., Bowring, S.A., 2008. Mesoarchean assembly and stabilization
1252 of the eastern Kaapvaal craton: A structural-thermochronological perspective.
1253 Tectonics 27, 1-27.
1254 Sláma, J., Kosler, J., Condon, D.J., Crowley, J.L., Gerdes, A., Hanchar, J.M.,
1255 Horstwood, M.S.A., Morris, G.A., Nasdala, L., Norberg, N., Schaltegger, U.,
1256 Schoene, B., Tubrett, M.N., Whitehouse, M.J., 2008. Plešovice zircon – A new

natural reference material for U–Pb and Hf isotopic microanalysis. Chemical Geology 249, 1–35.

Söderlund, U., Patchett, J.P., Vervoort, J.D., Isachsen, C.E., 2004. The 176Lu decay constant determined by Lu–Hf and U–Pb isotope systematics of Precambrian mafic intrusions. Earth and Planetary Science Letters 219, 311–324.

Stroh, P.T., Monrad, J.R., Fullagar, P.D., Naqvi, S.M., Hussain, S.M., Rogers, J.J.W., 1983. 3,000 M.y.-old Halekote trondhjemite: A record of stabilization of the Dharwar craton. Geological Society of India Memoirs 4, 365–376.

Stevenson, R.K., Patchett, P.J., 1990. Implications for the evolution of continental crust from Hf isotope systematics of Archean detrital zircons. Geochimica et Cosmochimica Acta 54, 1683-1697.

Taylor, P.N., Chadwick, B., Moorbath, S., Ramakrishnan, M., Viswanatha, M.N., 1984. Petrography, chemistry, and isotopic ages of Peninsular Gneiss, Dharwar acidvolcanic rocks and the Chitradurga granite with special reference to the lateArchaean evolution of the Karnataka craton. Precambrian Research 23, 349–375.

Vavra, G., Schmid, R., Gebauer, D., 1999. Internal morphology, habit and U-Th-Pb microanalysis of amphibolite-to-granulite- facies zircons: geochronology of the Ivrea Zone (Southern Alps). Contributions to Mineralogy and Petrology 134, 380-404.

Wang, X., Griffin, W.L., Chen, J., Huang, P., Li, X., 2011. U and Th contents and Th/U ratios of zircon in felsic and mafic magmatic rocks: improved zircon-melt distribution coefficient. Acta Geologica Sinica 85, 164-174.

1281 Weihed, P., Arndt, N., Billström, K., Duchesne, J.-C., Eilu, P., Martinsson, O.,
1282 Papunen,H., Lahtinen, R., 2005. Precambrian geodynamics and ore formation:
1283 the Fennoscandian Shield. Ore Geology Review 27, 273–322.
1284 Whitmeyer, S.J., Karlstrom, K.E., 2007. Tectonic model for the Proterozoic growth of
1285 North America. Geosphere 3, 220–259.
1286 Wiedenbeck, M., Allé, P., Corfu, F., Griffin, W.L., Meier, M., Oberli, F., von Quadt,
1287 A., Roddick, J.C., Spiegel, W., 1995, Three natural zircon standards for U–Th–
1288 Pb, Lu–Hf, trace element and REE analyses. Geostandard Newsletters 19, 1 –
1289 23.
1290 Wiedenbeck M, Hanchar JM, Peck WH, Sylvester P, Valley J, Whitehouse M, Kronz
1291 A, Morishita Y, Nasdala L, Fiebig J, Franchi I, Girard JP, Greenwood RC,
1292 Hinton R, Kita N, Mason PRD, Norman M, Ogasawara M, Piccoli R, Rhede D,
1293 Satoh H, Schulz-Dobrick B, Skår O, Spicuzza MJ, Terada K, Tindle A, Togashi
1294 S, Vennemann T, Xie Q, Zheng Y-F (2004) Further characterization of the
1295 91500 zircon crystal. Geostandards and Geoanalytical Research 28, 9-39.
1296 Woodhead, J.D., Hergt, J.M., 2005. A preliminary appraisal of seven natural zircon
1297 reference materials for *in situ* Hf isotope determination. Geostrandards and
1298 Geoanalytical Research 29, 183-195.
1299 Yoshida, M., Arima, M., Kano, T., Kunugiza, K., Venkata-Rao, M., Shirahata, H.,
1300 Sohma, T., Unnikrishnan-Warrier, C., Venkatesh-Ragavan, Yamaguchi, Y.,
1301 1994. Geological survey in Southern to Eastern Peninsular India, 1992. Journal
1302 of Geosciences 37, 31-54.
1303 Yoshida, M., Bindu, R.S., Kagami, H., Rajesham, T., Santosh, M., Shirahata, H., 1996.
1304 Geochronologic constraints of granulite terranes of South India and their

implications for the Precambrian assembly of Gondwana. Journal of Southeast Asian Earth Sciences, 14, 137–148.

Zeh, A., Gerdes, A.,Millonig, L., 2011. Hafnium isotope record of the Ancient Gneiss Complex, Swaziland, southern Africa: evidence for Archaean crust–mantle formation and crust reworking between 3.66 and 2.73 Ga. Journal of the Geological Society of London 168, 953–963.

Figure captions

Table 1. Summary of the Archean geology of the Western Dharwar craton after Naqvi and Rogers (1987), Yoshida et al. (1994), Naqvi et al. (2009), and Dey (2013).

Table 2. Details of rock sampling location and petrography.

Table 3. Summary of U-Pb and Lu-Hf isotope results for Indian zircons analyzed by LA-ICP-MS and LA-MC-ICP-MS

Table 4. Interpreted U-Pb ages and Lu-Hf isotope systematics for Indian zircons analyzed herein

Figure 1. Detailed geological map of the Dharwar craton adapted from Chardon et al. (2008) and Dey (2013). WDC and EDC refer to Western and Eastern Dharwar Cratons, respectively. Major schist belts have been reported and names are indicated as follows; B for Banasandra, Bb for Bababudan, Ch for Chitradurga, G for Ghattihosahalli, Ga for Gadag, Ho for Holenarsipur, J for Jayachamarajapura (J.C. Pura), K for Kalyadi, Ku

for Kudremuh, N for Nuggihalli, S for Sandur, Sh for Shimoga, and Sg for Sargur. The inset shows where Figure 1 locates respective to India.

Figure 2. Merged geological and structural map of the Holenarsipur Schist Belt (Western Dharwar Craton, Southern India), from Bouhallier et al. (1993), with location of samples collected for this study (red dots).

Figure 3. Photos of sampling locations with corresponding thin section images in polarized and cross-polarized light for samples 13DC12 (Figs. 3A-3C) and 13DC13 (Figs. 3D-3F). Note the hammer and the chisel, with orange handle, for scale in 3A and 3D, respectively. Mineral names are reported as Qz for quartz, Plg for plagioclase, Kf for K-Feldspar (essentially microcline), Bt for biotite, and Ms for muscovite.

Figure 4. Diagrams presenting the major characteristics of samples 13DC12 and 13DC13 based on major and minor element concentrations. Figure A is an An-Ab-Or normative plot that discriminates granitoid types (after O'Connor, 1965 and Barker, 1979). Figure B is a diagram that indicates granite chemical affinity according to the classification proposed by Shand (1943). Figure C is MALI index after Frost et al. (2001) with field compositions after Martin and Moyen (2012) and Laurent et al. (2014). Figure D is a classification of late-Archean granitoids proposed in Laurent et al. (2014). Figure E is a ternary diagram that presents the compositional field of melts produced by a range of possible sources (i.e., low-K and high-K mafic rocks, as well as tonalities and metasediments). This diagram can be used to infer granite sources using major element concentrations (after Laurent et al., 2014).

Figure 5. Coupled U-Pb and Lu-Hf isotope results for zircons from sample 13DC12. Dashed lines represent closed-system evolution of the Lu-Hf isotope system using the $^{176}Lu/^{177}Hf$ indicated next to each line, which correspond to the lowest and highest values measured for this zircon population, and assuming that the initial $^{176}Hf/^{177}Hf$ is the average of those visible in the inset. Note the general good match between datapoints and evolution lines.

Figure 6. Summary of 13DC12 zircon U-Pb geochronology. Figure A is a Concordia plot displaying the most concordant and oldest least discordant U-Pb data from 13DC12. Figure B presents the weighted average $^{207}Pb/^{206}Pb$ age for U-Pb data shown in Figure A. Figure C is a Concordia diagram that shows U-Pb data for all other zircons from 13DC12.

Figure 7. Coupled U-Pb and Lu-Hf isotope results for zircons from sample 13DC13. As in Figure 4, dashed lines represent closed-system evolution of the Lu-Hf isotope system using the $^{176}Lu/^{177}Hf$ indicated next to each line, which correspond to the lowest and highest values measured, and assuming that the initial $^{176}Hf/^{177}Hf$ is the average of the oldest zircons.

Figure 8. Coupled U-Pb and Lu-Hf isotope results for zircons from sample 13DC15. The dashed line represents closed-system evolution of the Lu-Hf isotope system using the $^{176}Lu/^{177}Hf$ measured in 13DC15_1b and the initial $^{176}Hf/^{177}Hf$ from 13DC15_1a.

Figure 9. Compilation of available U-Pb and Lu-Hf isotope data for detrital zircons from the Western Dharwar Craton (Sarma et al., 2012; Lancaster et al., 2015; Maibam

et al., 2016), combined with data from this study, and those for Gorur gneiss from Bhaskar Rao et al. (2008). Also shown is the age range for Sargur-group komatiites analyzed by Jayananda et al. (2008) using the Sm-Nd isotope system. Bulk Silicate Earth (BSE) parameters are those from Iizuka et al. (2015) and arc-mantle evolution is deduced from a present-day ε_{Hf} of +13.3 (Dhuime et al., 2011; Iizuka et al., 2013). Dashed lines indicate the evolution paths for reservoirs with mafic ($^{176}Lu/^{177}Hf = 0.02$) and felsic (TTG; $^{176}Lu/^{177}Hf = 0.005$) compositions. See text for details.

Captions to supplementary Figures and Tables:

Table S1. Major and minor oxide abundances for the orthogneisses analyzed in this study

Table S2. LA-ICP-MS and LA-MC-ICP-MS operating conditions

Table S3. U-Pb isotope results for the zircon standard 91500 analyzed by LA-ICP-MS.

Table S4. U-Pb isotope results for Indian zircons analyzed by LA-ICP-MS.

Table S5: Lu-Hf isotope results for zircon standards analyzed by LA-MC-ICP-MS

Table S6. Lu-Hf isotope results for Indian zircons analyzed by LA-MC-ICP-MS

Figure S1. Concordia plot and weighted average $^{207}Pb/^{206}Pb$ for the zircon standard 91500 that was used as a quality check in this study.

1404 Figure S2. Plots showing the accuracy of Hf isotope measurements performed on
1405 standards in this study. ε_{Hf} values presented in this figure correspond to those visible in
1406 Table S5 which were calculated by normalization to the accepted values of the
1407 corresponding zircon standard also provided in Table S5.
1408
1409 Figure S3. Concordia plot for zircons from the granitic gneiss (13DC12) with
1410 corresponding cathodo-luminescence images.
1411
1412 Figure S4. Concordia plot for zircons from the trondhjemitic gneiss (13DC13) with
1413 corresponding cathodo-luminescence images.
1414
1415 Figure S5. Concordia plot of all U-Pb data for 13DC13 zircons (A) and $^{207}Pb/^{206}Pb$ age
1416 vs. Th/U plot for corresponding zircons (B). White-filled symbols correspond to low-
1417 Th/U zircons whereas those filled with grey and black correspond to zircons with Th/U
1418 that comply with the common magmatic range and high-Th/U zircons, respectively.
1419
1420 Figure S6. Concordia plot for zircons from 13DC15 with corresponding transmitted
1421 light and cathodo-luminescence images.
1422

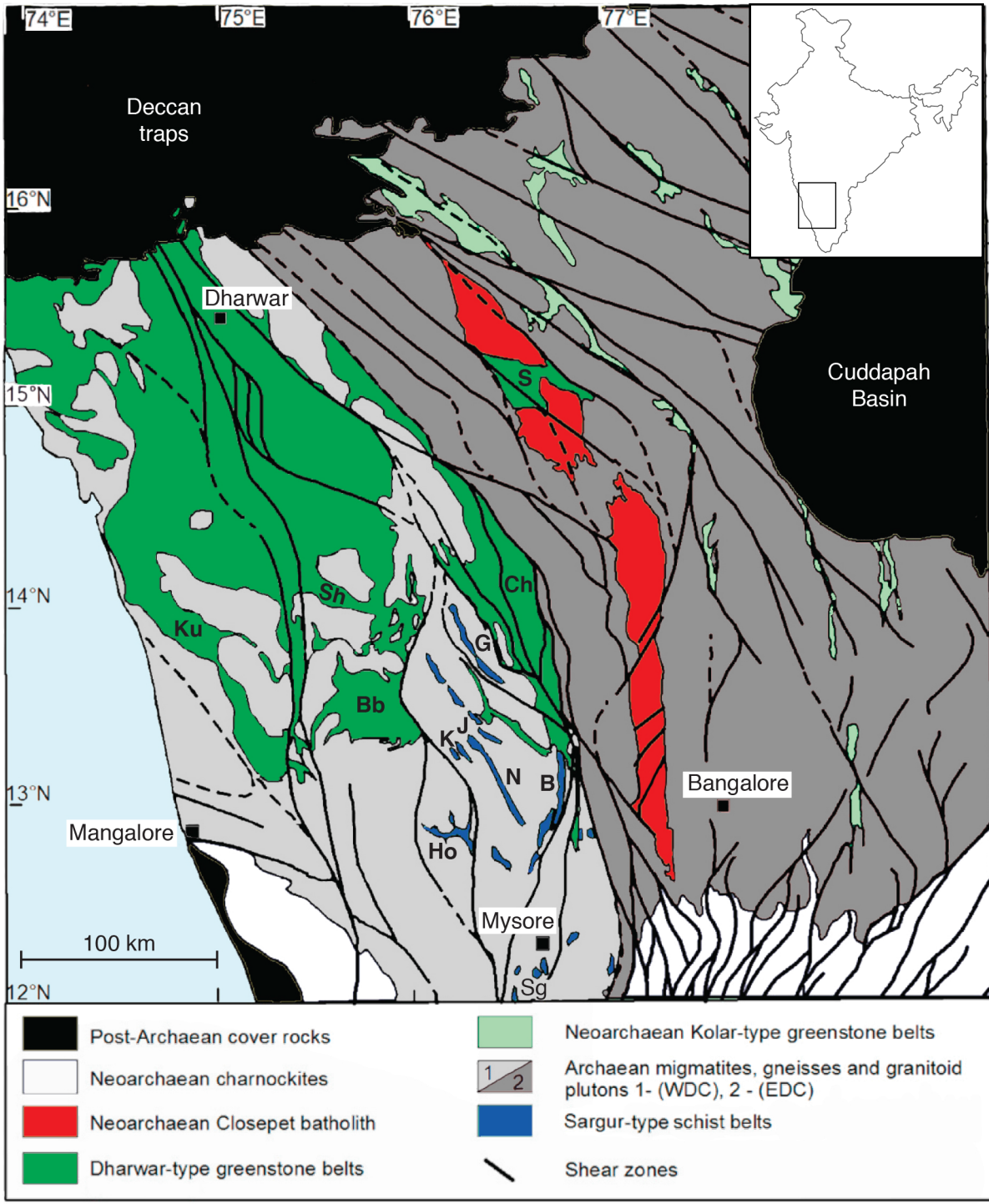
74°E
75°E
76°E
77°E
Deccan traps
16°N
Dharwar
15°N
S
Cuddapah Basin
14°N
Sh
Ch
Ku
G
Bb
K
J
N
B
Bangalore
13°N
Mangalore
Ho
Mysore
100 km
12°N
Sg
Post-Archaean cover rocks
Neoarchaean charnockites
Neoarchaean Closepet batholith
Dharwar-type greenstone belts
Neoarchaean Kolar-type greenstone belts
1
2
Archaean migmatites, gneisses and granitoid plutons 1- (WDC), 2 - (EDC)
Sargur-type schist belts
Shear zones

Figure 1

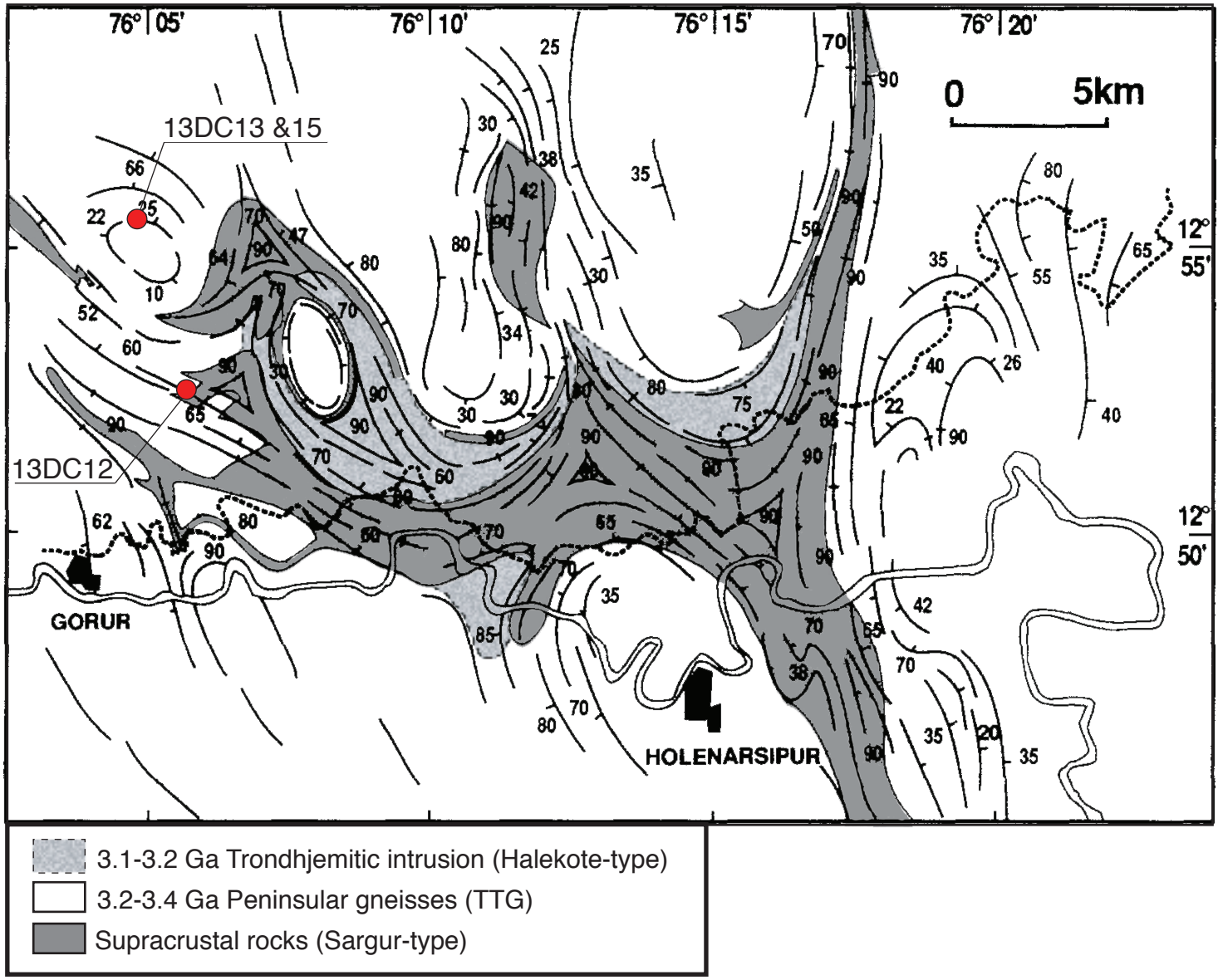
76° 05'
76° 10'
76° 15'
76° 20'
0 5km
13DC13 &15
13DC12
12° 55'
12° 50'
GORUR
HOLENARSIPUR
3.1-3.2 Ga Trondhjemitic intrusion (Halekote-type)
3.2-3.4 Ga Peninsular gneisses (TTG)
Supracrustal rocks (Sargur-type)

Figure 2

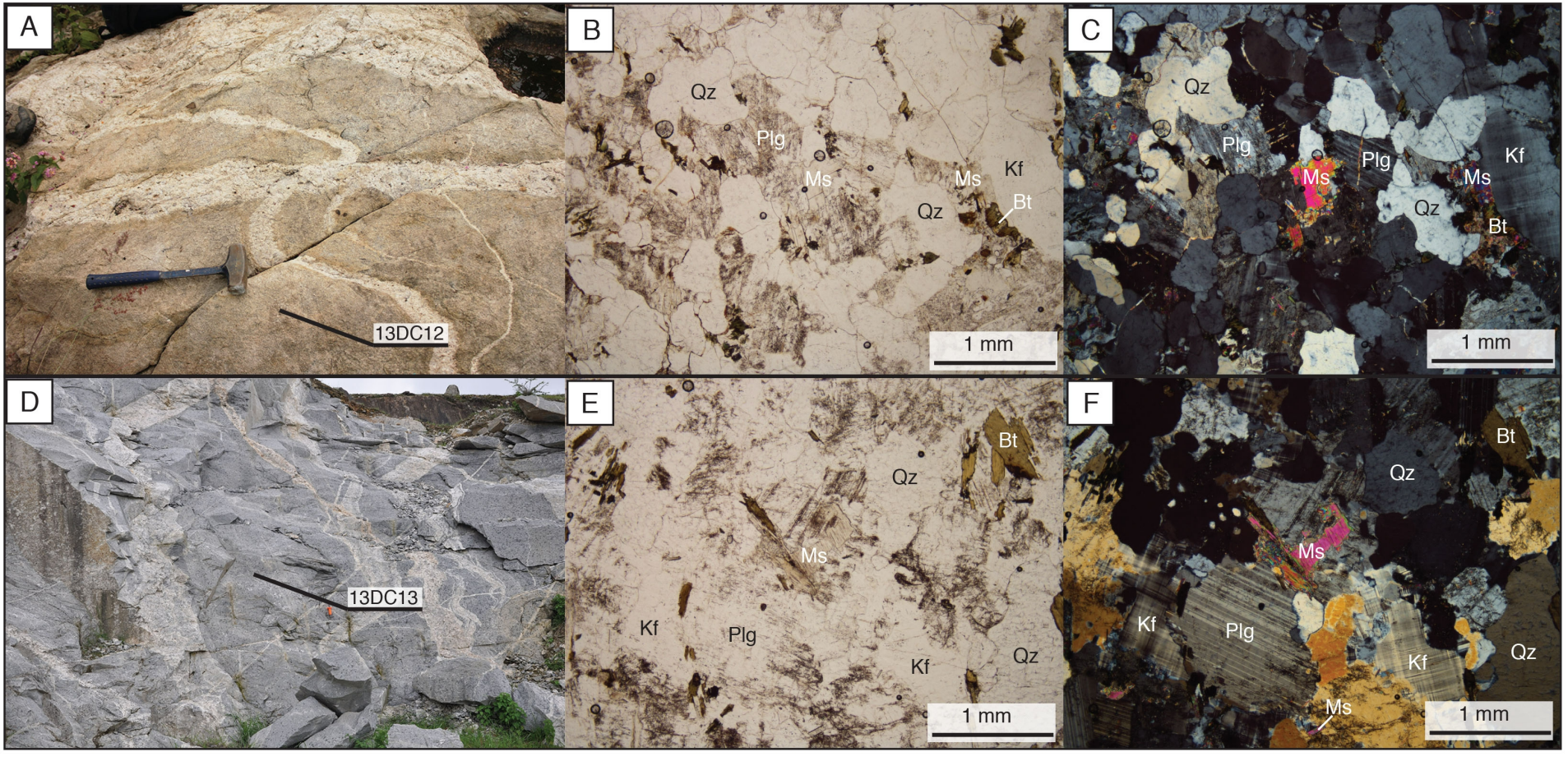
A
13DC12
B
Qz
Plg
Ms
Ms
Kf
Qz
Bt
1 mm
C
Qz
Plg
Ms
Plg
Kf
Ms
Qz
Bt
1 mm
D
13DC13
E
Bt
Qz
Ms
Kf
Plg
Kf
Qz
1 mm
F
Bt
Qz
Ms
Kf
Plg
Kf
Qz
Ms
1 mm

Figure 3

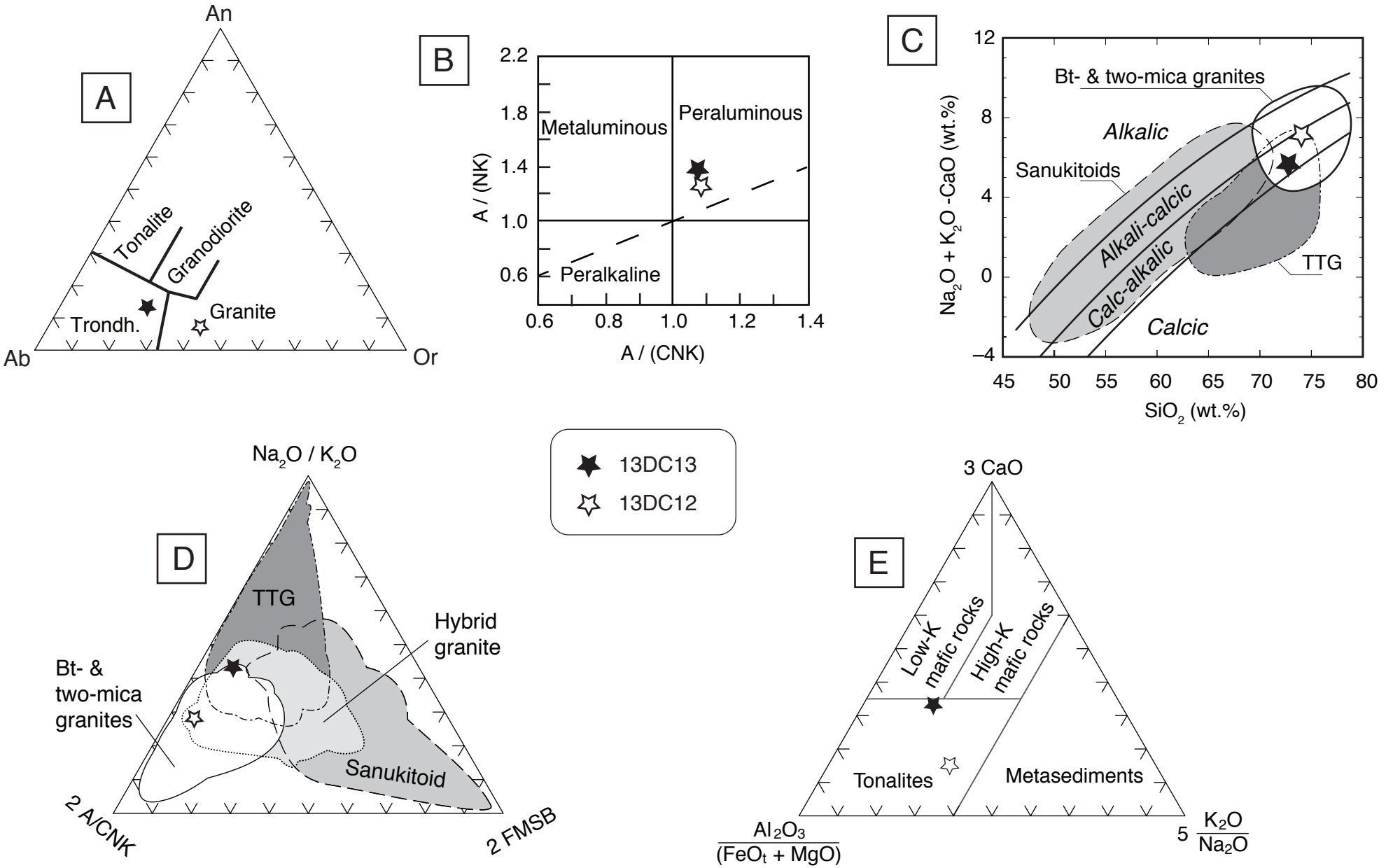
A
An
Ab
Or
Tonalite
Granodiorite
Trondh.
Granite
B
Metaluminous
Peraluminous
Peralkaline
A / (NK)
A / (CNK)
C
Bt- & two-mica granites
Alkalic
Sanukitoids
Alkali-calcic
Calc-alkalic
Calcic
TTG
Na2O + K2O -CaO (wt.%)
SiO2 (wt.%)
13DC13
13DC12
D
Na2O / K2O
TTG
Hybrid granite
Bt- & two-mica granites
Sanukitoid
2 A/CNK
2 FMSB
E
3 CaO
Low-K mafic rocks
High-K mafic rocks
Tonalites
Metasediments
Al2O3 / (FeOt + MgO)
5 K2O / Na2O

Figure 4

Figure 5

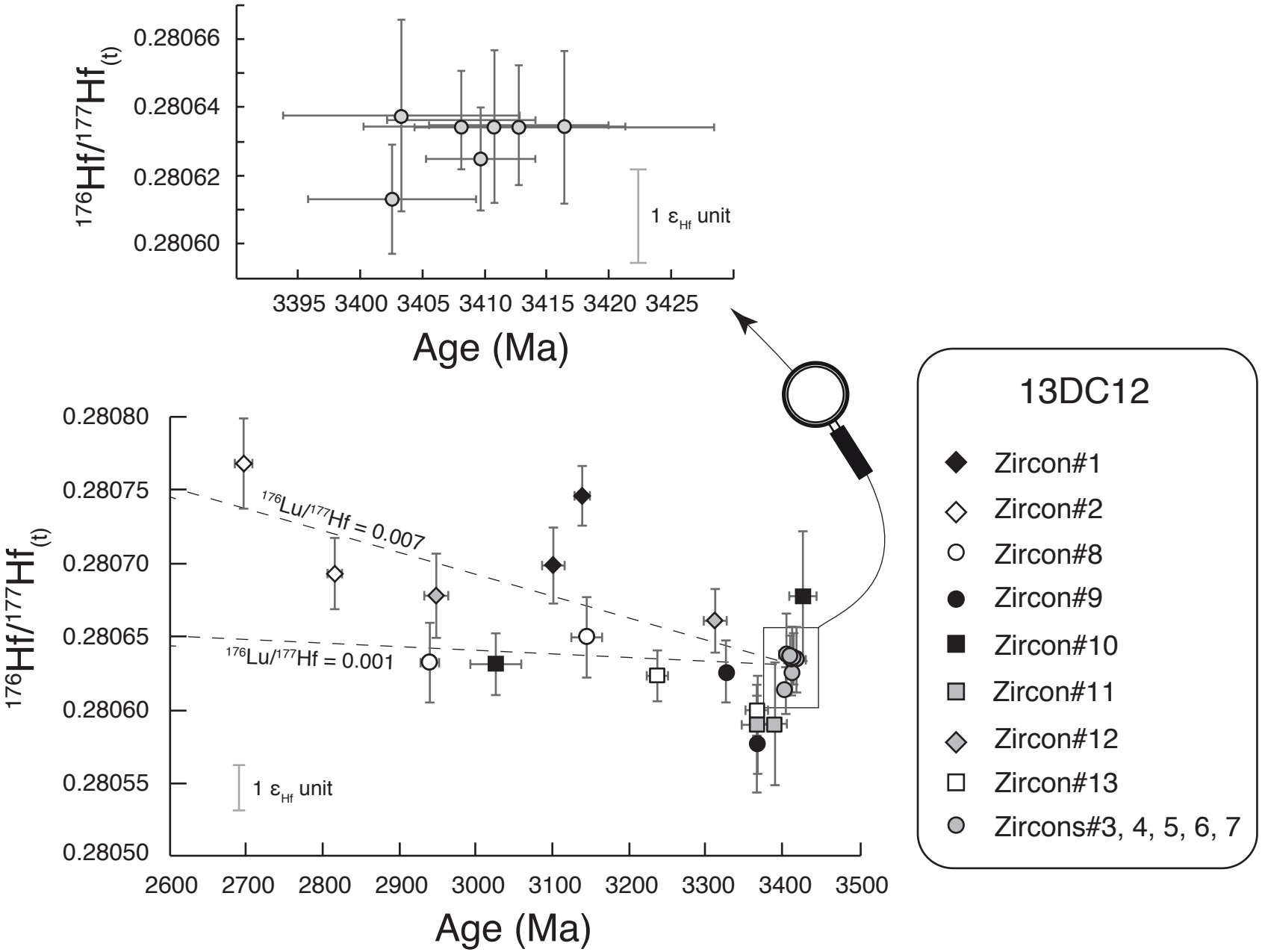
0.28066
0.28064
0.28062
0.28060
176Hf/177Hf(t)
1 εHf unit
3395 3400 3405 3410 3415 3420 3425
Age (Ma)
0.28080
0.28075
0.28070
0.28065
0.28060
0.28055
0.28050
176Lu/177Hf = 0.007
176Lu/177Hf = 0.001
1 εHf unit
2600 2700 2800 2900 3000 3100 3200 3300 3400 3500
Age (Ma)
13DC12
Zircon#1
Zircon#2
Zircon#8
Zircon#9
Zircon#10
Zircon#11
Zircon#12
Zircon#13
Zircons#3, 4, 5, 6, 7

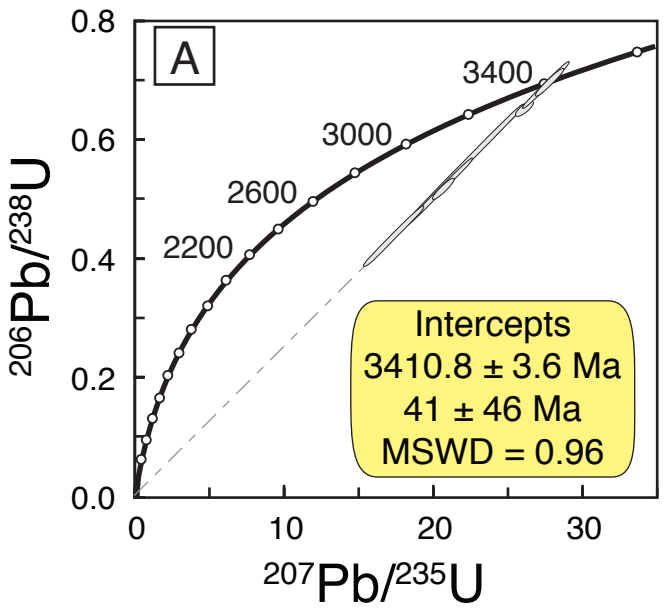
A
3400
3000
2600
2200
Intercepts
3410.8 ± 3.6 Ma
41 ± 46 Ma
MSWD = 0.96
0.0
0.2
0.4
0.6
0.8
0
10
20
30
206Pb/238U
207Pb/235U

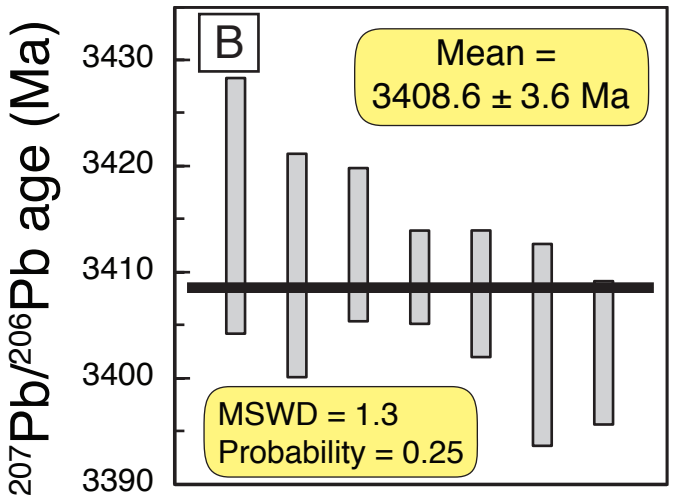
B
Mean =
3408.6 ± 3.6 Ma
MSWD = 1.3
Probability = 0.25
3390
3400
3410
3420
3430
207Pb/206Pb age (Ma)

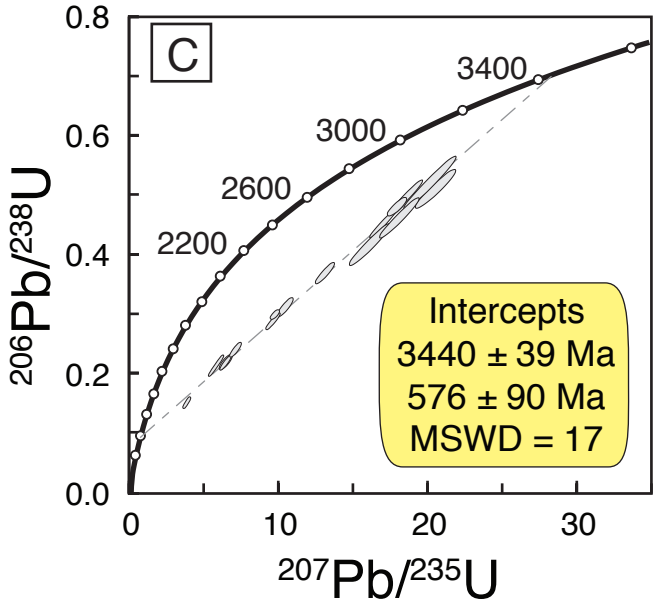
C
3400
3000
2600
2200
Intercepts
3440 ± 39 Ma
576 ± 90 Ma
MSWD = 17
0.0
0.2
0.4
0.6
0.8
0
10
20
30
206Pb/238U
207Pb/235U

Figure 6

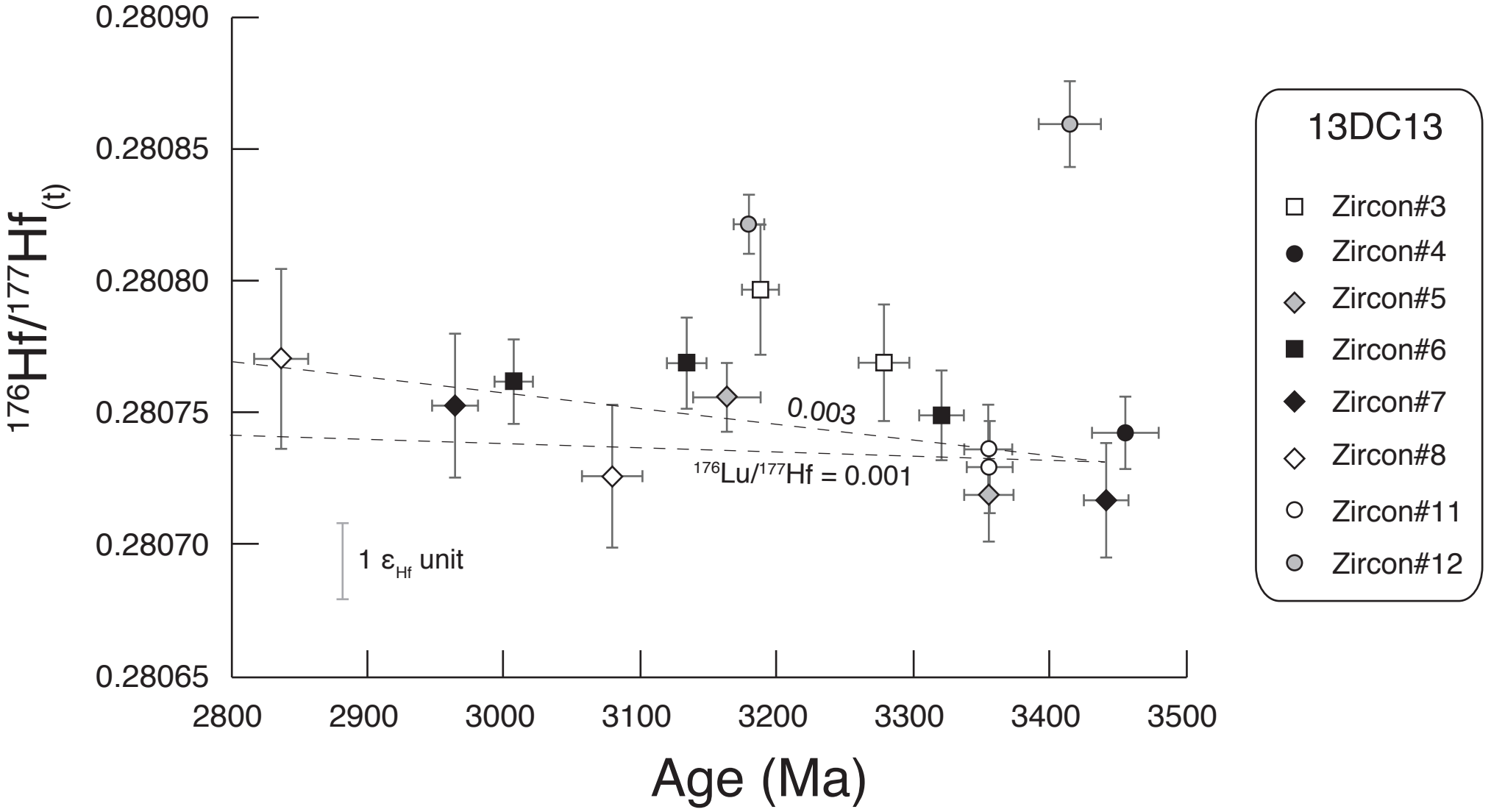
0.28090
0.28085
0.28080
0.28075
0.28070
0.28065
$^{176}Hf/^{177}Hf_{(t)}$
2800
2900
3000
3100
3200
3300
3400
3500
Age (Ma)
0.003
$^{176}Lu/^{177}Hf = 0.001$
1 ε_{Hf} unit
13DC13
Zircon#3
Zircon#4
Zircon#5
Zircon#6
Zircon#7
Zircon#8
Zircon#11
Zircon#12

Figure 7

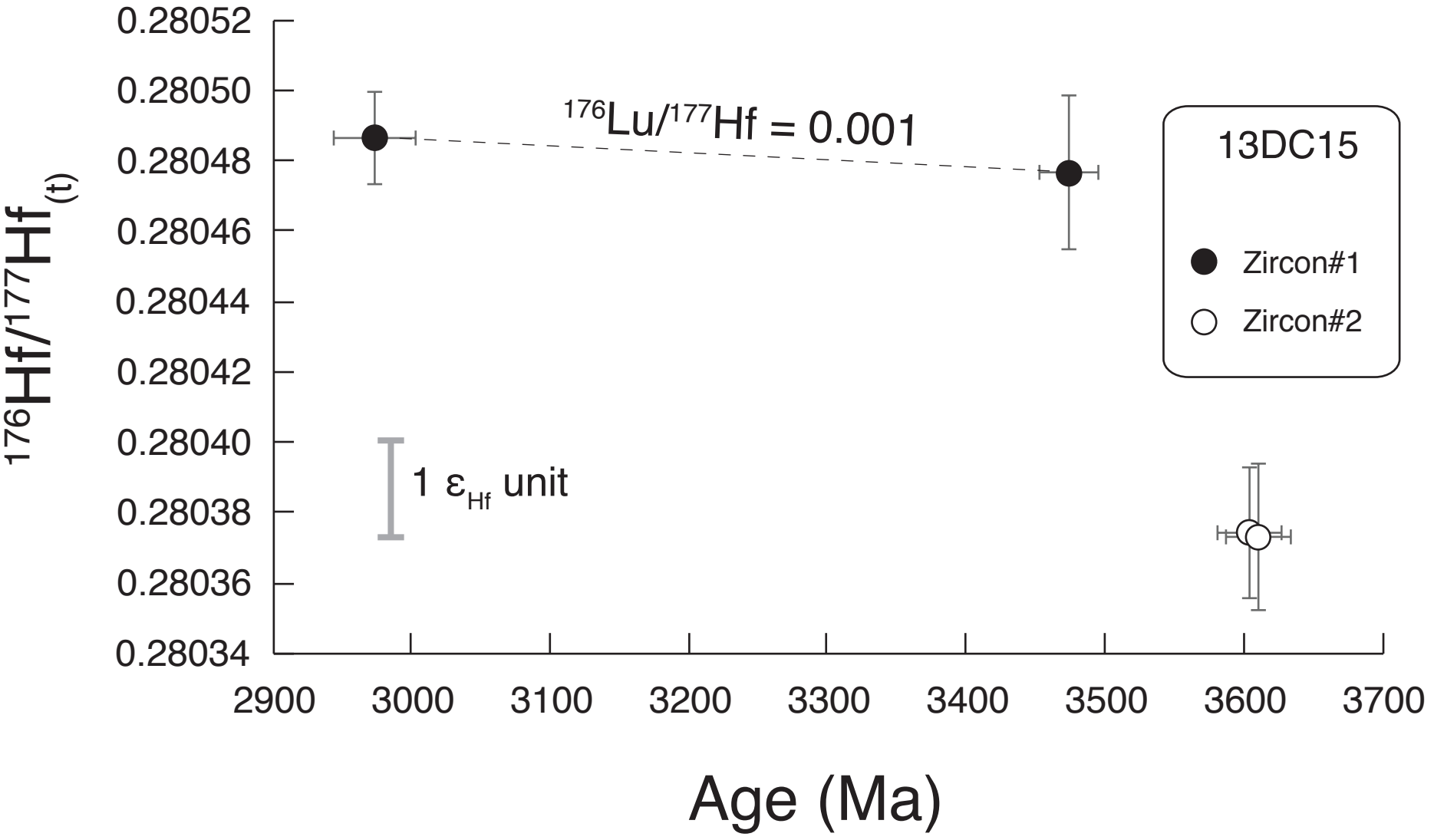
0.28052
0.28050
0.28048
0.28046
0.28044
0.28042
0.28040
0.28038
0.28036
0.28034
$^{176}Hf/^{177}Hf_{(t)}$
$^{176}Lu/^{177}Hf = 0.001$
1 ε_{Hf} unit
13DC15
Zircon#1
Zircon#2
2900
3000
3100
3200
3300
3400
3500
3600
3700
Age (Ma)

Figure 8

Figure 9

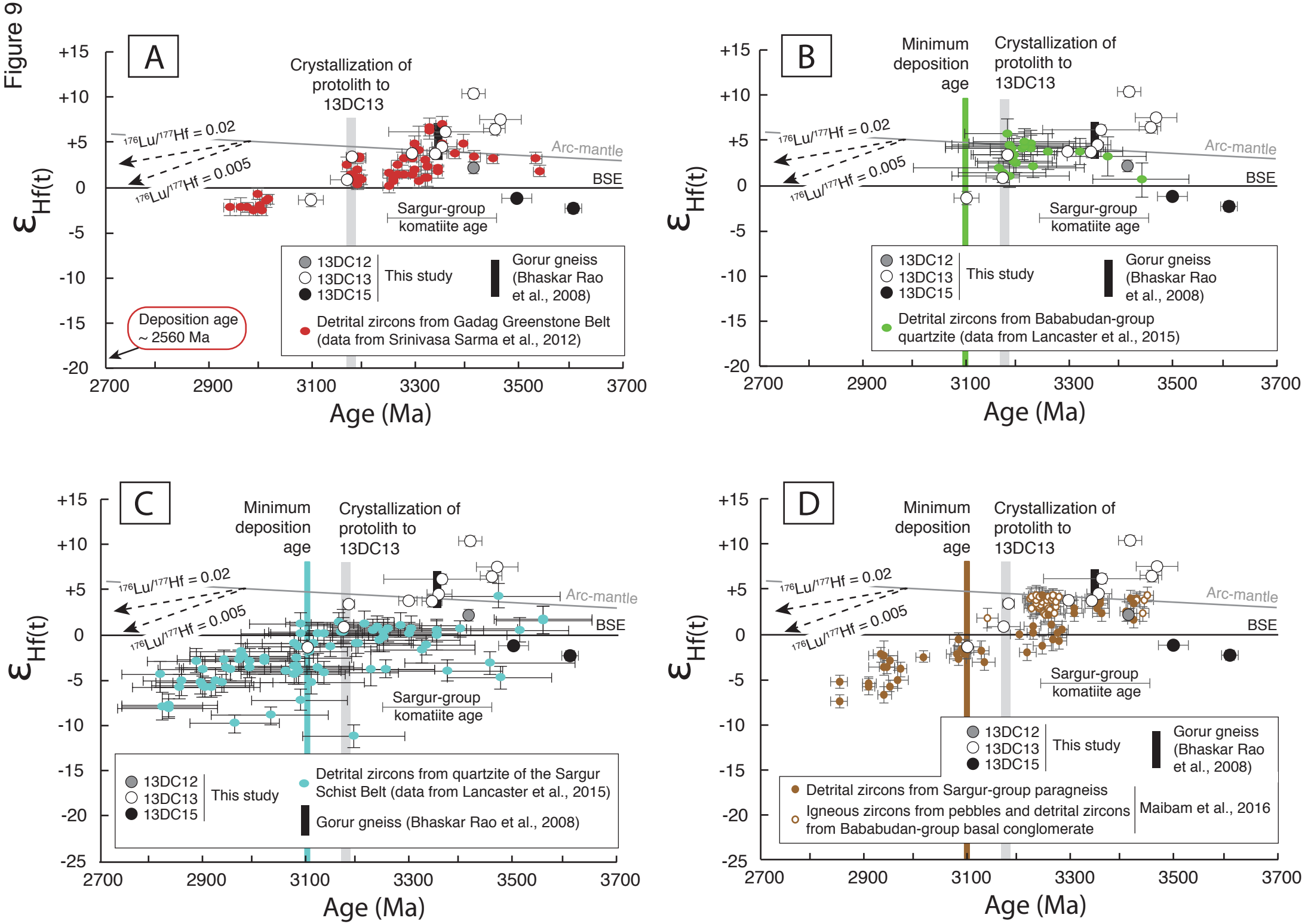
A
Crystallization of protolith to 13DC13
$^{176}Lu/^{177}Hf = 0.02$
$^{176}Lu/^{177}Hf = 0.005$
Arc-mantle
BSE
Sargur-group komatiite age
Deposition age ~ 2560 Ma
13DC12
13DC13
13DC15
This study
Gorur gneiss (Bhaskar Rao et al., 2008)
Detrital zircons from Gadag Greenstone Belt (data from Srinivasa Sarma et al., 2012)
$\varepsilon_{Hf(t)}$
Age (Ma)
B
Minimum deposition age
Crystallization of protolith to 13DC13
Detrital zircons from Bababudan-group quartzite (data from Lancaster et al., 2015)
C
Minimum deposition age
Crystallization of protolith to 13DC13
Detrital zircons from quartzite of the Sargur Schist Belt (data from Lancaster et al., 2015)
D
Minimum deposition age
Crystallization of protolith to 13DC13
Detrital zircons from Sargur-group paragneiss
Igneous zircons from pebbles and detrital zircons from Bababudan-group basal conglomerate
Maibam et al., 2016

Table 1. Summary of the Archean geology of the Western Dharwar craton after Naqvi and Rogers (1987), Yoshida et al. (1994), Naqvi et al. (2009), and Dey (2013)

Supracrustal rocks	Granitic rocks	Lithologies	Additional information
	Closepet granite (~2500 to ~2600 Ma)	K-rich granite	
Dharwar Supergroup (~2500 to ~2900 Ma) **Chitradurga group**		Conglomerate, quartzite, greywacke, pelite, BIF, basalt	Oldest reported detrital zircon in Gadag greenstone belt: 3542 ± 9 Ma (Sarma et al., 2012)
-------Unconformity------- **Bababudan group (3.2-3.0 Ga?)**		Conglomerate, quartzite, basalt, BIF	Oldest reported detrital zircon: 3634 ± 10 Ma (Bhaskar Rao et al., 2008)
-------Unconformity-------			
	Diapiric bodies (~3100 to ~3200 Ma)	Trondhjemite (Halekote) and granite/granodiorite (Chikmagalur)	Contains remnants of older greenstones and basement gneisses (e.g., Meen et al., 1992; Jayananda et al., 2015; this study). Inherited igneous zircon: 3607 ± 16 Ma (this study)
Sargur group (~3000 to ~3400 Ma)		Quartzite, pelite, calc-silicate, basalt, komatiite, BIF, layered mafic-ultramafics	Oldest age of 3352 ± 110 Ma from komatiites (Jayananda et al., 2008). Detrital zircons indicate a range from 3580 to 3130 Ma (Nutman et al., 1992). Lancaster et al. (2015) reported an oldest detrital zircon age of 3555 ± 95 Ma.
	Peninsular gneisses (~3200 to ~3400 Ma)	Tonalite-trondhjemite-granodiorite and granite	Oldest generations: 3342 ± 6 Ma (Gorur gneiss; Beckinsale et al., 1980; Jayananda et al., 2015), 3350 ± 9 Ma (Chikmagalur gneiss; Jayananda et al., 2015), and 3410.8 ± 3.6 Ma (this study)
	Older basement (up to ~3600 Ma)	TTG?	Existence inferred from detrital and inherited zircons (e.g., Nutman et al., 1992; Bhaskar Rao et al., 2008; Lancaster et al., 2015; this study)

Table 2. Sample locations and petrographic details of the samples analyzed in this study

Sample name	**Locality**	GPS Coordinates		**Rock type**
13DC12	Near Byadarahalli (Karnataka)	N12°52.463'	E076°05.686'	Granitic gneiss
13DC13	Near Javenahalli (Karnataka)	N12°55.461'	E076°04.809'	Trondhjemitic gneiss
13DC15	Near Javenahalli (Karnataka)	N12°55.461'	E076°04.809'	Bt-rich enclave within 13DC13

* Qz is for quartz, Plg for plagioclase, K-Feld for alkali feldspar, Bt for biotite, Msc for muscovite, Op for opaque pha

Mineralogy
Qz, Plg, K-Feld, Bt, Msc, ± Op
Qz, Plg, K-Feld, Bt, Msc, ± Op
Bt, Qz, Plg, ± K-Feld, ± Msc, ± Chl

ıses, and Chl for chlorite

Table 3. Summary of U-Pb and Lu-Hf isotope results for Indian zircons analyzed by LA-ICP-MS

Sample	U	Th	Pb	Th/U_c	Age (Ma)	2σ	Disc.	$^{176}Hf/^{177}Hf$	2 σ	$^{176}Lu/^{177}Hf$
	(ppm)				(Ma)				($x10^{-6}$)	
Granitic gneiss										
13DC12_1a	1334	257	561	0.41	3137	10	54%	0.281023	18	0.00460
13DC12_1b	1691	394	751	0.44	3100	15	51%	0.280990	22	0.00489
13DC12_2a	2837	1205	763	0.49	2696	11	71%	0.281124	29	0.00689
13DC12_2b	2072	1762	720	0.61	2815	9	61%	0.280890	23	0.00365
13DC12_3_1	538	201	442	0.51	3411	11	26%	0.280772	21	0.00209
13DC12_3_2	260	119	292	0.61	3416	12	7%	0.280772	21	0.00209
13DC12_4	253	48	230	0.39	3403	7	18%	0.280723	15	0.00167
13DC12_5a	262	80	270	0.30	3413	7	0%	0.280757	16	0.00186
13DC12_5b	302	99	311	0.30	3410	4	1%	0.280734	14	0.00165
13DC12_6	1277	1155	994	0.63	3403	10	37%	0.280875	24	0.00361
13DC12_7	471	631	504	0.99	3408	6	26%	0.280766	12	0.00198
13DC12_8a	2849	1454	1027	0.71	2939	12	62%	0.280855	25	0.00394
13DC12_8b	1352	463	640	0.46	3143	20	50%	0.281032	24	0.00633
13DC12_9a	615	660	498	0.63	3324	7	33%	0.280767	19	0.00219
13DC12_9b	456	284	462	0.48	3365	6	11%	0.280685	32	0.00167
13DC12_10a	581	483	519	0.74	3425	18	25%	0.280884	43	0.00313
13DC12_10b	1523	1530	550	0.56	3024	33	63%	0.280816	20	0.00317
13DC12_11a	1088	827	856	0.63	3388	15	33%	0.280869	36	0.00426
13DC12_11b	1060	802	805	0.66	3366	21	39%	0.280766	30	0.00272
13DC12_12a	1328	1141	554	0.83	2947	16	58%	0.280886	25	0.00369
13DC12_12b	1958	3334	742	0.13	3310	15	28%	0.280833	15	0.00271
13DC12_13a	640	201	374	0.37	3235	14	43%	0.280733	15	0.00177
13DC12_13b	271	86	218	0.52	3365	15	24%	0.280739	13	0.00214
Trondhjemitic gneiss										
13DC13_3a	348	292	363	1.02	3278	19	6%	0.280841	20	0.00114
13DC13_3b	341	314	318	1.02	3187	14	10%	0.280885	24	0.00143
13DC13_4_1	512	27	455	0.22	3424	17	10%	0.280856	12	0.00170
13DC13_4_2	538	381	601	0.53	3455	24	3%	0.280856	12	0.00170
13DC13_5a_1	2772	123	2057	0.11	3116	25	14%	0.280873	11	0.00191
13DC13_5a_2	3668	459	3205	0.14	3163	25	2%	0.280873	11	0.00191
13DC13_5b_1	1395	80	1044	0.08	3276	15	24%	0.280837	16	0.00182
13DC13_5b_2	680	28	694	0.05	3355	18	-7%	0.280837	16	0.00182
13DC13_6a	1380	25	700	0.02	3133	15	40%	0.280893	16	0.00206
13DC13_6b	122	83	154	0.58	3320	16	-14%	0.280856	15	0.00167
13DC13_6c	2410	55	933	0.03	3007	14	52%	0.280926	14	0.00284
13DC13_7a	2222	342	801	0.11	2964	17	54%	0.280899	26	0.00256
13DC13_7b	576	512	633	0.66	3441	16	5%	0.280948	18	0.00348
13DC13_8a	2097	560	497	1.22	2836	20	80%	0.280872	33	0.00186
13DC13_8b	615	259	268	1.21	3079	22	29%	0.280836	26	0.00186
13DC13_11a	265	170	254	0.79	3354	18	14%	0.280888	15	0.00234
13DC13_11b	225	156	234	0.82	3356	17	5%	0.280912	16	0.00283
13DC13_12a	291	101	299	0.32	3414	23	0%	0.280929	15	0.00105
13DC13_12b	232	12	191	0.05	3179	11	3%	0.280864	9	0.00069
Biotite-rich enclave										
13DC15_1a	241	75	240	0.43	3473	21	2%	0.280571	21	0.00140
13DC15_1b	494	86	314	0.18	2973	30	23%	0.280548	11	0.00108
13DC15_2a	293	177	320	0.47	3603	23	9%	0.280450	17	0.00109
13DC15_2b	315	191	336	0.54	3610	23	11%	0.280475	20	0.00146

S and LA-MC-ICP-MS

2 σ ($x10^{-5}$)	$^{176}Hf/^{177}Hf_{in}$	2 σ ($x10^{-6}$)	$\varepsilon_{Hf\ in}$	2 σ
13	0.280746	20	-0.3	0.7
21	0.280699	26	-2.9	0.9
14	0.280768	31	-10	1.1
8	0.280693	24	-9.8	0.9
9	0.280635	22	+2.3	0.8
9	0.280634	22	+2.4	0.8
5	0.280613	16	+1.3	0.6
7	0.280635	18	+2.3	0.6
3	0.280625	15	+1.9	0.5
20	0.280638	28	+2.2	1.0
9	0.280636	14	+2.3	0.5
14	0.280632	27	-9.1	1.0
21	0.280650	27	-3.6	1.0
12	0.280626	21	-0.1	0.8
5	0.280577	33	-0.9	1.2
10	0.280678	44	+4.1	1.6
6	0.280631	21	-7.1	0.8
31	0.280591	42	+0.2	1.5
20	0.280590	33	-0.4	1.2
23	0.280678	29	-7.2	1.0
23	0.280661	22	+0.8	0.8
10	0.280623	17	-2.3	0.6
15	0.280600	17	-0.1	0.6
9	0.280769	22	+3.9	0.8
6	0.280797	25	+2.7	0.9
6	0.280744	14	+6.5	0.5
6	0.280743	14	+7.2	0.5
4	0.280758	13	-0.4	0.5
4	0.280756	13	+0.7	0.5
7	0.280722	18	+2.2	0.6
7	0.280719	18	+4.0	0.6
4	0.280769	17	+0.4	0.6
6	0.280749	17	+4.2	0.6
7	0.280762	16	-2.8	0.6
13	0.280753	27	-4.2	1.0
17	0.280717	22	+5.9	0.8
7	0.280771	34	-6.6	1.2
7	0.280726	27	-2.4	1.0
7	0.280736	17	+4.6	0.6
7	0.280730	17	+4.3	0.6
3	0.280860	16	+10.4	0.6
3	0.280822	11	+3.4	0.4
6	0.280477	22	-1.8	0.8
2	0.280487	13	-13.4	0.5
9	0.280374	19	-2.4	0.7
4	0.280373	21	-2.3	0.7

Table 4. Interpreted U-Pb ages and Lu-Hf isotope systematics for Indian zircons analyzed here

Sample	Age (Ma)	2σ	$^{176}Hf/^{177}Hf_{in}$	2 σ	$\varepsilon_{Hf\ in}$	2 σ
Granitic gneiss (13DC12)	3410.8	3.6	0.280631	0.000018	+2.2	0.6
Trondhjemitic gneiss (13DC13)						
Zircon #4 (group 1)	3468	41	0.280742	0.000014	+7.5	0.5
Zircon #7 (group 1)	3456	20	0.280721	0.000017	+6.4	0.6
Zircon #12a (group 1)	3414	23	0.280860	0.000016	+10.4	0.6
Zircon #3 (group 2)	3359	110	0.280778	0.000016	+6.1	0.6
Zircon #11 (group 2)	3356	25	0.280733	0.000012	+4.5	0.4
Zircon #5b (group 2)	3342	19	0.280720	0.000018	+3.7	0.6
Zircon #6 (group 3)	3295	18	0.280752	0.000010	+3.7	0.4
Zircon #5a (group 4)	3170	32	0.280756	0.000013	+0.8	0.5
Zircon #12b (group 4)	3179	11	0.280822	0.000011	+3.4	0.4
Zircon #8 (group 5)	3101	25	0.280739	0.000021	-1.4	0.7
Biotite-rich enclave (13DC15)						
Zircon #1	3499	29	0.280476	0.000011	-1.3	0.4
Zircon #2	3607	16	0.280374	0.000014	-2.3	0.5

ein

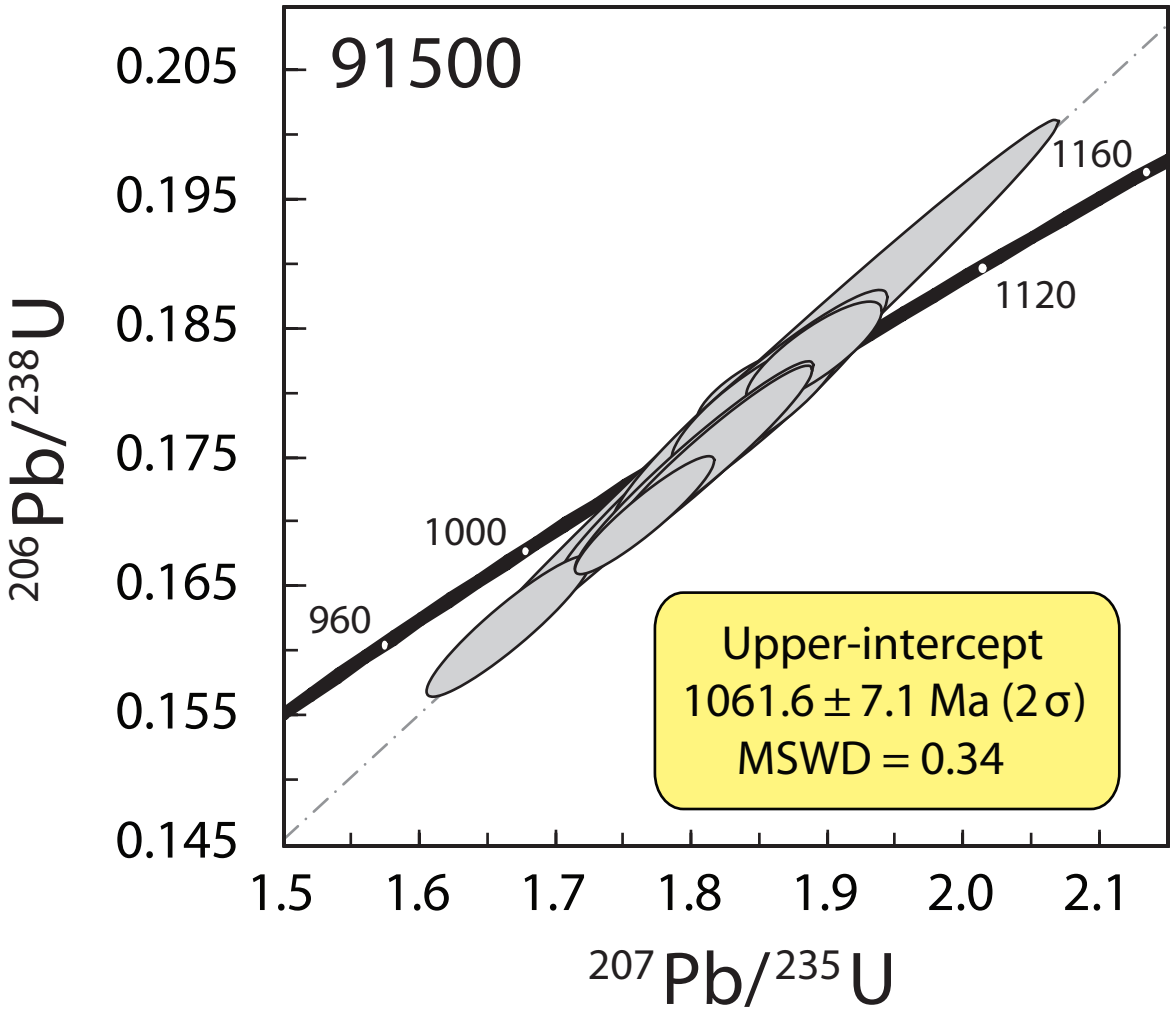
91500
0.205
0.195
0.185
0.175
0.165
0.155
0.145
1.5
1.6
1.7
1.8
1.9
2.0
2.1
1160
1120
1000
960
Upper-intercept
1061.6 ± 7.1 Ma (2 σ)
MSWD = 0.34
206Pb/238U
207Pb/235U

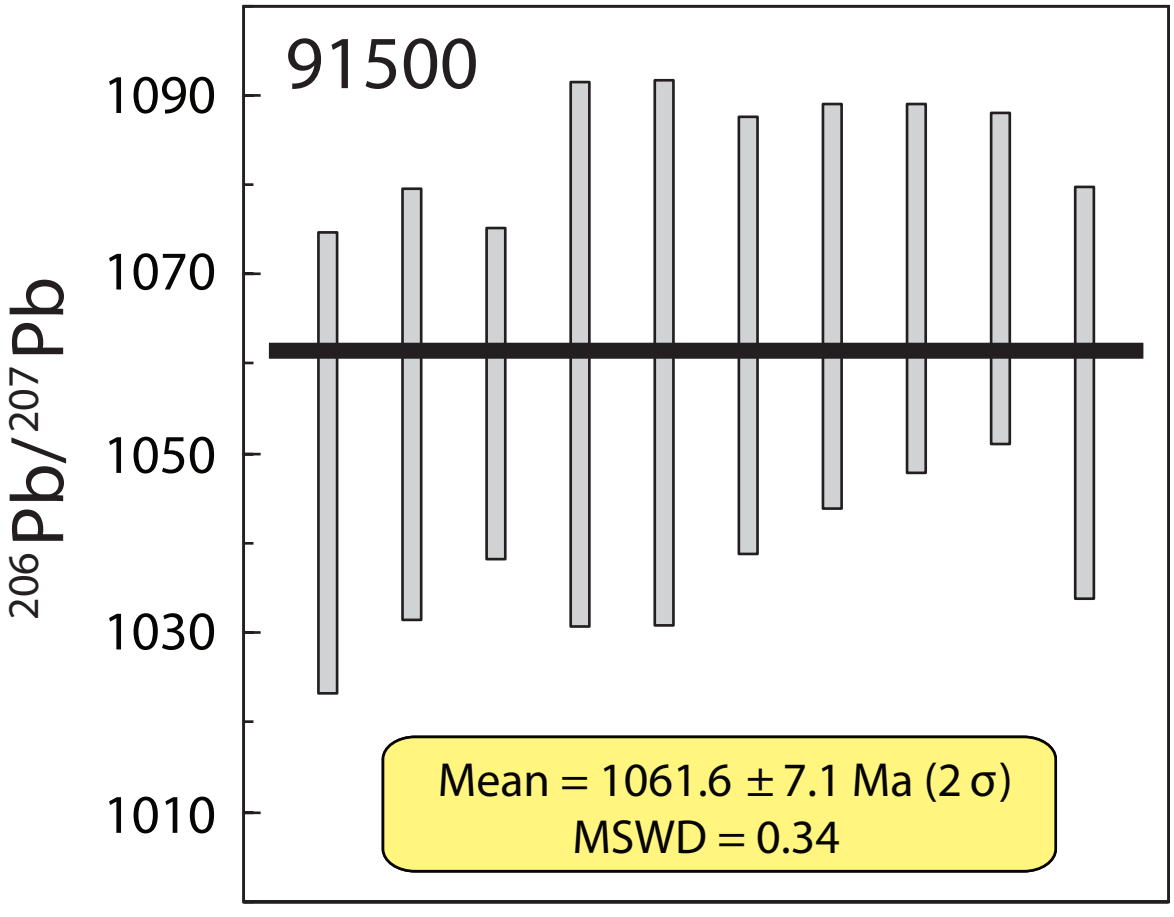
91500
1090
1070
1050
1030
1010
Mean = 1061.6 ± 7.1 Ma (2 σ)
MSWD = 0.34
206Pb/207Pb

Figure S1

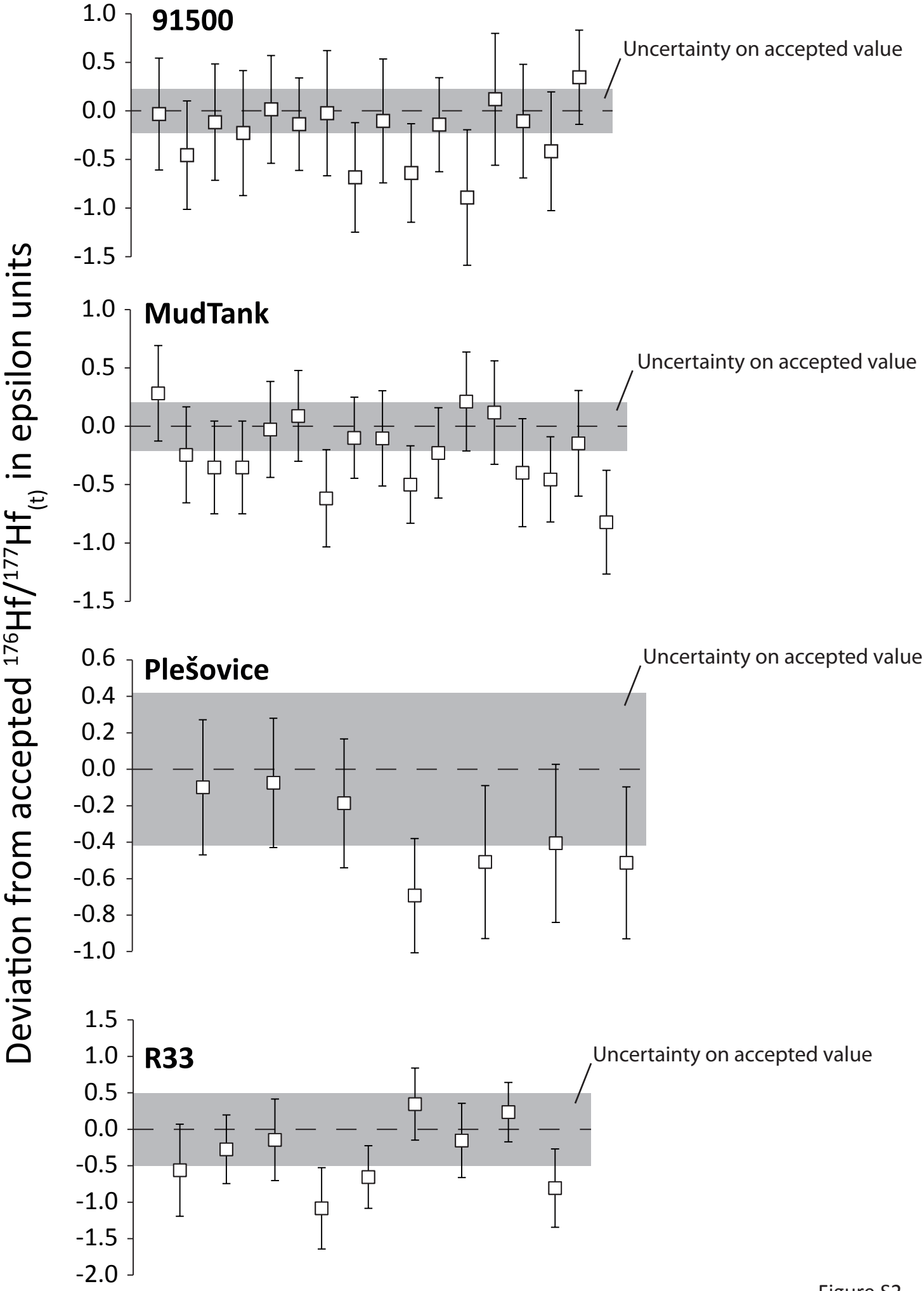
91500
Uncertainty on accepted value
1.0
0.5
0.0
-0.5
-1.0
-1.5
MudTank
Uncertainty on accepted value
1.0
0.5
0.0
-0.5
-1.0
-1.5
Plešovice
Uncertainty on accepted value
0.6
0.4
0.2
0.0
-0.2
-0.4
-0.6
-0.8
-1.0
R33
Uncertainty on accepted value
1.5
1.0
0.5
0.0
-0.5
-1.0
-1.5
-2.0
Deviation from accepted $^{176}Hf/^{177}Hf_{(t)}$ in epsilon units

Figure S2

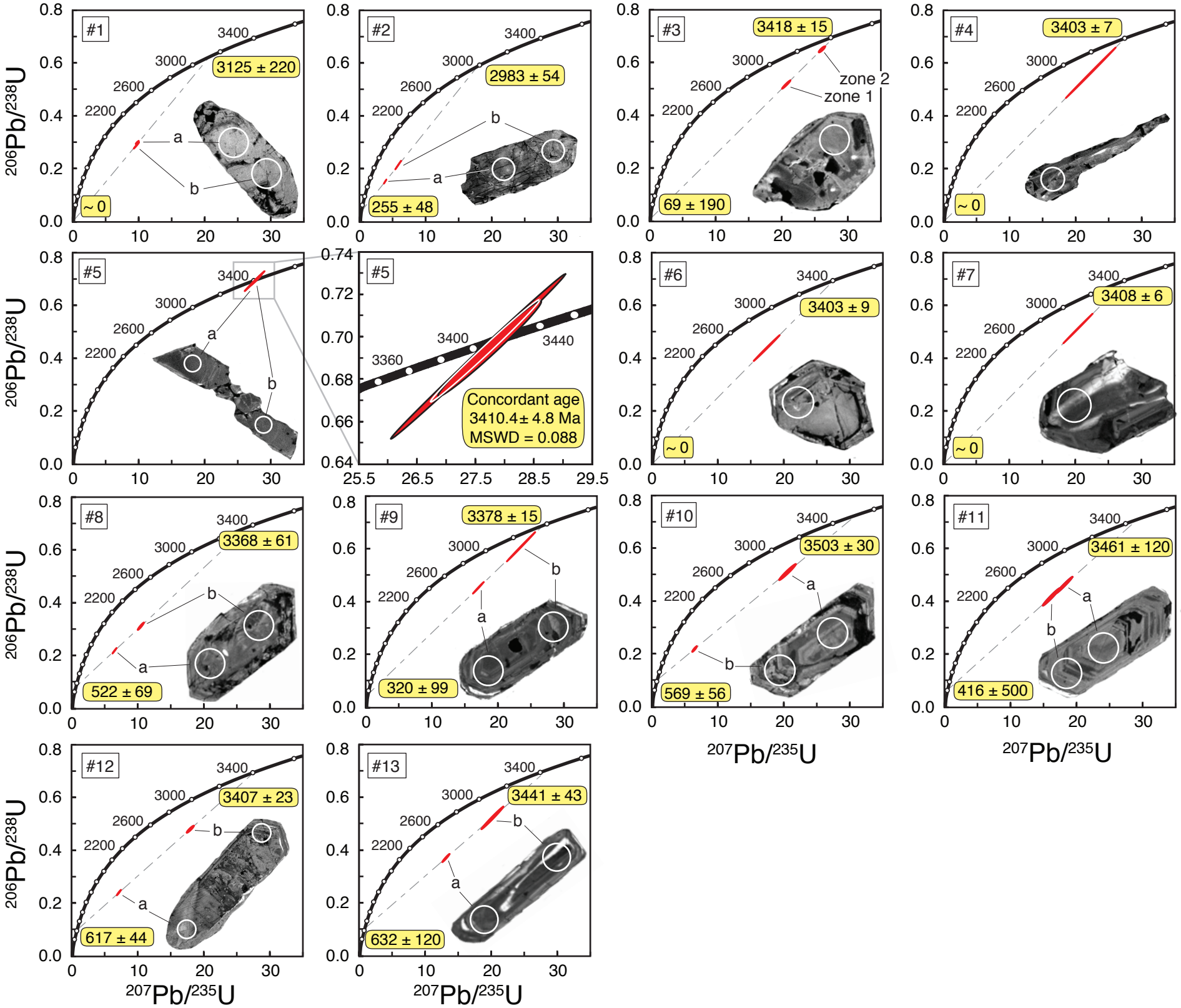
#1
3125 ± 220
~ 0
#2
2983 ± 54
255 ± 48
#3
3418 ± 15
zone 2
zone 1
69 ± 190
#4
3403 ± 7
~ 0
#5
#5
3360
3400
3440
Concordant age
3410.4± 4.8 Ma
MSWD = 0.088
#6
3403 ± 9
~ 0
#7
3408 ± 6
~ 0
#8
3368 ± 61
522 ± 69
#9
3378 ± 15
320 ± 99
#10
3503 ± 30
569 ± 56
#11
3461 ± 120
416 ± 500
#12
3407 ± 23
617 ± 44
#13
3441 ± 43
632 ± 120
206Pb/238U
207Pb/235U

Figure S3

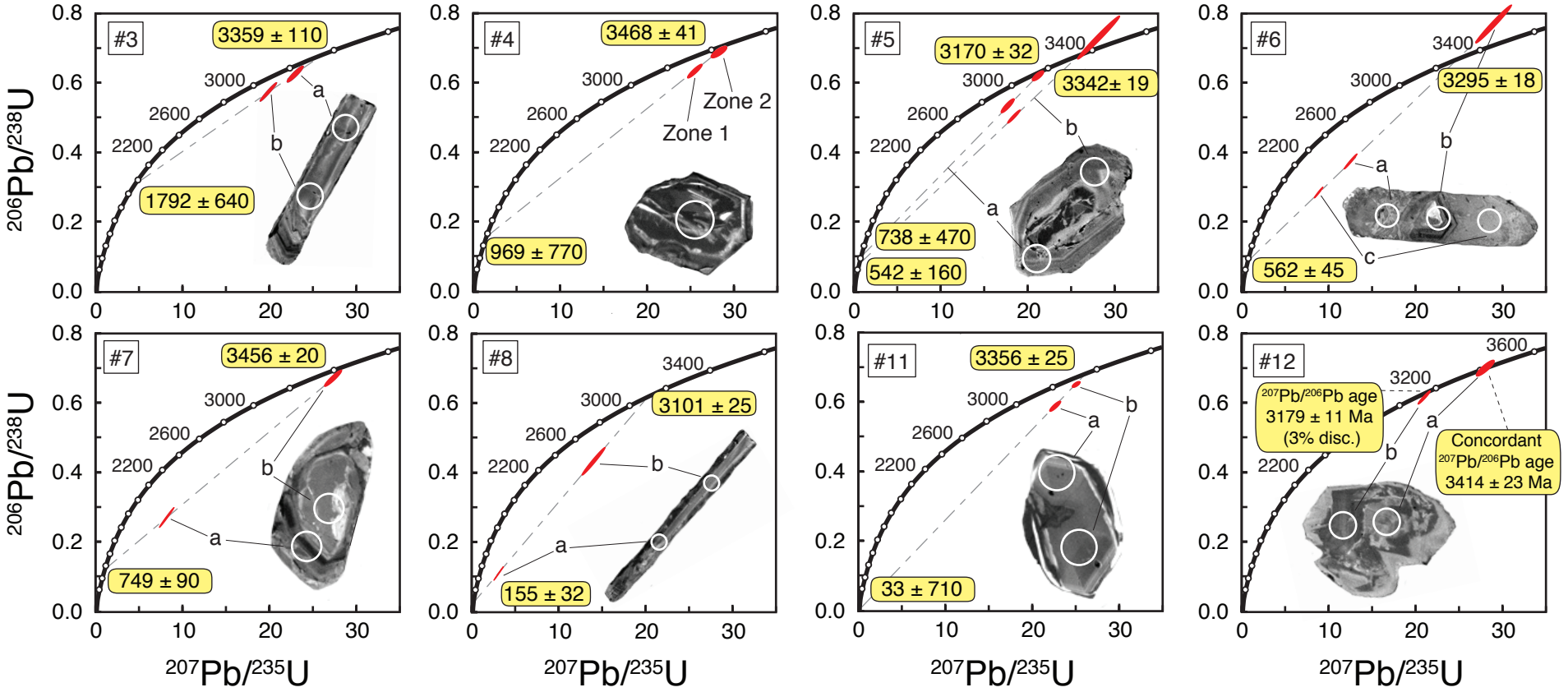
#3
3359 ± 110
1792 ± 640
#4
3468 ± 41
Zone 2
Zone 1
969 ± 770
#5
3170 ± 32
3342± 19
738 ± 470
542 ± 160
#6
3295 ± 18
562 ± 45
#7
3456 ± 20
749 ± 90
#8
3101 ± 25
155 ± 32
#11
3356 ± 25
33 ± 710
#12
207Pb/206Pb age
3179 ± 11 Ma
(3% disc.)
Concordant
207Pb/206Pb age
3414 ± 23 Ma
206Pb/238U
207Pb/235U

Figure S4

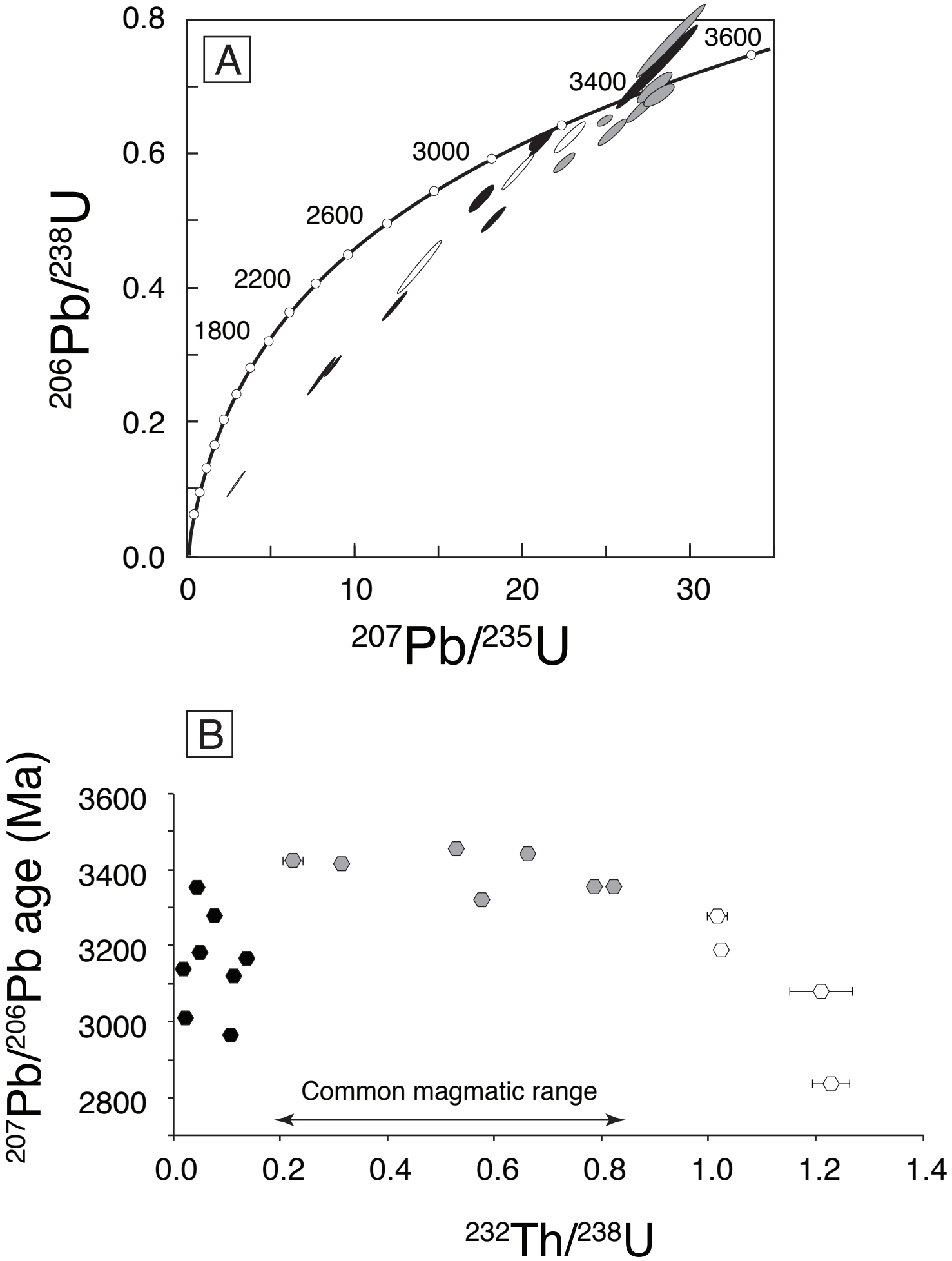
A
0.8
0.6
0.4
0.2
0.0
0
10
20
30
3600
3400
3000
2600
2200
1800
$^{206}Pb/^{238}U$
$^{207}Pb/^{235}U$
B
3600
3400
3200
3000
2800
0.0
0.2
0.4
0.6
0.8
1.0
1.2
1.4
Common magmatic range
$^{207}Pb/^{206}Pb$ age (Ma)
$^{232}Th/^{238}U$

Figure S5

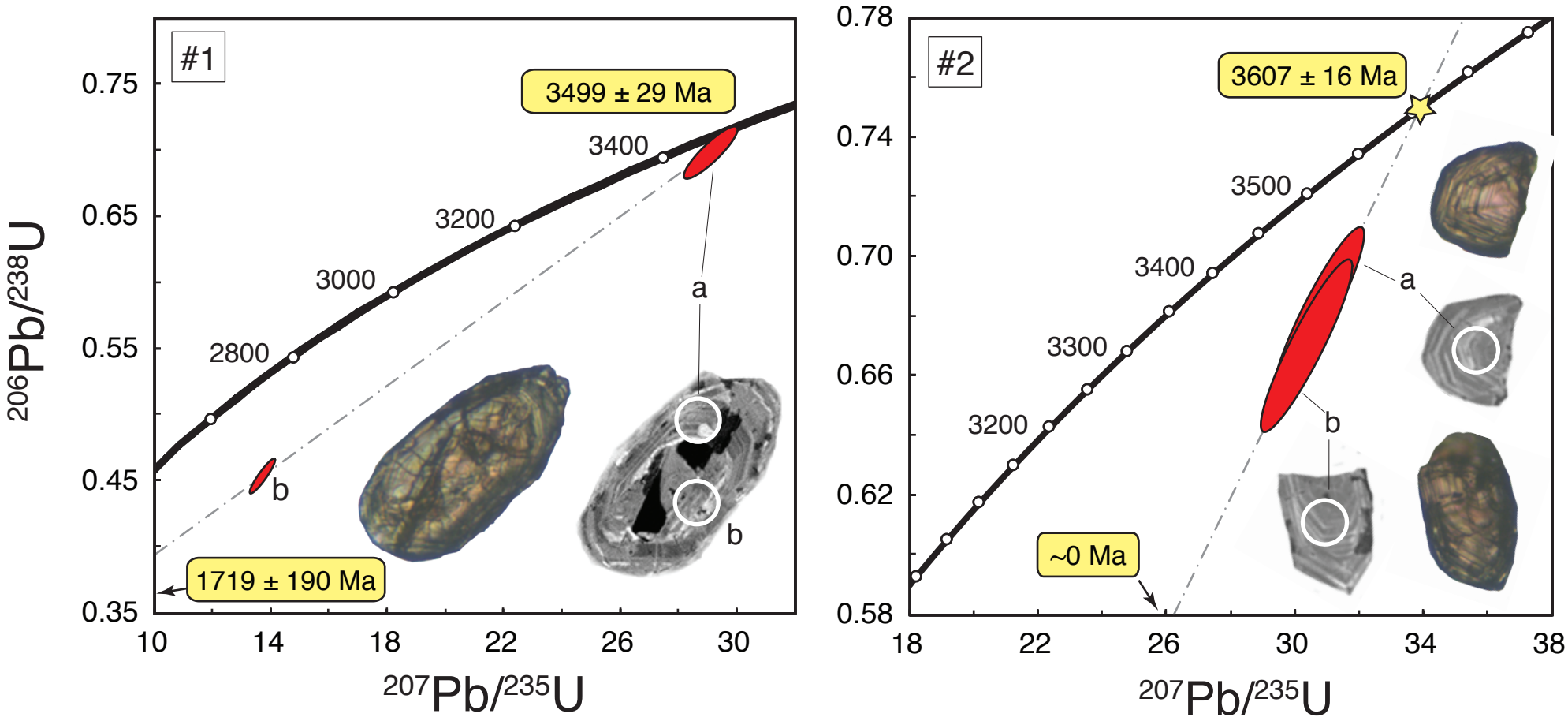
#1
3499 ± 29 Ma
3400
3200
3000
2800
a
b
b
1719 ± 190 Ma
0.75
0.65
0.55
0.45
0.35
10
14
18
22
26
30
206Pb/238U
207Pb/235U
#2
3607 ± 16 Ma
3500
3400
3300
3200
a
b
~0 Ma
0.78
0.74
0.70
0.66
0.62
0.58
18
22
26
30
34
38
207Pb/235U

Figure S6

Table S1. Major and minor oxide abundances for the orthogneisses analyzed in this study

	13DC12	13DC13
SiO2	74.01	72.57
TiO2	0.11	0.27
Al2O3	13.85	15.04
Fe2O3	1.47	1.69
MnO	0.02	0.02
MgO	0.19	0.50
CaO	0.95	1.82
Na2O	3.94	4.89
K2O	4.31	2.54
P2O5	0.11	0.08
Ba	0.048	0.051
Sr	0.009	0.041
L.O.I.	0.83	0.55
Total	99.85	100.06
Or	0.41	0.24
Ab	0.53	0.64
An	0.06	0.12
A/(CNK)	1.1	1.1
A/(NK)	1.2	1.4

Table S2. LA-ICP-MS and LA-MC-ICP-MS operating conditions

Analysis	*U-Pb geochronology*	*Lu-Hf isotope system*
Laboratory	University of New Hampshire	Université Blaise Pascal
ICP-MS model	Nu Instruments AttoM	Thermo Neptune +
Forward Power	1300 W	1200 W
Auxiliary gas (Ar)	~0.8 l/min	0.66 l/min
Ar sample	~0.7 l/min	0.86 l/min
Oxide ThO/Th	~0.5%	-
Additional gas	-	N2
Additional gas flow	-	4.5 ml/min
Laser model	New Wave Research UP-213	Resonetics Resolution M-50
Wavelength	213 nm	193 nm
Pulse duration	<4 ns	<4 ns
Energy	50% / ~0.07 mJ	~3.2 mJ
Fluence	9-10 J/cm^2	~3.8 J/cm2
Frequency	5 Hz	6 Hz
Spot size	30 μm	40 μm
Carrier gas	He	He
Carrier gas flow	~0.8 l/min	0.7 l/min
Data acquisition		**Data acquisition**
Protocol	Time resolved analysis	Time resolved analysis
Scanning mode	Peak-jumping	Static multi-collection
Dwell time per isotope	4 ms	1s
Sweeps per cycle	10	-
Dead-time correction	14 ns	-
Settling time	20 μs	-
Background counting time	30 s	20s
Sample measurement time	60 s	50s
Measurement type	Standard bracketing	Internal normalization
External standard	AS3, 91500	91500, Mud Tank, Plešovice, R33

Table S3. U-Pb isotope results for the zircon standard 91500 analyzed by LA-ICP-MS.

		Isotope Rati			
Sample name	**%$^{206}Pb_{rad}$**	**$^{207}Pb/^{235}U$**	**2 σ**	**$^{206}Pb/^{238}U$**	**2 σ**
91500					
91500_1	99.05	1.666	0.050	0.162	0.004
91500_3	99.67	1.765	0.042	0.171	0.004
91500_5	99.61	1.792	0.072	0.174	0.007
91500_6	99.23	1.813	0.061	0.175	0.006
91500_7	99.68	1.890	0.041	0.183	0.003
91500_8	98.94	1.802	0.072	0.174	0.007
91500_9	98.92	1.847	0.036	0.180	0.003
91500_10	99.44	1.847	0.051	0.179	0.004
91500_11	99.49	1.843	0.083	0.179	0.008
91500_12	99.75	1.846	0.183	0.180	0.018

ios						*Ages (M*		
$^{207}Pb/^{206}Pb$	2 σ	$^{208}Pb/^{206}Pb$	2 σ	$^{232}Th/^{238}U_C$	2 σ	$^{207}Pb/^{235}U$	2 σ	$^{206}Pb/^{238}U$
0.0746	0.0009	0.1099	0.0025	0.365	0.009	996	19	968
0.0750	0.0007	0.1112	0.0023	0.369	0.008	1033	15	1016
0.0746	0.0007	0.1112	0.0020	0.369	0.008	1043	26	1036
0.0750	0.0008	0.1112	0.0025	0.369	0.009	1050	22	1041
0.0748	0.0009	0.1112	0.0028	0.369	0.010	1077	14	1084
0.0749	0.0008	0.1094	0.0030	0.363	0.011	1046	26	1036
0.0743	0.0010	0.1118	0.0035	0.371	0.013	1062	13	1069
0.0747	0.0011	0.1106	0.0034	0.367	0.013	1062	18	1063
0.0747	0.0011	0.1125	0.0042	0.373	0.015	1061	29	1061
0.0745	0.0009	0.1106	0.0025	0.367	0.009	1062	63	1065
		Average		***0.37***	***0.01***			

0.344	***0.001***	***Wiedenbeck et al., 1995***
0.38	***0.09***	***Wiedenbeck et al., 2004***

1a)				*Semi-quantitative estimates*					
2 σ	**$^{207}Pb/^{206}Pb$**	**2 σ**	**Discordance**	**Pb (ppm)**	**2 σ**	**U (ppm)**	**2 σ**	**Th (ppm)**	**2 σ**
25	1057	23	9%	9.0	2.0	42.4	9.6	13.0	1.7
21	1070	18	5%	13.2	2.4	59.7	7.9	21.0	2.8
38	1057	19	2%	19.7	1.7	84.5	5.8	34.6	1.1
31	1069	20	3%	11.9	0.8	52.5	6.2	16.0	0.9
18	1063	24	-2%	17.4	0.9	72.1	3.3	26.8	0.8
37	1067	23	3%	15.3	2.6	68.3	10.3	21.1	2.8
14	1049	26	-2%	13.2	0.9	56.4	4.1	18.6	1.1
23	1061	30	0%	16.0	2.6	70.0	10.0	21.8	2.6
41	1061	30	0%	17.2	1.5	73.2	5.4	24.1	0.9
97	1056	24	-1%	14.2	3.3	61.1	11.4	18.8	1.7
			Average	***14.4***	***2.1***	***66.3***	***7.9***	***23.0***	***4.5***
				15.0	***4.0***	***80.0***	***16.0***	***29.9***	***4.2***
				Wiedenbeck et al., 2004					

Table S4. U-Pb isotope results for Indian zircons analyzed by LA-ICP-MS.

		Isotope Ratios					
Sample name	**%$^{206}Pb_{rad}$**	**$^{207}Pb/^{235}U$**	**2 σ**	**$^{206}Pb/^{238}U$**	**2 σ**	**$^{207}Pb/^{206}Pb$**	**2 σ**
Granitic gneiss							
13DC12_1a	99.3	9.7	0.3	0.289	0.010	0.2426	0.0015
13DC12_1b	99.3	9.8	0.2	0.299	0.005	0.2369	0.0022
13DC12_2a	99.5	3.9	0.2	0.152	0.006	0.1847	0.0013
13DC12_2b	99.2	5.9	0.4	0.214	0.014	0.1986	0.0012
13DC12_3_1	99.6	20.7	0.5	0.519	0.013	0.2887	0.0020
13DC12_3_2	99.6	26.1	0.4	0.653	0.009	0.2898	0.0023
13DC12_4	99.9	22.5	3.0	0.567	0.077	0.2872	0.0012
13DC12_5a	99.9	27.7	0.7	0.696	0.018	0.2891	0.0013
13DC12_5b	99.9	27.5	1.2	0.692	0.031	0.2885	0.0008
13DC12_6	99.8	17.4	1.6	0.439	0.040	0.2873	0.0018
13DC12_7	99.9	20.4	1.8	0.513	0.046	0.2882	0.0011
13DC12_8a	98.1	6.5	0.3	0.219	0.008	0.2143	0.0016
13DC12_8b	99.7	10.5	0.4	0.312	0.011	0.2435	0.0031
13DC12_9a	99.4	17.1	0.7	0.453	0.018	0.2732	0.0012
13DC12_9b	99.9	23.5	1.8	0.608	0.045	0.2803	0.0011
13DC12_10a	99.8	21.2	1.1	0.527	0.027	0.2913	0.0034
13DC12_10b	98.9	7.0	0.4	0.224	0.011	0.2261	0.0047
13DC12_11a	99.3	18.1	1.0	0.462	0.026	0.2846	0.0028
13DC12_11b	99.5	16.2	1.1	0.418	0.027	0.2805	0.0038
13DC12_12a	99.3	7.2	0.3	0.241	0.009	0.2154	0.0021
13DC12_12b	99.8	17.9	0.5	0.481	0.011	0.2708	0.0026
13DC12_13a	99.5	13.2	0.5	0.370	0.013	0.2581	0.0023
13DC12_13b	99.9	20.2	1.4	0.522	0.035	0.2803	0.0026
Trondhjemitic gneiss							
13DC13_3a	99.9	22.9	0.7	0.625	0.019	0.2652	0.0032
13DC13_3b	99.9	19.8	0.8	0.573	0.022	0.2504	0.0022
13DC13_4_1	99.9	25.4	0.7	0.633	0.016	0.2911	0.0032
13DC13_4_2	99.9	28.2	0.7	0.687	0.014	0.2971	0.0047
13DC13_5a_1	99.6	17.6	0.6	0.534	0.017	0.2394	0.0038
13DC13_5a_2	99.6	21.1	0.5	0.620	0.012	0.2466	0.0039
13DC13_5b_1	99.8	18.3	0.6	0.502	0.016	0.2649	0.0025
13DC13_5b_2	99.9	28.1	2.0	0.730	0.051	0.2786	0.0032
13DC13_6a	99.9	12.5	0.6	0.373	0.018	0.2420	0.0022
13DC13_6b	99.9	28.9	1.7	0.769	0.044	0.2725	0.0029
13DC13_6c	99.9	8.8	0.4	0.285	0.013	0.2236	0.0020
13DC13_7a_1	99.8	8.1	0.7	0.270	0.023	0.2177	0.0023
13DC13_7b	99.9	27.2	0.8	0.671	0.019	0.2944	0.0031
13DC13_8a	98.7	3.0	0.4	0.109	0.016	0.2012	0.0025
13DC13_8b	98.9	13.9	1.1	0.432	0.033	0.2339	0.0033
13DC13_11a	99.9	22.6	0.5	0.587	0.012	0.2785	0.0032
13DC13_11b	99.9	25.0	0.4	0.650	0.007	0.2787	0.0030
13DC13_12a	99.9	27.9	0.8	0.700	0.018	0.2894	0.0043
13DC13_12b	99.9	21.1	0.6	0.615	0.015	0.2491	0.0018
Biotite-rich enclave							
13DC15_1a	99.9	28.9	0.7	0.697	0.015	0.3006	0.0042
13DC15_1b	99.2	13.7	0.7	0.454	0.022	0.2189	0.0041
13DC15_2a	99.9	30.7	1.2	0.681	0.023	0.3271	0.0050

13DC15_2b	99.9	30.4	1.2	0.670	0.024	0.3285	0.0050

				Ages (Ma)					
$^{208}Pb/^{206}Pb$	2 σ	$^{232}Th/^{238}U_C$	2 σ	$^{207}Pb/^{235}U$	2 σ	$^{206}Pb/^{238}U$	2 σ	$^{207}Pb/^{206}Pb$	2 σ
0.1097	0.0021	0.410	0.008	2403	31	1635	49	3137	10
0.1171	0.0026	0.44	0.01	2415	18	1689	26	3100	15
0.1344	0.0092	0.49	0.03	1609	33	913	35	2696	11
0.1653	0.0028	0.61	0.01	1955	54	1249	73	2815	9
0.1349	0.0050	0.51	0.02	3124	25	2697	55	3411	11
0.1603	0.0037	0.61	0.01	3350	15	3240	35	3416	12
0.1016	0.0018	0.39	0.01	3204	123	2897	323	3403	7
0.0791	0.0025	0.30	0.01	3410	25	3405	68	3413	7
0.0802	0.0022	0.304	0.009	3403	43	3392	118	3410	4
0.1653	0.0049	0.63	0.02	2957	85	2346	183	3403	10
0.2601	0.0050	0.99	0.02	3110	82	2670	197	3408	6
0.1918	0.0047	0.71	0.02	2042	34	1277	45	2939	12
0.1221	0.0042	0.46	0.02	2478	35	1751	56	3143	20
0.1662	0.0160	0.63	0.06	2938	38	2407	81	3324	7
0.1274	0.0047	0.48	0.02	3248	70	3063	185	3365	6
0.1939	0.0086	0.74	0.03	3146	49	2728	114	3425	18
0.1519	0.0091	0.56	0.04	2111	46	1305	58	3024	33
0.1673	0.0060	0.63	0.02	2997	53	2449	115	3388	15
0.1733	0.0153	0.66	0.06	2886	61	2251	123	3366	21
0.2243	0.0061	0.83	0.02	2131	33	1391	46	2947	16
0.0337	0.0025	0.127	0.009	2987	24	2531	49	3310	15
0.0989	0.0063	0.37	0.02	2691	33	2028	60	3235	14
0.1370	0.0070	0.52	0.03	3099	63	2706	149	3365	15
0.2704	0.0086	1.02	0.03	3221	31	3130	75	3278	19
0.2734	0.0060	1.02	0.02	3082	37	2922	91	3187	14
0.0590	0.0098	0.22	0.04	3325	26	3163	62	3424	17
0.1390	0.0048	0.53	0.02	3425	25	3373	53	3455	24
0.0305	0.0012	0.114	0.005	2969	33	2757	70	3116	25
0.0377	0.0012	0.141	0.005	3142	24	3110	47	3163	25
0.0205	0.0014	0.077	0.005	3008	31	2624	68	3276	15
0.0120	0.0017	0.045	0.006	3421	67	3535	191	3355	18
0.0052	0.0006	0.020	0.002	2640	45	2045	84	3133	15
0.1528	0.0061	0.58	0.02	3450	56	3678	163	3320	16
0.0068	0.0007	0.025	0.003	2314	40	1614	64	3007	14
0.0291	0.0017	0.108	0.006	2244	74	1543	117	2964	17
0.1744	0.0042	0.66	0.02	3392	29	3310	72	3441	16
0.3320	0.0225	1.22	0.08	1414	106	667	93	2836	20
0.3256	0.0317	1.21	0.12	2745	70	2314	148	3079	22
0.2083	0.0053	0.79	0.02	3208	22	2979	48	3354	18
0.2180	0.0053	0.82	0.02	3307	15	3228	27	3356	17
0.0831	0.0045	0.32	0.02	3416	29	3420	70	3414	23
0.0138	0.0029	0.05	0.01	3145	25	3091	62	3179	11
0.0491	0.0027	0.43	0.01	3450	24	3410	56	3473	21
0.1137	0.0101	0.18	0.04	2729	48	2413	99	2973	30
0.1222	0.0081	0.47	0.03	3510	36	3349	91	3603	23

0.1414	0.0048	0.54	0.02	3498	37	3307	92	3610	23

	Semi-quantitative estimates					
Disc.	**Pb (ppm)**	**2 σ**	**U (ppm)**	**2 σ**	**Th (ppm)**	**2 σ**
54%	561.1	54.2	1334.2	75.5	257.1	24.1
51%	750.8	69.0	1691.0	97.5	393.6	21.5
71%	762.7	58.6	2836.9	138.0	1205.3	56.3
61%	719.5	82.0	2072.4	128.7	1761.5	119.7
26%	441.7	31.8	537.6	26.3	201.2	7.2
7%	291.9	28.6	259.7	20.9	119.2	6.5
18%	229.6	35.6	252.7	25.7	47.9	8.1
0%	270.3	24.3	262.1	14.3	79.6	4.3
1%	311.2	144.1	301.8	64.9	99.1	35.8
37%	994.0	459.5	1277.1	279.2	1155.2	416.1
26%	503.5	232.0	470.9	100.2	630.9	224.8
62%	1026.5	476.1	2848.9	611.6	1453.8	519.7
50%	639.5	299.2	1351.8	293.4	463.4	168.2
33%	498.3	58.6	615.0	31.8	659.5	34.4
11%	462.0	63.7	455.9	36.4	283.8	24.0
25%	519.1	65.7	581.2	30.2	483.1	30.4
63%	549.7	70.8	1523.3	87.3	1529.7	84.0
33%	856.2	118.6	1088.2	70.1	827.2	53.2
39%	804.5	383.7	1060.1	255.7	802.4	316.6
58%	554.2	264.1	1328.0	317.9	1141.1	473.1
28%	742.4	355.2	1958.5	473.3	3333.7	665.8
43%	373.6	181.5	640.1	154.4	201.4	81.2
24%	217.8	26.1	271.2	28.5	86.3	11.8
6%	362.9	36.3	348.2	22.4	291.7	16.8
10%	318.5	34.0	341.1	24.9	314.0	17.9
10%	454.9	60.5	512.0	16.6	27.1	3.4
3%	601.3	127.5	537.8	54.1	380.8	44.1
14%	2056.7	251.9	2772.3	171.0	123.0	9.9
2%	3204.9	609.0	3668.1	425.6	459.0	62.8
24%	1043.6	64.4	1395.5	35.8	80.5	4.2
-7%	693.8	178.2	679.7	34.8	28.3	4.5
40%	700.3	67.2	1380.3	55.6	24.8	1.6
-14%	153.6	20.8	122.4	7.6	83.0	7.3
52%	933.0	156.1	2409.8	204.5	54.9	4.3
54%	800.6	416.3	2221.8	334.3	342.3	35.0
5%	633.2	23.9	576.3	13.3	512.3	9.6
80%	497.2	163.9	2097.3	130.5	560.3	34.1
29%	267.8	50.0	615.1	65.1	259.1	34.6
14%	254.4	37.7	265.0	18.6	169.7	20.1
5%	234.5	34.5	224.7	15.6	155.7	18.4
0%	299.1	46.4	290.7	21.1	101.5	12.7
3%	191.0	11.8	232.3	5.1	12.1	1.4
2%	239.9	28.6	240.6	24.3	75.1	9.4
23%	313.6	24.1	494.5	20.9	86.1	9.8
9%	320.1	18.1	292.7	10.4	177.2	4.5

11%	336.1	10.8	314.8	7.4	191.2	4.0

Table S5: Lu-Hf isotope results for zircon standards analyzed by LA-MC-ICP-MS

Standard name	Age (Ma)	176Hf/177Hf	2 ste	176Lu/177Hf	2 ste	176Yb/177Hf
91500	*1065*	*0.282305*	*0.000006*	*0.000121–.000381*		*0.0036–0.0099*
91500_1		0.282305	0.000016	0.000418	0.000001	0.014910
91500_2		0.282293	0.000016	0.000438	0.000001	0.015459
91500_3		0.282302	0.000017	0.000407	0.000001	0.014321
91500_4		0.282299	0.000018	0.000409	0.000001	0.014367
91500_5		0.282307	0.000016	0.000437	0.000001	0.015457
91500_6		0.282302	0.000013	0.000423	0.000001	0.014444
91500_7		0.282305	0.000018	0.000420	0.000001	0.014222
91500_8		0.282286	0.000016	0.000390	0.000001	0.013120
91500_9		0.282302	0.000018	0.000383	0.000001	0.012902
91500_10		0.282286	0.000014	0.000356	0.000000	0.011996
91500_11		0.282301	0.000014	0.000374	0.000000	0.012674
91500_12		0.282280	0.000020	0.000386	0.000001	0.012975
91500_13		0.282309	0.000019	0.000390	0.000001	0.013130
91500_14		0.282302	0.000016	0.000386	0.000001	0.012839
91500_15		0.282294	0.000017	0.000414	0.000001	0.013977
91500_16		0.282315	0.000014	0.000405	0.000001	0.013517
	Average	0.282299	0.000018	0.000402	0.000046	0.013769
Mud tank	*570*	*0.282507*	*0.000006*	*0.000042*	-	*0.0012*
MudTank_1		0.282515	0.000012	0.000018	0.000000	0.000780
MudTank_2		0.282500	0.000012	0.000017	0.000000	0.000746
MudTank_3		0.282497	0.000011	0.000020	0.000000	0.000854
MudTank_4		0.282497	0.000011	0.000020	0.000000	0.000854
MudTank_5		0.282506	0.000012	0.000019	0.000000	0.000814
MudTank_6		0.282509	0.000011	0.000023	0.000000	0.000948
MudTank_7		0.282489	0.000012	0.000017	0.000000	0.000745
MudTank_8		0.282504	0.000010	0.000018	0.000000	0.000737
MudTank_9		0.282504	0.000012	0.000017	0.000000	0.000703
MudTank_10		0.282493	0.000009	0.000017	0.000000	0.000707
MudTank_11		0.282500	0.000011	0.000017	0.000000	0.000708
MudTank_12		0.282513	0.000012	0.000018	0.000000	0.000759
MudTank_13		0.282510	0.000013	0.000018	0.000000	0.000723
MudTank_14		0.282496	0.000013	0.000017	0.000000	0.000727
MudTank_15		0.282494	0.000010	0.000020	0.000000	0.000805
MudTank_16		0.282503	0.000013	0.000018	0.000000	0.000766
MudTank_17		0.282484	0.000013	0.000018	0.000000	0.000732
	Average	0.282501	0.000017	0.000018	0.000003	0.000771
Plešovice	*337*	*0.282482*	*0.000012*	*0.000042–0.000141*		*0.0012–.0041*
Plešovice_gr1_1		0.282479	0.000010	0.000079	0.000002	0.004115
Plešovice_gr1_2		0.282480	0.000010	0.000088	0.000000	0.004563
Plešovice_gr1_3		0.282476	0.000010	0.000085	0.000001	0.004391
Plešovice_gr1_4		0.282462	0.000009	0.000088	0.000000	0.004573
Plešovice_gr1_5		0.282467	0.000012	0.000085	0.000000	0.004412
Plešovice_gr1_6		0.282470	0.000012	0.000106	0.000000	0.005312
Plešovice_gr1_7		0.282467	0.000012	0.000087	0.000000	0.004454
	Average	0.282472	0.000013	0.000088	0.000017	0.004546
R33	*419*	*0.282764*	*0.000014*	*0.001989*	-	*0.052*

R33_gr1_1		0.282749	0.000018	0.002085	0.000063	0.076698
R33_gr1_2		0.282755	0.000013	0.001832	0.000091	0.067295
R33_gr1_3		0.282757	0.000016	0.001660	0.000056	0.059885
R33_gr1_4		0.282728	0.000016	0.001249	0.000050	0.044724
R33_gr1_5		0.282740	0.000012	0.001351	0.000011	0.047085
R33_gr2_1		0.282785	0.000014	0.003456	0.000014	0.120370
R33_gr2_2		0.282771	0.000014	0.003375	0.000016	0.117759
R33_gr2_3		0.282785	0.000012	0.003821	0.000033	0.135503
R33_gr2_4		0.282747	0.000015	0.002672	0.000039	0.094189
	Average	0.282757	0.000039	0.002389	0.001943	0.084834

* Present day value normalized to the respective zircon standard best average $^{176}Hf/^{177}Hf$ as provided by the q

2 ste	178Hf/177Hf	2 ste	ε_{Hf}(ref)*	2 ste	Reference
)					*Blichert-Toft (2008)*
0.000109	1.467259	0.000047	0.0	0.6	
0.000094	1.467260	0.000031	-0.5	0.6	
0.000087	1.467289	0.000037	-0.1	0.6	
0.000081	1.467286	0.000044	-0.2	0.6	
0.000091	1.467252	0.000040	0.0	0.6	
0.000129	1.467262	0.000037	-0.1	0.5	
0.000114	1.467275	0.000043	0.0	0.6	
0.000103	1.467261	0.000032	-0.7	0.6	
0.000095	1.467261	0.000042	-0.1	0.6	
0.000101	1.467288	0.000032	-0.6	0.5	
0.000095	1.467239	0.000038	-0.1	0.5	
0.000116	1.467256	0.000040	-0.9	0.7	
0.000093	1.467282	0.000035	0.1	0.7	
0.000053	1.467292	0.000036	-0.1	0.6	
0.000096	1.467308	0.000037	-0.4	0.6	
0.000099	1.467261	0.000039	0.3	0.5	
0.002056	1.467271	0.000036	0.4	0.7	
-					*Woodhead and Hergt (2005)*
0.000009	1.467283	0.000024	0.3	0.4	
0.000008	1.467256	0.000026	-0.2	0.4	
0.000013	1.467266	0.000030	-0.4	0.4	
0.000013	1.467266	0.000030	-0.4	0.4	
0.000007	1.467258	0.000029	0.0	0.4	
0.000006	1.467275	0.000021	0.1	0.4	
0.000006	1.467268	0.000023	-0.6	0.4	
0.000007	1.467276	0.000025	-0.1	0.3	
0.000005	1.467293	0.000026	-0.1	0.4	
0.000007	1.467280	0.000027	-0.5	0.3	
0.000006	1.467272	0.000025	-0.2	0.4	
0.000010	1.467314	0.000034	0.2	0.4	
0.000005	1.467279	0.000027	0.1	0.4	
0.000011	1.467256	0.000031	-0.4	0.5	
0.000005	1.467266	0.000032	-0.5	0.4	
0.000007	1.467283	0.000034	-0.1	0.5	
0.000006	1.467281	0.000026	-0.8	0.4	
0.000132	1.467275	0.000029	-0.2	0.6	
					Sláma et al. (2008)
0.000043	1.467261	0.000029	-0.1	0.4	
0.000035	1.467280	0.000032	-0.1	0.4	
0.000100	1.467276	0.000021	-0.2	0.4	
0.000035	1.467276	0.000024	-0.7	0.3	
0.000016	1.467257	0.000026	-0.5	0.4	
0.000048	1.467278	0.000026	-0.4	0.4	
0.000070	1.467278	0.000028	-0.5	0.4	
0.000741	1.467272	0.000019	-0.4	0.5	
-					*Fisher et al. (2014)*

0.003340	1.467262	0.000031	-0.6	0.6
0.004302	1.467280	0.000031	-0.3	0.5
0.001717	1.467243	0.000037	-0.1	0.6
0.002176	1.467269	0.000025	-1.1	0.6
0.000720	1.467270	0.000033	-0.7	0.4
0.000759	1.467256	0.000027	0.3	0.5
0.000502	1.467293	0.000031	-0.2	0.5
0.000336	1.467277	0.000026	0.2	0.4
0.000906	1.467256	0.000035	-0.8	0.5
0.067200	1.467267	0.000030	-0.3	0.9

ɹuoted reference

Table S6. Lu-Hf isotope results for Indian zircons analyzed by LA-MC-ICP-MS

Name	Age (Ma)	2 σ	Discordance (%)	176Hf/177Hf	2 σ	176Lu/177Hf
Granitic gneiss						
13DC12_1a	3137	10	54%	0.281023	0.000018	0.00460
13DC12_1b	3100	15	51%	0.280990	0.000022	0.00489
13DC12_2a	2696	11	71%	0.281124	0.000029	0.00689
13DC12_2b	2815	9	61%	0.280890	0.000023	0.00365
13DC12_3	3411	11	26%	0.280772	0.000021	0.00209
13DC12_3	3416	12	7%	0.280772	0.000021	0.00209
13DC12_4	3403	7	18%	0.280723	0.000015	0.00167
13DC12_5a	3413	7	0%	0.280757	0.000016	0.00186
13DC12_5b	3410	4	1%	0.280734	0.000014	0.00165
13DC12_6	3403	10	37%	0.280875	0.000024	0.00361
13DC12_7	3408	6	26%	0.280766	0.000012	0.00198
13DC12_8a	2939	12	62%	0.280855	0.000025	0.00394
13DC12_8b	3143	20	50%	0.281032	0.000024	0.00633
13DC12_9a	3324	7	33%	0.280767	0.000019	0.00219
13DC12_9b	3365	6	11%	0.280685	0.000032	0.00167
13DC12_10a	3425	18	25%	0.280884	0.000043	0.00313
13DC12_10b	3024	33	63%	0.280816	0.000020	0.00317
13DC12_11a	3388	15	33%	0.280869	0.000036	0.00426
13DC12_11b	3366	21	39%	0.280766	0.000030	0.00272
13DC12_12a	2947	16	58%	0.280886	0.000025	0.00369
13DC12_12b	3310	15	28%	0.280833	0.000015	0.00271
13DC12_13a	3235	14	43%	0.280733	0.000015	0.00177
13DC12_13b	3365	15	24%	0.280739	0.000013	0.00214
Trondhjemitic gneiss						
13DC13_3a	3278	19	6%	0.280841	0.000020	0.00114
13DC13_3b	3187	14	10%	0.280885	0.000024	0.00143
13DC13_4_1	3424	17	10%	0.280856	0.000012	0.00170
13DC13_4_2	3455	24	3%	0.280856	0.000012	0.00170
13DC13_5a_1	3116	25	14%	0.280873	0.000011	0.00191
13DC13_5a_2	3163	25	2%	0.280873	0.000011	0.00191
13DC13_5b_1	3276	15	24%	0.280837	0.000016	0.00182
13DC13_5b_2	3355	18	-7%	0.280837	0.000016	0.00182
13DC13_6a	3133	15	40%	0.280893	0.000016	0.00206
13DC13_6b	3320	16	-14%	0.280856	0.000015	0.00167
13DC13_6c	3007	14	52%	0.280926	0.000014	0.00284
13DC13_7a	2964	17	54%	0.280899	0.000026	0.00256
13DC13_7b	3441	16	5%	0.280948	0.000018	0.00348
13DC13_8a	2836	20	80%	0.280872	0.000033	0.00186
13DC13_8b	3079	22	29%	0.280836	0.000026	0.00186
13DC13_11a	3354	18	14%	0.280888	0.000015	0.00234
13DC13_11b	3356	17	5%	0.280912	0.000016	0.00283
13DC13_12a	3414	23	0%	0.280929	0.000015	0.00105
13DC13_12b	3179	11	3%	0.280864	0.000009	0.00069
Biotite-rich enclave						
13DC15_1a	3473	21	2%	0.280571	0.000021	0.00140
13DC15_1b	2973	30	23%	0.280548	0.000011	0.00108
13DC15_2a	3603	23	9%	0.280450	0.000017	0.00109

13DC15_2b	3610	23	11%	0.280475	0.000020	0.00146

2 σ	176Yb/177Hf	2 σ	178Hf/177Hf	2 σ	176Hf/177Hf i	2 σ
0.00013	0.1756	0.0061	1.46728	0.00004	0.280746	0.000020
0.00021	0.1899	0.0100	1.46726	0.00004	0.280699	0.000026
0.00014	0.2782	0.0068	1.46728	0.00004	0.280768	0.000031
0.00008	0.1358	0.0034	1.46727	0.00006	0.280693	0.000024
0.00009	0.0784	0.0041	1.46723	0.00003	0.280635	0.000022
0.00009	0.0784	0.0041	1.46723	0.00003	0.280634	0.000022
0.00005	0.0580	0.0016	1.46731	0.00003	0.280613	0.000016
0.00007	0.0644	0.0026	1.46727	0.00002	0.280635	0.000018
0.00003	0.0593	0.0011	1.46727	0.00003	0.280625	0.000015
0.00020	0.1296	0.0104	1.46728	0.00004	0.280638	0.000028
0.00009	0.0694	0.0037	1.46727	0.00002	0.280636	0.000014
0.00014	0.1406	0.0058	1.46729	0.00004	0.280632	0.000027
0.00021	0.2515	0.0068	1.46726	0.00004	0.280650	0.000027
0.00012	0.0684	0.0040	1.46730	0.00007	0.280626	0.000021
0.00005	0.0522	0.0024	1.46729	0.00005	0.280577	0.000033
0.00010	0.1032	0.0028	1.46723	0.00005	0.280678	0.000044
0.00006	0.1167	0.0044	1.46730	0.00004	0.280631	0.000021
0.00031	0.1539	0.0125	1.46728	0.00005	0.280591	0.000042
0.00020	0.0952	0.0086	1.46734	0.00008	0.280590	0.000033
0.00023	0.1298	0.0093	1.46725	0.00003	0.280678	0.000029
0.00023	0.0833	0.0052	1.46728	0.00002	0.280661	0.000022
0.00010	0.0596	0.0027	1.46731	0.00003	0.280623	0.000017
0.00015	0.0828	0.0080	1.46729	0.00003	0.280600	0.000017
0.00009	0.0401	0.0037	1.46729	0.00004	0.280769	0.000022
0.00006	0.0489	0.0022	1.46733	0.00004	0.280797	0.000025
0.00006	0.0559	0.0020	1.46729	0.00003	0.280744	0.000014
0.00006	0.0559	0.0020	1.46729	0.00003	0.280743	0.000014
0.00004	0.0680	0.0006	1.46728	0.00002	0.280758	0.000013
0.00004	0.0680	0.0006	1.46728	0.00002	0.280756	0.000013
0.00007	0.0569	0.0021	1.46728	0.00003	0.280722	0.000018
0.00007	0.0569	0.0021	1.46728	0.00003	0.280719	0.000018
0.00004	0.0587	0.0018	1.46732	0.00004	0.280769	0.000017
0.00006	0.0587	0.0024	1.46727	0.00003	0.280749	0.000017
0.00007	0.0832	0.0010	1.46731	0.00003	0.280762	0.000016
0.00013	0.0769	0.0033	1.46724	0.00009	0.280753	0.000027
0.00017	0.1165	0.0060	1.46729	0.00003	0.280717	0.000022
0.00007	0.0601	0.0020	1.46733	0.00005	0.280771	0.000034
0.00007	0.0592	0.0019	1.46728	0.00006	0.280726	0.000027
0.00007	0.0838	0.0030	1.46727	0.00003	0.280736	0.000017
0.00007	0.0985	0.0020	1.46723	0.00003	0.280730	0.000017
0.00003	0.0336	0.0010	1.46729	0.00003	0.280860	0.000016
0.00003	0.0223	0.0012	1.46726	0.00003	0.280822	0.000011
0.00006	0.0415	0.0016	1.46730	0.00004	0.280477	0.000022
0.00002	0.0349	0.0004	1.46730	0.00003	0.280487	0.000013
0.00009	0.0354	0.0037	1.46726	0.00005	0.280374	0.000019

0.00004	0.0502	0.0010	1.46726	0.00005	0.280373	0.000021

εHf in	2 σ
-0.3	0.7
-2.9	0.9
-10.0	1.1
-9.8	0.9
2.3	0.8
2.4	0.8
1.3	0.6
2.3	0.6
1.9	0.5
2.2	1.0
2.3	0.5
-9.1	1.0
-3.6	1.0
-0.1	0.8
-0.9	1.2
4.1	1.6
-7.1	0.8
0.2	1.5
-0.4	1.2
-7.2	1.0
0.8	0.8
-2.3	0.6
-0.1	0.6
3.9	0.8
2.7	0.9
6.5	0.5
7.2	0.5
-0.4	0.5
0.7	0.5
2.2	0.6
4.0	0.6
0.4	0.6
4.2	0.6
-2.8	0.6
-4.2	1.0
5.9	0.8
-6.6	1.2
-2.4	1.0
4.6	0.6
4.3	0.6
10.4	0.6
3.4	0.4
-1.8	0.8
-13.4	0.5
-2.4	0.7

-2.3 0.7